UDK 621.3:(53+54+621+66)(05)(497.1)=00 ISSN 0352-9045

INFORMACIJE MIDEM

Strokovno društvo za mikroelektroniko elektronske sestavne dele in materiale

4◦2010

Strokovna revija za mikroelektroniko, elektronske sestavne dele in materiale
Journal of Microelectronics, Electronic Components and Materials

INFORMACIJE MIDEM, LETNIK 40, ŠT. 4(136), LJUBLJANA, december 2010

MIDEM 2010

46th INTERNATIONAL CONFERENCE
ON MICROELECTRONICS, DEVICES AND MATERIALS
and the WORKSHOP on
OPTICAL SENSORS

September 29.- October 1.2010
Radenci, Slovenia

UDK621.3:(53+54+621+66), ISSN0352-9045 Informacije MIDEM 40(2010)4, Ljubljana

Obnovitev članstva v strokovnem društvu MIDEM in iz tega izhajajoče ugodnosti in obveznosti

Spoštovani,

V svojem več desetletij dolgem obstoju in delovanju smo si prizadevali narediti društvo privlačno in koristno vsem članom.Z delovanjem društva ste se srečali tudi vi in se odločili, da se v društvo včlanite. Življenske poti, zaposlitev in strokovno zanimanje pa se z leti spreminjajo, najrazličnejši dogodki, izzivi in odločitve so vas morda usmerili v povsem druga področja in vaš interes za delovanje ali članstvo v društvu se je z leti močno spremenil, morda izginil. Morda pa vas aktivnosti društva kljub temu še vedno zanimajo, če ne drugače, kot spomin na prijetne čase, ki smo jih skupaj preživeli. Spremenili so se tudi naslovi in način komuniciranja.

Ker je seznam članstva postal dolg, očitno pa je, da mnogi nekdanji člani nimajo več interesa za sodelovanje v društvu, se je Izvršilni odbor društva odločil, da stanje članstva uredi in **vas zato prosi, da izpolnite in nam pošljete obrazec priložen na koncu revije.**

Naj vas ponovno spomnimo na ugodnosti, ki izhajajo iz vašega članstva. Kot član strokovnega društva prejemate revijo »Informacije MIDEM«, povabljeni ste na strokovne konference, kjer lahko predstavite svoje raziskovalne in razvojne dosežke ali srečate stare znance in nove, povabljene predavatelje s področja, ki vas zanima. O svojih dosežkih in problemih lahko poročate v strokovni reviji, ki ima ugleden IMPACT faktor. S svojimi predlogi lahko usmerjate delovanje društva.

Vaša obveza je plačilo članarine 25 EUR na leto. Članarino lahko plačate na transakcijski račun društva pri A-banki: 051008010631192. Pri nakazilu ne pozabite navesti svojega imena!

Upamo, da vas delovanje društva še vedno zanima in da boste članstvo obnovili. Žal pa bomo morali dosedanje člane, ki članstva ne boste obnovili do konca leta 2010, brisati iz seznama članstva.

Prijavnice pošljite na naslov:

MIDEM pri MIKROIKS

Stegne 11

1521 Ljubljana

Ljubljana, december 2010

Izvršilni odbor društva

RECENT TRENDS IN DIELECTROPHORESIS

Guolin Xu[1], Francis E.H. Tay[1,2], Guillaume Tresset[3], Florina S. Iliescu[4], Andrei Avram[5], Ciprian Iliescu[1]

[1]Institute of Bioengineering and Nanotechnoloy, Singapore,
[2]National University of Singapore, Dept. of Mechanical Engineering,
[3]Laboratoire de Physique des Solides, University Paris-Sud, CNRS, France,
[4]Republic Polytechnic, School of Applied Science, Singapore,
[5]National Institute for Research and Development in Microtechnologies, Bucharest, Romania

Key words: dielectrophoresis, BioMEMS, dielectrophoretic devices, dielectrophoretic chip, DEP 3D filter

Abstract: The paper presents the recent development of one important BioMEMS application: dielectrophoresis. A classification of dielectrophoretic devices, recent work in the field as well as theoretical consideration and numerical simulation will be presented in the first part of the paper. The second part of the paper presents some dielectrophoretic chip developed by the authors. Different structures of DEP devices such as DEP devices with 3D electrodes, DEP chip with asymmetric electrodes as well as an isolating DEP 3D filter are presented. The main biological applications of these microfluidic devices are: cell trapping and separation of two cellular populations. Some field-flow separation methods performed on the above mentioned chips are described.

Najnovejši trendi pri dielektroforezi

Kjučne besede: dielektroforeza, BioMEMS, dielektroforezne naprave, dielektroforezni čipi, DEP 3D filtri

Izvleček: Članek opisuje razvoj ene najpomembnejših BioMEMS aplikacij-dielektroforezo. V prvem delu članka bo predstavljena klasifikacija naprav za dielektroforezo, kakor tudi numerične simualcije samega pojava. V drugem delu je predstavljeno nekaj dielektroforeznih čipov, ki smo jih razvili na inštitutu za bioinženiring in nanotehnologijo v Singapurju. Predstavljene so tudi različne strukture DEP vezij: DEP vezja s 3D elektrodami, DEP čipi z asimetričnimi elektrodami in izoliran DEP 3D filter. Glavne biološke aplikacije teh mikrofluidnih naprav so: ujetje celic in loÄevanje dveh celičnih populacij. Opisanih je tudi nekaj ločevalnih metod, ki se izvajajo na zgoraj omenjenih čipih.

1. Introduction

Lab-on-chip devices are essential elements for biomedical instrumentation /1/. Microfluidic dispensing and controlling devices /2/, also the afferent technologies for microfluidic chip fabrication on glass /3/, polydimethyl-siloxane (PDMS) /4/, plastic /5/ or even UV curable polymer /6/ were developed.

In our group the research was focus on few directions: devices for drug delivery /7/, cell cultures on microfluidic platforms /8/, characterization of biological samples using impedance spectroscopy /9/ separation of white blood cells using magnetophoresis /10/ and dielectrophoresis /11/. The paper presents the recent trends in dielectrophoresis and main achievement of our team.

2. General consideration about dep

The term "dielectrophoresis" was first coined by Pohl /12/. DEP is a motion of dielectric particles caused by polarization effects in a non-uniform electric field. A particle suspended in a medium of different dielectric characteristics became electrically polarized. Due to the difference in electric field strength on the two sides of the particle, a net dielectrophoretic force pulls it towards the higher electric field gradient region (positive DEP) or pushes it towards the lower electric field gradient region (negative DEP).(Figure 1)

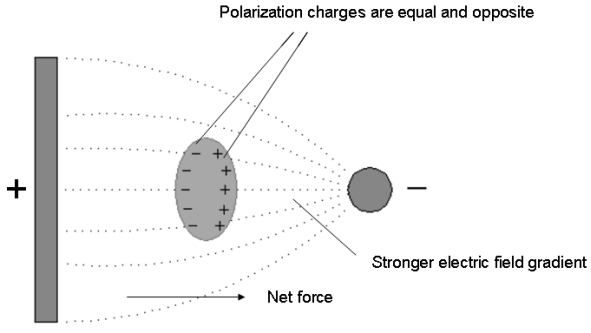

Fig. 1: Principle of dielectrophoresis

Early dielectrophoretic devices were made from thin electrical wires or other machined metal electrodes /13-15/. For many years, their applications were limited to the micro-scale particles, due to the size of the electrodes, which were not small enough to generate high electric field gradient. After 1990, with the development of microfabrica-

tion technologies, a large number of micro- or nano-scale complex electrode arrays designed for particle manipulation were precisely fabricated and integrated to form miniaturized dielectrophoresis chips.

2.1 Analytical consideration

The time-average dielectrophoretic force for the general field was defined as: /16/

$$\left\langle \bar{F}(t) \right\rangle = 2\pi\varepsilon_1 R^3 \left\{ \mathrm{Re}[K]\nabla E_0^2 + 2\,\mathrm{Im}[K](E_{x0}^2\nabla\varphi_x + E_{y0}^2\nabla\varphi_y + E_{z0}^2\nabla\varphi_z \right\} \quad (1)$$

E_{i0} and $\varphi_i (i = x; y; z)$ represented the magnitude and phase, respectively, of the field components in the principal axis directions. This expression contained two terms that contributed to the DEP motion.

1) The first term related the *real* component of the induced dipole moment in the particle and to spatial non-uniformity of the field magnitude. This force directed the particle towards higher or lower electric field regions, depending on whether the $\mathrm{Re}[K]$ was positive or negative. This was the conventional DEP term. The classical DEP force can be given by:

$$F_{DEP} = 2\pi R^3 \varepsilon_1 \,\mathrm{Re}[K]\nabla E_0^2 \quad (2)$$

2) The second term related the *imaginary* component of the induced dipole moment and to spatial non-uniformity of the field phase. This force directed the particle against or along the direction of travel of the electric field depending on whether the phases of the field components are larger $(\mathrm{Im}[K] > 0)$ or smaller $(\mathrm{Im}[K] < 0)$. This was called Travelling Wave Dielectrophoresis (TWD). The expression can be given by /16/:

$$F_{TWD} = \frac{4\pi^2 \varepsilon_m r^3 \,\mathrm{Im}[K(\omega)] E^2}{\lambda} \quad (3)$$

When $\mathrm{Re}[K] = 0$ or $\mathrm{Im}[K] = 0$, the particle experienced no positive or negative DEP force. The frequency at which the particle showed no DEP force was called crossover frequency. The crossover frequency depended on dielectric properties of particle and medium.

K was the well-known complex Clausius–Mossotti factor, defined as:

$$K = \frac{\varepsilon_2^* - \varepsilon_1^*}{\varepsilon_2^* + 2\varepsilon_1^*}, \quad \varepsilon^* = \varepsilon - j\frac{\sigma}{\omega} \quad (4)$$

ε_2^* and ε_1^* were the complex permittivity of the particle and medium respectively. The complex permittivity for a dielectric material can be described by its permittivity ε, conductivity σ, and angular frequency w of the applied electrical field E_0. Taking the example of conventional DEP item, the DEP force acting on a spherical particle was a function of Clausius–Mossotti factor Re (K), which determined the direction of the DEP force. The Clausius-Mossotti factor was a function of electric field frequency, as shown in Figure 2. At a range of frequencies, the particle experienced positive DEP while it showed negative DEP at another range of frequencies. The frequency where the particle showed no positive and negative DEP was called crossover frequency. The change of the permittivity and conductivity of the particles and medium caused the shift of the crossover frequency. Thus at a selected frequency range, one population of particles experienced positive DEP while the other population exhibited negative DEP. This provided a possible basis to separate the mixture of different particles.

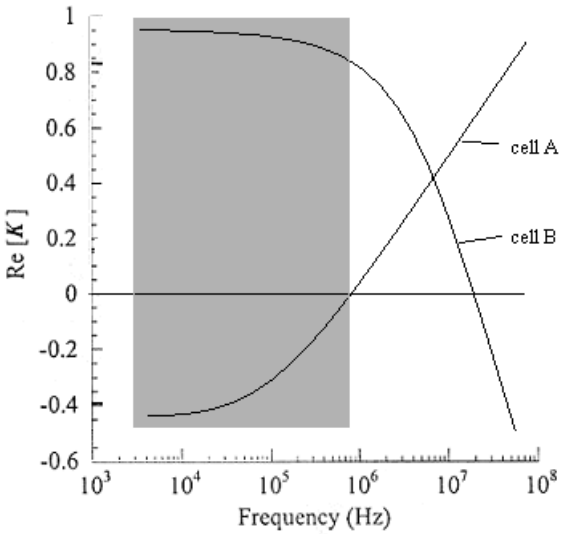

Fig. 2: Variation of the Re (K) as a function of frequency

A particle suspended in a solution was not subjected to DEP force only. It was exposed to many other forces such as hydrodynamic force, gravitational force, and electro-hydrodynamic force. For sub-microparticles, Brownian force must be considered. It was still a big challenge to overcome the Brownian force for manipulation of the sub-microparticles. A detailed calculation of various forces was described in /16/. The movement of the particle in a fluid was determined by the resultant force of many factors. Considering the influence of different types of forces, different separation mechanisms can be performed based on different microfabricated DEP devices.

However, quantification methods of the real value of DEP force on individual cell/ particles was just started. Therefore, pico-Newton resolution of the force was required. A first step was performed by Wei et al /18/ using optical tweezers as a force sensor. They claimed not only the sensitivity of the method for DEP force measurements, but also a selectivity that clearly distinguished the DEP force from all the other forces in the system, such as: electrophoresis, electro-osmosis, heat-induced convection, and Brownian forces. The method was suitable for quantifying the frequency-dependent DEP force and the crossover frequency of different particles.

2.2 Classification of DEP devices

Lately, a special attention was given to dielectrophoresis. This was proved by the increased number of publications especially over the last 5 years /18/. Recent reviews regarding dielectrophoresis were presented in /19-23/.

The dielectrophoretic force that generated the movement was strongly dependent on the gradient of the electric field. According to the methods used for achieving this gradient, different solutions were proposed.

Travelling wave DEP (Figure 3) was the method of changing the phase of the applied electric field /24, 25/ to achieve the gradient of the electric field between two parallel electrodes. Recent work performed by Choi et al in /26/ proved the potential of travelling wave DEP for high throughput separation of particles. An interesting application was presented by Lei et al in /27/, where the traveling wave dielectrophoresis was used for blood pumping in a microfluidic channel.

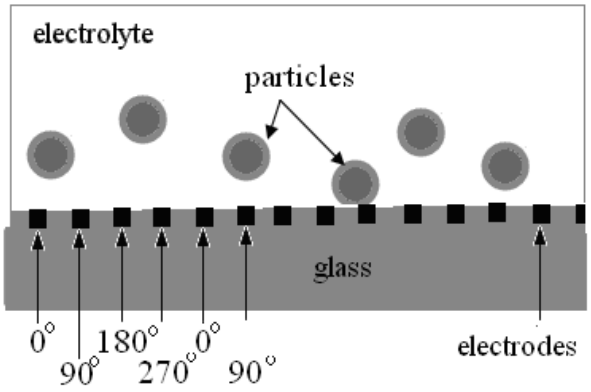

Fig. 3: Working principle of travelling wave dielectrophoresis

Isolating DEP (illustrated in Figure 4), the method presented in Figure 3b, consisted of generating electric field gradient of using of non-homogenous dielectric medium between two parallel-plate electrodes /28, 29/. Parikesit et al /30/ demonstrated that i-DEP can induce size-dependent trajectories of DNA macromolecules. Lewpiriyawong et al proposed in /31/ a conventional microfluidic H filter fabricated in PDMS. This filter induced a non-uniform electric field and generated a negative DEP force on the particles. Jen *et al* /32/ proposed an iDEP microchip to selectively trap dead HeLa cells and collect the viable cells by the hydrodynamic flow in the outlet with four isolated pillars that generated distortion in an uniform electric field.

Chiou *et al* proposed an optically induced DEP method where the gradient of the electric field was generated with a help of an optical image on a photodiode surface /33/. In the same direction, Lee *et al* proposed in /34/ a separation technique of particles under light-intensity gradient. A photoconductive layer was illuminated and a dielectrophoresis force was generated. This force competed with the hydrodynamic force. Hwang *et al* in /35/ discussed an optoelectrofluidic platform for differentiation of normal oocytes using a positive-DEP force that was induced by dynamic image projected from a liquid crystal display.

Moving DEP, presented in /36/ by Kua *et al* was a method where particles, initially trapped in a non-uniform electric

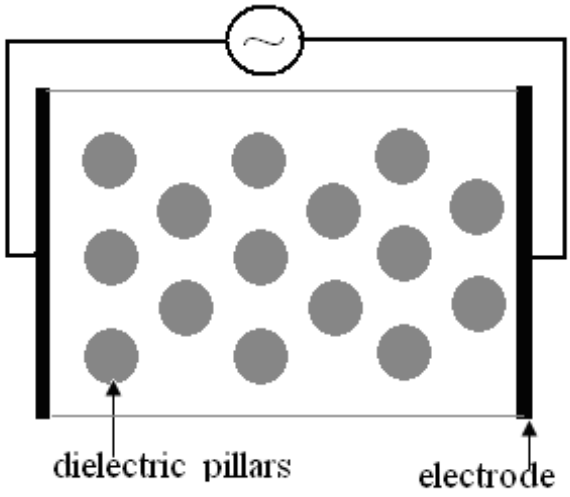

Fig. 4: Working principle of isolating dielectrophoresis

field, were moved using a travelling electric field. The mathematical modeling of the method was presented in /37/.

Another method used the spatial or temporal conductivity gradient. The medium conductivity was gradually increased generating an electric field gradient /38, 39/.

Another method described the gradient of the electric field which was generated by the non-uniform shape of the electrodes. The electrodes can be thin films /40, 41/ - Figure 3c, 3D pillars /42-44/, 3D electrodes that simultaneously defined the microfluidic channel /45/ or were embedded in the wall of the microfluidic channel /46, 47/ and also combination between a thin electrode and a 3D electrode /48/. H.C. Chang's group improved the dielectrophoretic force that acted on different particles in microfluidic device by buffer selection and cross linking /49, 50/. Cheng *et al* /51/ presented an integrated AC dielectrophoretic microfluidic platform based on planar electrodes. 3D DEP were formed gates by placing the electrodes on top and at the bottom of the microfluidic channel. A 3D-DEP cage was presented by Choi *et al* in /52/. Gradient of the electric field can be generated also in vertical direction using interdigitated electrodes; in this case the particles were either trapped at the bottom of the microfluidic channel by positive DEP or levitated using negative DEP /53/. Interdigitated electrodes were also used an interesting application proposed by Flanagan *et al* in /54/: they characterized the stem cells and their different progeny using dielectrophoresis (which induced a frequency-dependent dipole in cells).

There were three groups of applications of DEP phenomenon on cell:

- cell separation,
- cell lysis,
- cell patterning.

A main focus in DEP research was cell sorting- separation of two or more population, or even separation of rare cells

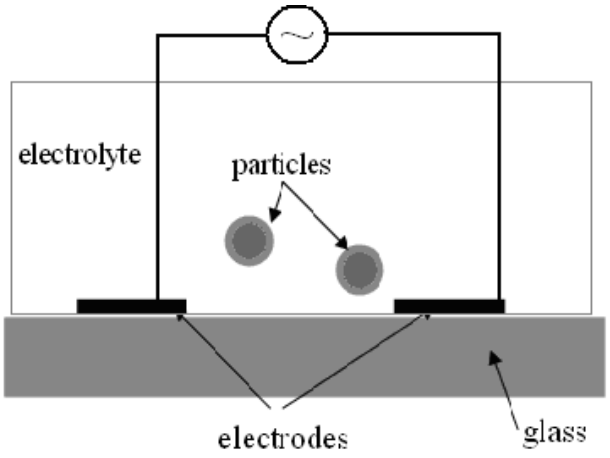

Fig. 5: Schematic representation of classical DEP (electrified gradient is generated by the irregular shape of the electrodes.

from a cell population. Reviews on cell separation were presented by Hughes /55/ and Gascoyne and Vykoukal /56/. These techniques can be summarized as: (a) flow separation, (b) field flow fractionation, (c) travel wave dielectrophoresis.

The flow separation method consisted of trapping, at different locations, the population that exhibited pDEP and nDEP. It used the hydrodynamic force to collect one of these cell populations flowing as a particle suspension solution over an electrode array. Flow separators were reported and demonstrated in /57-60/. The field-flow fraction /61, 62/ used a fluid velocity gradient to separate particles while DEP force was used to locate particles from different regions of the microfluidic channel. Traveling wave DEP can be also used as a separation technique. Related work was reported /63, 64/.

Lysing cells was an important step in the analysis of intracellular contents. This operation can be performed on microfluidic chip in correlation with cell concentration using dielectrophoretic force. Related work was presented in /65-68/.

Cell patterning was another application of dielectrophoresis with two main directions: single cell and multiple cells. In /69/ Ho *et al* proved patterning of hepatic and endothelial cells in a microfluidic chamber using DEP traps. **Rosenthal** and **Voldman reported in /70/** microfabricated DEP traps designed to pattern large arrays of single cells. Suzuki *et al* used nDEP and an interdigited array with four independent microelectrode subunits for cellular micropatern (C2C12 cells) /71/. Mittal *et al* /72/ used nDEP microwells for single-cell patterning in physiological media. Thomas *et al* /73/ proposed two complementary ring electrodes on different layers insulated by a dielectric layer that captured single cell inside the inner ring electrode.

3. Dep chip with 3d electrodes

3.1 Structure of the device

The DEP device structure, presented in Figure 6, consisted of three main layers: two glass wafers (top and bottom) and an inter-layer of conductive silicon that formed the microfluidic channels and the two DEP electrodes. A metallization layer on the bottom glass surface was connected to the bulk silicon electrodes via holes for easy assembly to a PCB. Inlet and outlet tubes were glued on the devices for fluid access.

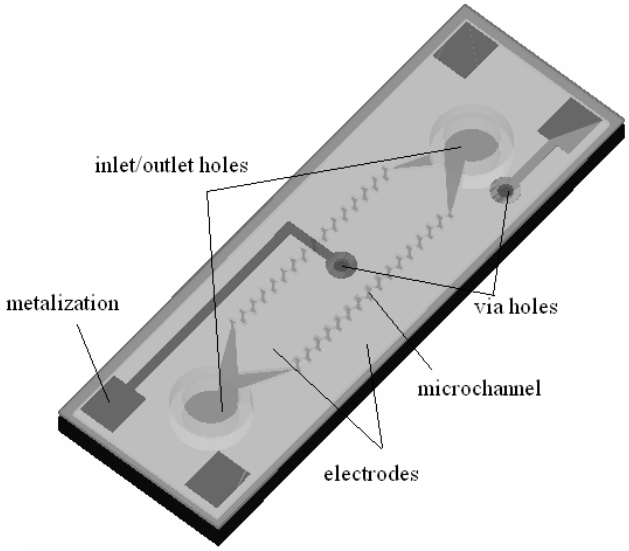

Fig. 6: DEP device with 3D electrodes

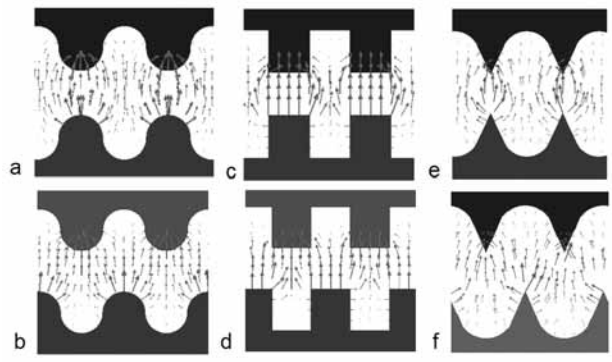

Fig. 7: Configurations of electrode for FEA analysis

Table 1: Electric field strength and gradient for different electrode configura-tions with 10V_{pp} actuation voltage (the distance between electrodes was 100μm)

Design	a	b	c	d	e	f
E [x 10^4V/m]	4.22	4.07	3.68	3.75	8.87	3.61
∇E^2 [X10^5 V^2/m^3]	2.91	1.76	2.29	2.38	12.8	5.53

To generate the DEP force for cell manipulation an AC voltage with a frequency of 1 kHz-100 MHz must be applied

to the electrodes so that an electric field and its gradient can be generated. From equation (1), the DEP force was proportional to the gradient of the square of electric field, which was determined by the geometry of electrodes and the insulator.

For the presented DEP device, the electrode arrangement was developed to maximize the electric field while minimizing the electrical dead volumes. This ensured that the DEP force was always sufficient to overcome Stokes' force and concentrate the cells at a relative low actuation voltage while minimizing fluidic dead volumes. This was a unique requirement for the design described since the electrode geometry also defined the fluidic geometry.

To estimate the electric field generated, triangular, rectangular and semi-circular type electrodes were analysed using the Maxwell electrostatic finite element analysis (FEA) software. Figure 7 showed examples of electrode configurations. Table 1 listed the maximum electric field and its gradient generated by each electrode configuration. A detail study regarding the gradient of the electric field was presented in /74/.

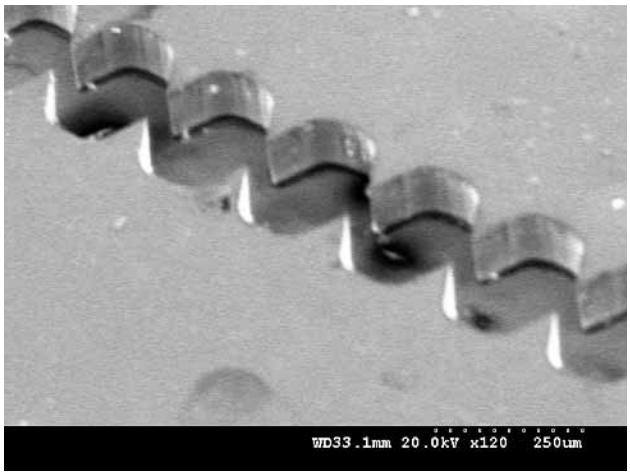

Fig. 8: SEM picture with the microchannel

3.2. Cell trapping in a DEP device with 3D electrodes

The testing of the device was performed using yeast cells. 100 mg of yeast, 100 mg of glucose and 2 ml DI water were incubated in an Eppendof tube at 37°C for 2 hours. The cells were then concentrated by centrifugation at 1000 rpm for 1 minute. The supernatant solution was removed and the cell pellet was washed by adding into the tube 2 ml of DI water. The centrifugation and washing process was repeated three times before the cells were collected and re-suspended in the separation buffer. The separation buffer was a mixture of phosphate buffered saline (PBS) and DI water. The conductivity of the separation buffer was

Fig. 9: Photo with DEP chips

adjusted to about 50 μS/cm using NaCl. The final concentration of the cells was $1x10^7$ cell/ml.

A function generator with a sinusoidal wave output was used to generate the drive signal. A linear amplifier was used to amplify the output voltage of the function generator in order to drive the DEP device. The drive signal was increased gradually from 0 to 25 V. The signal frequency was anywhere in the range of 20 kHz to 100 kHz.

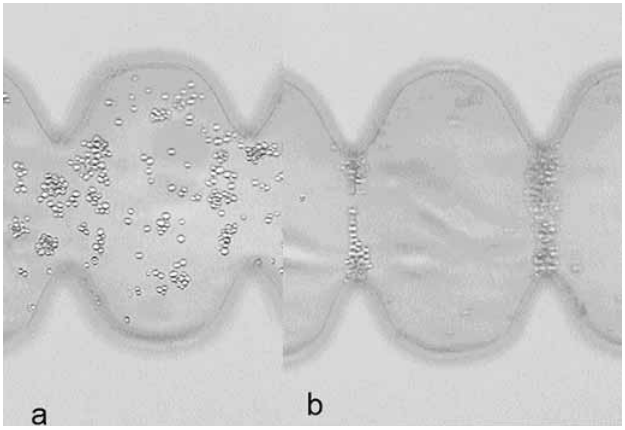

Fig. 10: The results of the trapping. Optical image with the trapping by positive DEP of yeast cells: (a) Before applying voltage, and (b) after.

The main advantage of the device with 3D electrodes consisted of a reduced Joule effect. A detailed analysis regarding Joule effect in different DEP devices was presented in /74/.

3.3. Sequential field-flow cell separation method in a DEP chip with 3D electrodes

The method was described in /75/ and consisted of four steps as illustrated in Figure 11. First, the microchannel was filled with the mixture of the two populations of parti-

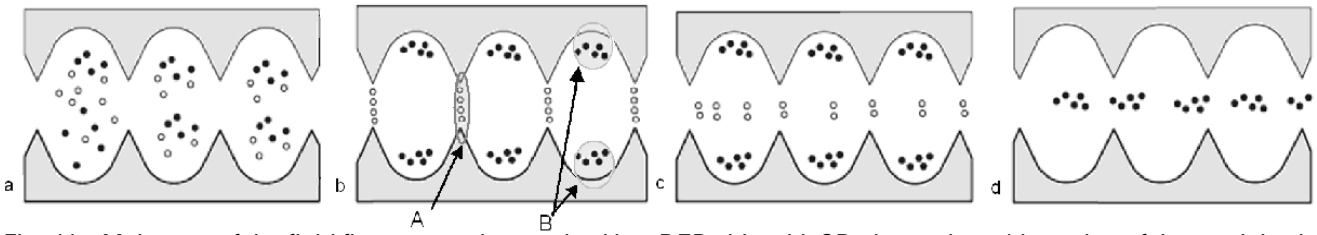

Fig. 11: Main step of the field-flow separation method in a DEP chip with 3D electrodes: a) insertion of the particles in the chip, b) cells separation using pDEP and nDEP, c) moving the first population by increasing the velocity of the fluid, d) the second population is released after removing the electric field.

cle (Figure 11a). Second, the particle populations were trapped at different locations along the microfluidic channels (Figure 11b). The population which exhibited positive dielectrophoresis was trapped in the area where the distance between the electrodes was the minimum while the other population that exhibited negative dielectrophoresis was trapped in places where the distance between electrodes was at its maximum. In the next step, increasing the flow in the microchannels resulted in an increased hydrodynamic force that swept the cell population trapped by positive dielectrophoresis out of the chip (Figure 11c). In the last step the electric field was removed and the second population was swept out and collected at the outlet (Figure 11d). The testing was performed with live/dead yeast cells.

3.4 Continuous field-flow separation of two cell populations in a DEP chip 3D electrodes

The method was similar to the previous one with the observation that the separation process was performed under continuous flow. The method was presented in detail in /76/ and consisted of two cell populations (live/dead) which flow through a microfluidic channel. The vertical walls of the channel were the electrodes of the DEP device. The irregular shape of the electrodes generated both electric field and fluid velocity gradients. As a result, the particles that exhibited negative DEP were trapped in the fluidic dead zones, while the particles that experienced positive DEP were concentrated in the regions with high velocity and thus collected at the outlet. The device was tested with dead and living yeast cells.

3.5 Bidirectional field –flow separation method

For the above presented methods the main disadvantage was the collection of the population trapped in the wells. This disadvantage can be eliminated using a chip with 2 inlets and two outlets, method described in /77/.

The methodology, illustrated in Figure 14, was as follows: first the solution with the mixture of two particle population was injected into the microfluidic chamber (Figure 14a); next the two populations were separated in different locations according to their electrical properties (Figure 14b);

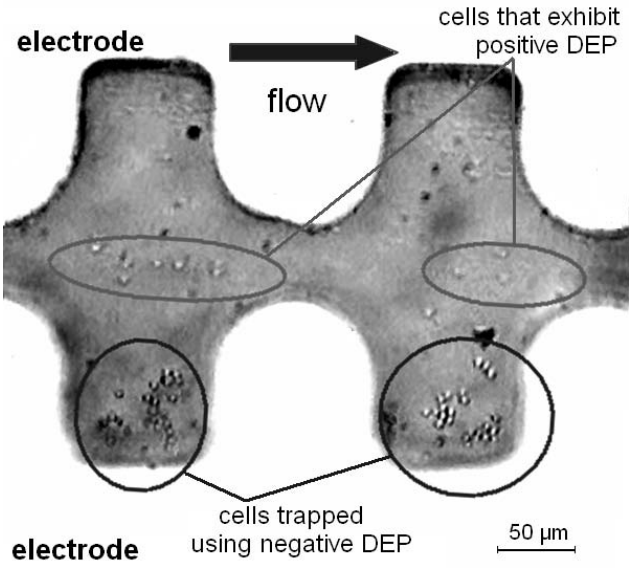

Fig. 12: Optical image of the separation process

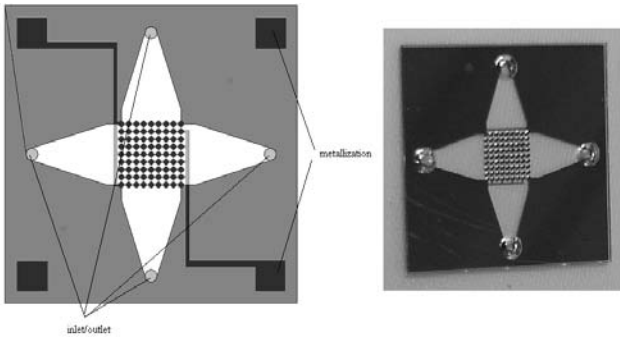

Fig. 13: Schematic drawing and optical image with the device use

subsequently, one population was collected at one of the outlet by flowing a fresh buffer solution (Figure 14c) while the other one was collected at the second outlet in the perpendicular direction (Figure 14d).

The two populations were separated using positive and negative DEP at different locations.

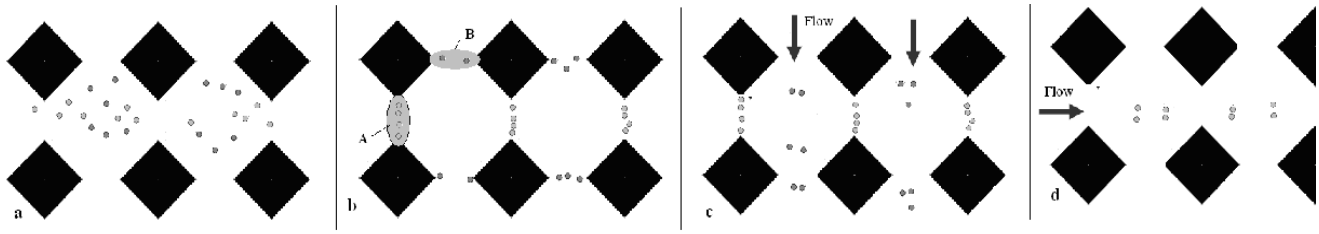

Fig. 14: Bidirectional field-flow separation method: a) insertion of the cell mixture, b) trapping of the cell in different location of the device, c) collection of the first cell population, d) collection of the second population.

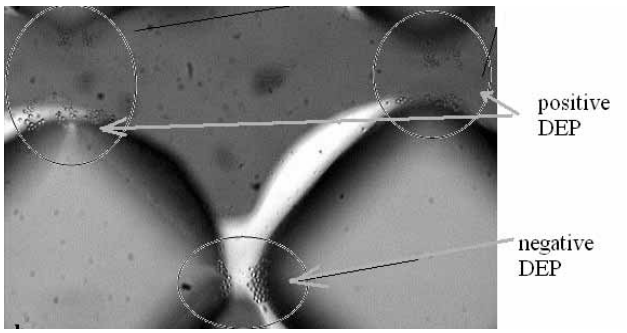

Fig. 15: Optical image taken during the separation process

4. Dep chip with asymmetric electrodes

4.1 Structure of the DEP chip with asymmetric electrodes

An asymmetric distribution of the electric field in the vertical plane can be possible using a special configuration of the electrodes: a bulk silicon electrode and a thin electrode (Figure 16).

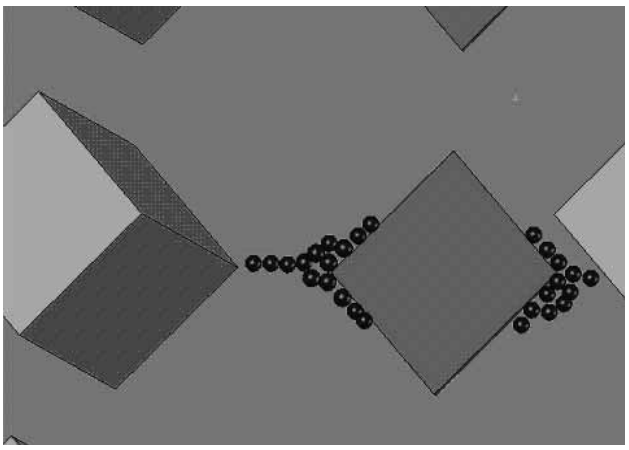

Fig. 16: DEP chip with 3D gradient

The thick electrode defined, at the same time, the walls, while the two glass dies formed the ceiling and floor of the microfluidic channel. The top glass die presented two etch-through inlet/outlet holes of the microfluidic channel. In the bottom glass die isotropic via-holes were performed through the glass for the lead-outs. The proposed DEP structure, with thin and thick electrodes, generated an asymmetric distribution of the electric field in the vertical plane. Therefore it created an enhanced electric field gradient. As a result, for positive DEP, the particles were trapped near the thin electrode, while for negative DEP the particles were levitated. Compared to the typical planar DEP devices, the proposed DEP structure presented an increased DEP force in the vertical direction. Details of the fabrication process of the device were presented in /48, 78/.

4.2 Cell trapping in a DEP device with asymmetric electrodes

The fabrication process of the DEP chip with asymmetric electrodes was similar to the process described previously. For the thin electrode a 1 µm-thick amorphous silicon layer (doped with Al) was used. The stress in the layer was measured to be less than 100 MPa compressive. The result of the testing of the DEP device using yeast cell was presented in Figure 16. The testing was performed in conditions similar to the testing of the DEP chip with 3D electrodes.

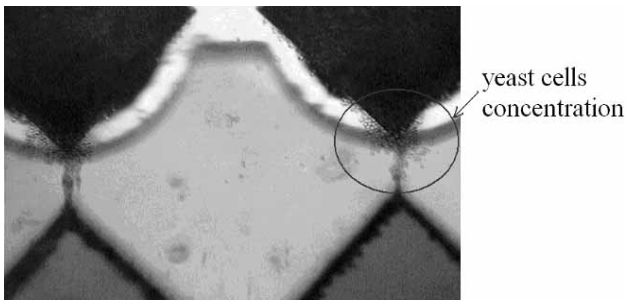

Fig. 16: Yeast cells trapped in the highest electric field regions around thin electrode tips due to positive DEP.

4.3 Continuous field-flow separation method in a DEP device with asymmetric electrodes

Figure 17 illustrated the separation method in a DEP chip with asymmetric electrodes. The mixture with two particle

populations was flowed through the microfluidic device. The magnitude of the electric field, its frequency and the medium properties were selected in such a way that one population exhibited positive DEP while the other one negative DEP. The electric field was applied as a continuous flow. Two results were recorded: (a) the particles that exhibited negative DEP were levitated due to a strong DEP force in a vertical direction that overcame the buoyancy force (b) the particles that experienced positive DEP were collected at the bottom of the device in the vicinity of the thin electrode. As a result, the cells that experienced negative DEP were collected at the outlet. When the electric field was released and the flow in the microfluidic channel was increased, the second population of cells was collected at the outlet.

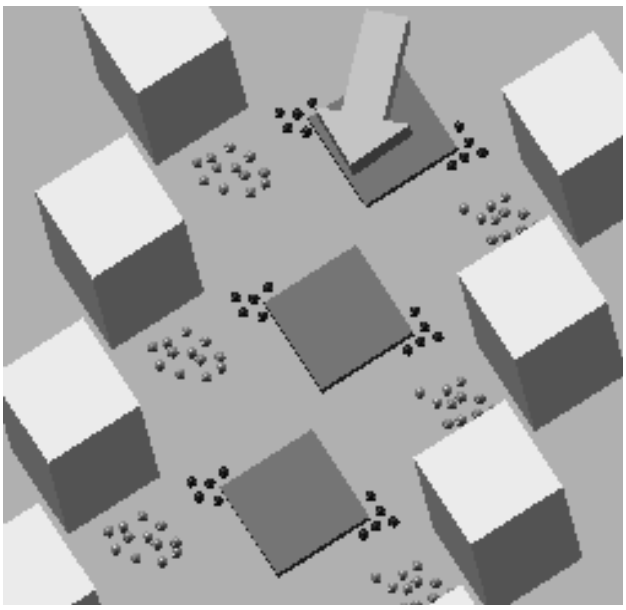

Fig. 17: Schematic view with the separation method: the population that exhibited positive DEP was trapped at the bottom of the device, while the population that experienced negative DEP was levitated and flowed out.

5. Conclusions

The paper presented an overview of the trends in dielectrophoresis as well as the contribution of the authors in this field with a special attention to structure of DEP devices with 3D electrodes or combinations between 3D and planar electrodes. The main advantages of the structures described were: (1) the electrodes defined the walls of the microfluidic channel, (2) usage of classical microfabrication techniques, (3) fabrication of the chip at wafer level, (4) the devices can work with a small volume of the samples, (5) a reduced Joule effect comparing with the DEP device with planar electrodes, (6) due to the reduced Joule effect the devices are suitable for biological applications

6. References

/1/ P.S. Dittrich, A. Manz, Lab-on-a-chip: microfluidics in drug discovery, Nature Reviews Drug Discovery, 5, 2006, 210-218.

/2/ J. West, M. Becker, S. Tombrink, A. Manz, Micro total analysis systems: latest achievements, Anal. Chem., 80, 2008, 4403–4419.

/3/ C. Iliescu, Microfluidics in glass: technologies and applications, Inf. MIDEM. 36, 2006, 204-211.

/4/ J. Friend, L. Yeo, Fabrication of microfluidic devices using polydimethylsiloxane, Biomicrofluidics, 4, 2010, 026502.

/5/ H. Taylor, D. Boning, C. Iliescu, B. Chen, Computationally efficient modelling of pattern dependencies in the micro-embossing of thermoplastic polymers, Microelectr. Eng., 85/5-6, 2008 1453-1456.

/6/ E.P. Dupont, R. Luisier, M.A.M. Gijs, NOA 63 as a UV-curable material for fabrication of microfluidic channels with native hydrophilicity, Microelectr. Eng 87/5-8, 2010 1253-1255.

/7/ B. Chen, J. Wei, C. Iliescu, Sonophoretic enhanced microneedles array (SEMA)-Improving the efficiency of transdermal drug delivery, Sens Act. B, 145/1, 2010, 54-60.

/8/ M. Ni, W. H. Tong, D. Choudhury, N. A. A. Rahim, C. Iliescu, H. Yu, Cell Culture on MEMS Platforms: A Review, Int. J. of Mol. Sci., 10/12, 2009, 5411-5441.

/9/ C. Iliescu, G. Xu, E. Barbarini, M. Avram, A. Avram, Microfluidic device for continuous magnetophoretic separation of white blood cells, Microsys. Tech., 15/8, 2008, 1157-1162.

/10/ C. Iliescu, D.P. Poenar, S.T. Selvan, Frequency dependence on the accuracy of electrical impedance spectroscopy measurements in microfluidic devices, J. Micromech. Microeng., 20/2, 2010, 022001.

/11/ C. Iliescu F.E.H. Tay, G.L. Xu, L. Yu, V. Samper, A dielectrophoretic chip packaged at wafer level, Microsys. Tech., 12/10-11, 2006, 987-992.

/12/ H.A. Pohl, Dielectrophoresis, Cambridge University Press, 1978.

/13/ T.B. Jones, J.P. Kraybill, Active feedback controlled dielectrophoretic levitation, J. Appl. Phys. 60, 1986, 1247–1252.

/14/ K.V.I.S. Kaler, T.B. Jones, Dielectrophoretic spectra of single cells determined by feedback-controlled levitation. Biophys. J., 57, 1990, 173–182.

/15/ J. Gimsa, P. Marszalek, U. Loewe, T.Y. Tsong, Dielectrophoresis and electrorotation of neurospora slime and murine myeloma cells. Biophys. J., 60, 1991, 749–760.

/16/ T.B. Jones, Electromechanics of particle, Cambridge Univ. Press, 1995.

/17/ A. Castellanos, A Ramos, A González, N G Green, H Morgan, Electrohydrodynamics and dielectrophoresis in microsystems: scaling laws, J. Phys. D 36, 2003, 2584-2597.

/18/ M-T. Wei, J. Junio, H.D. Ou-Yang, Direct measurements of the frequency-dependent dielectrophoresis force, Biomicrofluidics 3, 2009, 012003.

/19/ C. Zhang, K. Khoshmanesh, A. Mitchell, K. Kalantar-Zadeh, Dielectrophoresis for manipulation of micro/nano particles in microfluidic systems, Anal. Bioanal. Chem. 396/1, 2010, 401-420.

/20/ M.M. Meighan, S.J. R. Staton, M.A. Hayes, Bioanalytical separations using electric field gradient techniques, Electrophoresis 30/5, 2009, 852-865.

/21/ R. Pethig, Dielectrophoresis: Status of the theory, technology, and applications, Biomicrofluidics 4, 2010, 022811.

/22/ F.E.H. Tay, L. Yu, C. Iliescu, Particle manipulation by miniaturised dielectrophoretic devices, Defense Science Journal, 59/6, 2009, 595-604.

/23/ Y. Kang, D. Li, Electrokinetic motion of particles and cells in microchannels, Microfluid Nanofluid 6, 2009, 431–460.

/24/ R. Pethig, M.S. Talary, R.S. Lee, Enhancing traveling-wave dielectrophoresis with signal superposition, IEEE Eng. Med. Biol. Mag. 22/6, 2003, 43-50.

/25/ L. Cui, D. Holmes, H. Morgan, The dielectrophoretic levitation and separation of latex beads in microchips, Electrophoresis 22, 2001, 3893–3901.

/26/ E. Choi, B. Kim, J. Park, High-throughput microparticle separation using gradient traveling wave dielectrophoresis, J. Micromech. Microeng., 19, 2009, 125014.

/27/ U. Lei, C.W. Huang, J. Chen, C.Y. Yang, Y.J. Lo, A. Wo, C.F. Chen, T.W. Fung, A travelling wave dielectrophoretic pump for blood delivery, Lab Chip 9, 2009, 1349-1356.

/28/ E.B. Cummings, A. K. Singh, Dielectrophoresis in microchips containing arrays of insulating posts: theoretical and experimental results, Anal. Chem. 75, 2003, 4724–4731.

/29/ C. Iliescu, G. Xu, F.C. Loe, P.L. Ong, F.E.H. Tay, A 3D dielectrophoretic filter chip, Electrophoresis 28/7, 2007, 1107-1114.

/30/ G.O.F. Parikesit A.P. Markesteijn, O.M. Piciu, A. Bossche, J. Westerweel, I.T. Young, Y. Garini, Size-dependent trajectories of DNA macromolecules due to insulative dielectrophoresis in submicrometer-deep fluidic channels, Biomicrofluidics, 2, 2008, 024103.

/31/ N. Lewpiriyawong, C. Yang , Y.C. Lam, Dielectrophoretic manipulation of particles in a modified microfluidic H filter with multi-insulating blocks, Biomicrofluidics 2, 2008, 034105.

/32/ C-P. Jen, C.-T. Huang and H-Y. Shih, Hydrodynamic separation of cells utilizing insulator-based dielectrophoresis Microsystem Technologies, 16/7, 2010, 1097-1104.

/33/ P.Y. Chiou, A.T. Ohta, M.C. Wu, Massively parallel manipulation of single cells and microparticles using optical images, Nature, 436/21, 2005, 370-372.

/34/ S. Lee , H.J. Park , J.S. Yoon , K.H. Kang, Optoelectrofluidic field separation based on light-intensity gradients, Biomicrofluidics, 4, 2010, 034102.

/35/ H. Hwang, D.H. Lee, W. Choi, J.K. Park, Enhanced discrimination of normal oocytes using optically induced pulling-up dielectrophoretic force, Biomicrofluidics, 3, 2009, 014103. /36/ C.H. Kua, Y.C. Lam, I. Rodriguez, C. Yang, K. Youcef-Toumi, Dynamic cell fractiona-tion and transportation using moving dielectrophoresis, Anal. Chem., 79, 2007, 6975-6987.

/37/ C.H. Kua, Y.C. Lam, I. Rodriguez, C. Yang, K. Youcef-Toumi Cell motion model for moving dielectrophoresis, Anal. Chem, 80, 2008, 5454–5461.

/38/ M.D. Vahey, J. Voldman, High-throughput cell and particle characterization using isodielectric separation, Anal Chem, 81, 2009, 2446–2455.

/39/ G.H. Markx, P.A. Dyda, R. Pethig, Dielectrophoretic separation of bacteria using a conductivity gradient, J. Biotech., 51/2, 1996, 175-180.

/40/ S. Masuda, M. Washizu, T. Nanba, Novel method of cell fusion in field constriction area in fluid integrated circuit, IEEE Trans. Ind. Applications, 25/4, 1989, 732-737.

/41/ J. Park, B. Kim, S.K. Choi, S. Hong, S.H. Lee, K-I. Lee, An efficient cell separation system using 3D-asymmetric microelectrodes, Lab Chip 5, 2005, 1264–1270.

/42/ J. Voldman, M. Toner, M.L. Gray, M.A. Schmidt, Design and analysis of extruded quadrupolar dielectrophoretic traps, J. Electrostatics, 57, 2003, 69-90.

/43/ B.Y. Park, M.J. Madou, 3-D electrode designs for flow-through dielectrophoretic systems, Electrophoresis, 26, 2005, 3745-3757.

/44/ Y-K. Cho, T-H. Kim, J-G. Lee, On-chip concentration of bacteria using a 3D dielectrophoretic chip and subsequent laser-based DNA extraction in the same chip, J. Micromech. Microeng, 20, 2010, 065010.

/45/ C. Iliescu, G. Xu, V. Samper, F.E.H. Tay, Fabrication of a dielectrophoretic chip with 3D silicon electrodes, J. Micromech. Microeng, 15/3, 2005, 494-500.

/46/ L. Wang, L.A. Flanagan, N.L. Jeon, E. Monuki, A.P. Lee, Dielectrophoresis switching with vertical sidewall electrodes for microfluidic flow cytometry, Lab Chip, 7, 2007, 1114–1120.

/47/ L. Wang, J. Lu, S.A. Marchenko, E.S. Monuki, L.A. Flanagan, A.P. Lee, Dual frequency dielectrophoresis with interdigitated sidewall electrodes for microfluidic flowthrough separation of beads and cells, Electrophoresis, 30/5, 2009, 782-791.

/48/ C. Iliescu, L.M. Yu, G.L. Xu, F.E.H. Tay, A dielectrophoretic chip with a 3-D electric field gradient, J. Microelectromech. Syst., 15/6, 2006, 1506-1513.

/49/ Z. Gagnon, J. Mazur, H-C. Chang, Glutaraldehyde enhanced dielectrophoretic yeast cell separation, Biomicrofluidics, 3, 2009, 044108.

/50/ J.E. Gordon, Z. Gagnon, H-C. Chang, Dielectrophoretic discrimination of bovine red blood cell starvation age by buffer selection and membrane cross-linking, Biomicrofluidics, 1, 2007, 044102.

/51/ I -F. Cheng, H-C. Chang, D. Hou, H-C. Chang, An integrated dielectrophoretic chip for continuous bioparticle filtering, focusing, sorting, trapping, and detecting, Biomicrofluidics, 1, 2007, 021503.

/52/ J-W. Choi, S. Rosset, M. Niklaus, J.R. Adleman, H. Shea, D. Psaltis, 3-dimensional electrode patterning within a microfluidic channel using metal ion implantation, Lab Chip, 10, 2010, 783–788.

/53/ Z. Zou, S. Lee, C.H. Ahn, Sensors Journal, IEEE, 8/5, 2008, 527 – 535.

/54/ L.A. Flanagan, J. Lu, L. Wang, S.A. Marchenko, N.L. Jeon, A.P. Lee, E.S. Monuki, Unique dielectric properties distinguish stem cells and their differentiated progeny, Stem Cells, 26, 2008, 656–665.

/55/ M. P. Hughes, Strategies for dielectrophoretic separation in laboratory-on-a-chip systems, Electrophoresis, 23, 2002, 2569-2582.

/56/ P.R.C. Gascoyne, J. Vykoukal, Particle separation by dielectrophoresis, Electrophoresis, 23, 2002, 1973-1983.

/57/ J. Yang, Y. Huang, X-B Wang, F.F. Becker, P.R.C. Gascoyne, Cell separation on microfabricated electrodes using dielectrophoretic/gravitational field-flow fractionation, Anal. Chem., 71, 1999, 911-918.

/58/ C. Iliescu, G. Tresset, G. Xu, Continuous field-flow separation of particle populations in a dielectrophoretic chip with three dimensional electrodes, Appl. Phys. Lett., 90/23, 2007, 234104.

/59/ F. Yang, X. Yang, H. Jiang, P. Bulkhaults, P. Wood, W. Hrushesky, G. Wang, Dielectrophoretic separation of colorectal cancer cells, Biomicrofluidics 4, 2010, 013204.

/60/ A. Valero, T. Braschler, N. Demierre, P. Renaud, A miniaturized continuous dielectrophoretic cell sorter and its applications, Biomicrofluidics, 4, 2010, 022807.

/61/ G.H. Markx, R. Pethig, J. Rousselet, The dielectrophoretic levitation of latex beads, with reference to field-flow fractionation, J. Phys. D: Appl. Phys., 30, 1997, 2470.

/62/ K. Zhu, A. S. Kaprelyants, E.G. Salina, G.H. Markx, Separation by dielectrophoresis of dormant and nondormant bacterial cells of Mycobacterium smegmatis, Biomicrofluidics, 4, 2010, 022809.

/63/ M.P. Hughes, R. Pethig, X.B. Wang, Dielectrophoretic forces on particles in travelling electric fields, J. Phys. D: Appl. Phys., 29, 1996, 474.

/64/ P. Gascoyne, C. Mahidol, M. Ruchirawat, J. Satayavivad, P. Watcharasit, F.F. Becker, Microsample preparation by dielectrophoresis: isolation of malaria, Lab Chip, 2, 2002, 70-75.

/65/ C. Church, J. Zhu, G.Huang, T-R Tzeng, X. Xuan, Integrated electrical concentration and lysis of cells in a microfluidic chip, Biomicrofluidics, 4, 2010, 044101.

/66/ H. Lu, M. A. Schmidt, K.F. Jensen, A microfluidic electroporation device for cell lysis, Lab Chip, 5, 2005, 23–29.

/67/ S.W. Lee, Y.C. Tai, A micro cell lysis device, Sens. Actuators A, 73, 1999, 74-79.

/68/ Q. Ramadan, V. Samper, D. Poenar, Z. Liang, C. Yu, T.M. Lim, Simultaneous cell lysis and bead trapping in a continuous flow microfluidic device, Sens. Actuators B, 113/2, 2006, 944-955.

/69/ C.-T. Ho, R-Z. Lin, W-Y Chang, H-Y Chang, C-H. Liu, Rapid heterogeneous liver-cell on-chip patterning via the enhanced field-induced dielectrophoresis trap, Lab Chip, 6, 2006, 724-734.

/70/ A. Rosenthal, J. Voldman, Dielectrophoretic traps for single-particle patterning, Bioph. J., 88/3, 2005, 2193-2205.

/71/ M. Suzuki, T. Yasukawa, H. Shiku, T. Matsue, Negative dielectrophoretic patterning with different cell types, Biosens. Bioelectr., 24, 2008,1043-1047.

/72/ N. Mittal, A. Rosenthal, J. Voldman, nDEP microwells for single-cell patterning in physiological media, Lab Chip, 7, 2007, 1146-1153.

/73/ R.S. Thomas, H. Morgan, N.G. Green, Negative DEP traps for single cell immobilisation, Lab Chip, 9, 2009, 1534-1540.

/74/ F.E.H. Tay, L. Yu, C. Iliescu, Electrical and thermal characterization of a dielectrophoretic chip with 3D electrodes for cells manipulation, Electroch. Acta, 52/8, 2007, 2862-2868.

/75/ L. Yu, C. Iliescu, G. Xu, F.E.H. Tay, Sequential field-flow cell separation method in a dielectrophoretic chip with 3D electrodes, J. Microelectromech. Syst., 16/5, 2007, 1120-1129.

/76/ G. Tresset, C. Iliescu, Electrical control of loaded biomimetic femtoliter vesicles in microfluidic system, Appl. Phys. Lett., 90/17, 2007, 173901.

/77/ C. Iliescu, L. Yu, F. Tay, B. Chen, Bidirectional field flow particle separation method in a dielectrophoretic chip with 3D electrodes, Sens. Actuators B, 129/1, 2008, 491-496.

/78/ C. Iliescu, G. Tresset, G. Xu, Dielectrophoretic field-flow method for separating particle populations in a chip with asymmetric electrodes, Biomicrofluidics, 3, 2009, 044104.

Guolin Xu[1],
Francis E.H. Tay[1,2],
Guillaume Tresset[3],
Florina S. Iliescu[4],
Andrei Avram[5],
Ciprian Iliescu[1]*

[1] Institute of Bioengineering and Nanotechnoloy, Singapore

[2] National University of Singapore, Dept. of Mechanical Engineering,

[3] Laboratoire de Physique des Solides, University Paris-Sud, CNRS, France

[4] Republic Polytechnic, School of Applied Science, Singapore

[5] National Institute for Research and Development in Microtechnologies, Bucharest, Romania,

** corresponding author:*
Institute of Bioengineering and Nanotechnoloy,
31 Biopolis Way, The Nanos, #04-01,
Singapore 138669,
e-mail: ciliescu@ibn.a-star.edu.sg

Prispelo (Arrived): 01.09.2010 *Sprejeto (Accepted): 15.09.2010*

OVERVIEW OF FIBER OPTIC SENSING TECHNOLOGIES FOR STRUCTURAL HEALTH MONITORING

Daniele Inaudi

SMARTEC / Roctest

Key words: optical sensors, health monitoring, point sensors, long-gauge sensors, distributed sensors

Abstract: From many points of view, fibre optic sensors are the ideal transducers for structural monitoring. Being durable, stable and insensitive to external perturbations, they are particularly interesting for the long-term health assessment of civil structures.

Many different fibre optic sensor technologies exist and offer a wide range of performances and suitability for different applications. The most widely used sensing techniques include point sensors (Fibre Bragg Gratings and Fabry-Perot interferometers), long-gauge sensors (SOFO) and distributed sensors (Raman and Brillouin scattering sensors). These sensing technologies are now widely used in routine application for health monitoring of structures such as bridges, buildings, monuments, tunnels, dams, dykes, pipelines, landslides and many others.

This contribution reviews these systems and technologies and briefly presents some significant application examples.

Pregled tehnologij optičnega zaznavanja za uporabo v zdravstvenem monitoringu

Kjučne besede: optični senzorji, spremljanje stanja, koničasti senzorji, porazdeljeni senzorji

Izvleček: Senzorji z optičnimi vlakni so idealni pretvorniki za spremljanje stanja gradbenih konstrukcij. Zaradi svoje trajnosti, stabilnosti in neobčutljivosti do zunanjih motenj, so primerni za dolgoročno zasledovanje stanja gradbenih struktur. Obstaja veliko razliÄnih tehnologij, ki ponujajo širok spekter senzorjev za različne aplikacije. Najbolj pogosto uporabljene so tehnike točkovnega zaznavanja in tehnike porazdeljenih senzorjev. Te tehnike zaznavanja so splošno uporabljene v rutinskih aplikacijah za spremljanje stanja mostov, zgradb, spomenikov, tunelov, jezov, nasipov, vodovodov, zemeljskih plazov. V članku so predstavljeni sistemi, tehnologije in pomembne aplikacije.

1 Fiber optic sensors

There exist a great variety of fiber optic sensors /1/ for structural monitoring in both the academic and the industrial areas. In this overview we will concentrate on SOFO and DiTeSt sensors. These systems for civil health monitoring that have reached an industrial level and have been used in a number of field applications.

Figure 1 illustrates the four main types of fiber optic sensors:

- Point sensors have a single measurement point at the end of the fiber optic connection cable, similarly to most electrical sensors.
- Multiplexed sensors allow the measurement at multiple points along a single fiber line
- Long-base sensors integrate the measurement over a long measurement base. They are also known as long-gage sensors.
- Distributed sensors are able to sense at any point along a single fiber line, typically every meter over many kilometers of length

The greatest advantages of the FOS are intrinsically linked to the optical fiber itself that is either used as a link between the sensor and the signal conditioner, or becomes the sensor itself in the case of long-gauge and distributed sensors. In almost all FOS applications, the optical fiber is

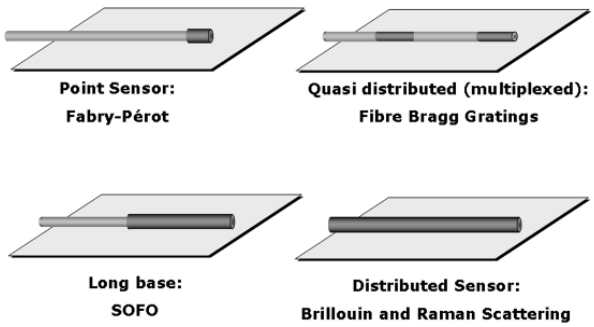

Fig. 1: Fiber Optic Sensor Types

a thin glass fiber that is protected mechanically by a polymer coating (or a metal coating in extreme cases) and further protected by a multi-layer cable structure designed to protect the fiber from the environment where it will be installed. Since glass is an inert material very resistant to almost all chemicals, even at extreme temperatures, it is an ideal material for use in harsh environments such as encountered in geotechnical applications. Chemical resistance is a great advantage for long term reliable health monitoring of civil engineering structures, making fiber optic sensors particularly durable. Since the light confined into the core of the optical fibers used for sensing purposes does not interact with any surrounding electromagnetic field, FOS are intrinsically immune to any electromagnetic (EM) interferences. With such unique advantage over sen-

sors using electrical cables, FOS are obviously the ideal sensing solution when the presence of EM, Radio Frequency or Microwaves cannot be avoided. For instance, FOS will not be affected by any electromagnetic field generated by lightning hitting a monitored bridge or dam, nor from the interference produced by a subway train running near a monitored zone. FOS are intrinsically safe and naturally explosion-proof, making them particularly suitable for monitoring applications of risky structures such as gas pipelines or chemical plants. But the greatest and most exclusive advantage of such sensors is their ability to offer long range distributed sensing capabilities.

1.2 SOFO Displacement Sensors

The SOFO system (Figure 2) is a fiber optic displacement sensor with a resolution in the micrometer range and an excellent long-term stability. It was developed at the Swiss Federal Institute of Technology in Lausanne (EPFL) and is now commercialized by SMARTEC in Switzerland /2/.

Fig. 2: SOFO system reading unit

The measurement setup uses low-coherence interferometry to measure the length difference between two optical fibers installed on the structure to be monitored (Figure 3). The measurement fiber is pre-tensioned and mechanically coupled to the structure at two anchorage points in order to follow its deformations, while the reference fiber is free and acts as temperature reference. Both fibers are installed inside the same pipe and the measurement basis can be chosen between 200mm and 10m. The resolution of the system is of 2 μm independently from the measurement basis and its precision of 0.2% of the measured deformation even over years of operation.

The SOFO system has been successfully used to monitor more than 150 structures, including bridges, tunnels, piles, anchored walls, dams, historical monuments, nuclear power plants as well as laboratory models.

1.3 Bragg Grating Strain Sensors

Bragg gratings are periodic alterations in the index of refraction of the fiber core that can be produced by adequately exposing the fiber to intense UV light. The produced gratings typically have length of the order of 10 mm. If white light is injected in the fiber containing the grating, the wavelength corresponding to the grating pitch will be reflected while all other wavelengths will pass through the grating undisturbed. Since the grating period is strain and temperature dependent, it becomes possible to measure these two parameters by analyzing the spectrum of the reflected light /3/. This is typically done using a tunable filter (such as a Fabry-Perot cavity) or a spectrometer. Resolutions of the order of 1 με and 0.1 °C can be achieved with the best demodulators. If strain and temperature variations are expected simultaneously, it is necessary to use a free reference grating that measures the temperature alone and use its reading to correct the strain values. Setups allowing the simultaneous measurement of strain and temperature have been proposed, but have yet to prove their reliability in field conditions. The main interest in using Bragg gratings resides in their multiplexing potential. Many gratings can be written in the same fiber at different locations and tuned to reflect at different wavelengths. This allows the measurement of strain at different places along a fiber using a single cable. Typically, 4 to 16 gratings can be measured on a single fiber line. It has to be noticed that since the gratings have to share the spectrum of the source used to illuminate them, there is a trade-off between the number of grating and the dynamic range of the measurements on each of them.

Fig. 3: SOFO Sensor installed on a rebar

Because of their length, fiber Bragg gratings can be used as replacement of conventional strain gages and installed by gluing them on metals and other smooth surfaces. With adequate packaging they can also be used to measure strains in concrete over basis length of typically 100 mm.

1.4 Fabry-Perot strain sensors

Extrinsic Fabry-Perot Interferometers (EFPIs) are constituted by a capillary silica tube containing two cleaved optical fibers facing each other's, but leaving an air gap of a few microns or tens of microns between them (see Figure 4) /4/. When light is launched into one of the fibers, a back-reflected interference signal is obtained. This is due to the reflection of the incoming light on the glass-to-air and on air-to-glass interfaces. This interference can be demodulated using coherent or low-coherence techniques to reconstruct the changes in the fiber spacing. Since the two fibers are attached to the capillary tube near its two extremities (with a typical spacing of 10 mm), the gap change will correspond to the average strain variation between the two attachment points.

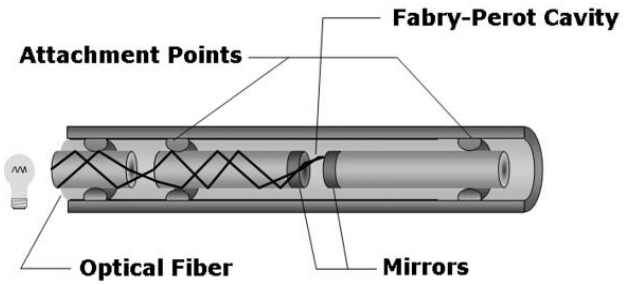

Fig. 4: Fabry-Perot Sensor

1.5 Raman Distributed Temperature Sensors

Raman scattering is the result of a non-linear interaction between the light traveling in a fiber and silica. When an intense light signal is shined into the fiber, two frequency-shifted components called respectively Raman Stokes and Raman anti-Stokes will appear in the back-scattered spectrum. The relative intensity of these two components depends on the local temperature of the fiber. If the light signal is pulsed and the back-scattered intensity is recorded as a function of the round-trip time, it becomes possible to obtain a temperature profile along the fiber /5/. Typically a temperature resolution of the order of 1°C and a spatial resolution of less than 1m over a measurement range up to 10 km are obtained for multi-mode fibers. A new system based on the use of singlemode fibers should extend the range to about 30km with a spatial resolution of 8 m and a temperature resolution of 2°C.

1.6 Brillouin Distributed Temperature sensors

Brillouin scattering sensors show an interesting potential for distributed strain and temperature monitoring. Systems able to measure strain or temperature variations of fibers with length up to 50 km with spatial resolution down in the meter range are now demonstrating their potential in field applications. For temperature measurements, the Brillouin sensor is a strong competitor to systems based on Raman scattering, while for strain measurements it has practically no rivals.

Brillouin scattering is the result of the interaction between optical and sound waves in optical fibers. Thermally excited acoustic waves (phonons) produce a periodic modulation of the refractive index. Brillouin scattering occurs when light propagating in the fiber is diffracted backward by this moving grating, giving rise to a frequency-shifted component by a phenomenon similar to the Doppler shift. This process is called spontaneous Brillouin scattering.

Acoustic waves can also be generated by injecting in the fiber two counter-propagating waves with a frequency difference equal to the Brillouin shift. Through electrostriction, these two waves will give rise to a traveling acoustic wave that reinforces the phonon population. This process is called stimulated Brillouin amplification. If the probe signal consists in a short light pulse and its reflected intensity is plotted against its time of flight and frequency shift, it will be possible to obtain a profile of the Brillouin shift along the fiber length.

The most interesting aspect of Brillouin scattering for sensing applications resides in the temperature and strain dependence of the Brillouin shift /6/. This is the result of the change the acoustic velocity according to variation in the silica density. The measurement of the Brillouin shift can be approached using spontaneous or stimulated scattering. The main challenge in using spontaneous Brillouin scattering for sensing applications resides in the extremely low level of the detected signal. This requires sophisticated signal processing and relatively long integration times.

Systems based on the stimulated Brillouin amplification have the advantage of working with a relatively stronger signal but face another challenge. To produce a meaningful signal the two counter-propagating waves must maintain an extremely stable frequency difference. This usually

Fig. 5: DiTeSt Reading Unit

requires the synchronization of two laser sources that must inject the two signals at the opposite ends of the fiber under test. The MET (Metrology laboratory) group at Swiss Federal Institute of Technology in Lausanne (EPFL) proposed a more elegant approach /6/. It consists in generating both waves from a single laser source using an integrated optics modulator. This arrangement offers the advantage of eliminating the need for two lasers and intrinsically insures that the frequency difference remains stable independently from the laser drift. SMARTEC and Omnisens (Switzerland) commercialize a system based on this setup and named DiTeSt (Figure 5). It features a measurement range of 10 km with a spatial resolution of 1 m or a range of 25 km with a resolution of 2 m. The strain resolution is 2 με and the temperature resolution 0.1 °C. The system is portable and can be used for field applications.

Since the Brillouin frequency shift depends on both the local strain and temperature of the fiber, the sensor setup will determine the actual sensitivity of the system. For measuring temperatures it is sufficient to use a standard telecommunication cable. These cables are designed to shield the optical fibers from an elongation of the cable. The fiber will therefore remain in its unstrained state and the frequency shifts can be unambiguously assigned to temperature variations. If the frequency shift of the fiber is known at a reference temperature it will be possible to calculate the absolute temperature at any point along the fiber. Measuring distributed strains requires a specially designed sensor. A mechanical coupling between the sensor and the host structure along the whole length of the fiber has to be guaranteed. To resolve the cross-sensitivity to temperature variations, it is also necessary to install a reference fiber along the strain sensor. Similarly to the temperature case, knowing the frequency shift of the unstrained fiber will allow an absolute strain measurement.

2. Selected projects

This section will introduce a few projects showing an effective use of fiber optic technology for the health monitoring of different types of structures, with different aims and during different phases of the structure's lifetime.

2.1 Colle Isarco Bridge

The development of a life extension and/or replacement strategy for highway structures is a crucial point in an effective bridge management system. An example of a global monitoring approach in establishing a bridge management system is represented by the project of the Colle d'Isarco viaduct on the Italian Brenner-Highway A22. The section of the highway that is subject to monitoring activities includes four columns, each of them supporting asymmetrical cantilevers in the north and south direction as can be seen in Figure 6 /7/.

Fig. 6: View of the Colle Isarco Bridge on the Brennero Highway in Italy

The overall length of this section is 378 m. The height of the girders near the supports number 8 and 9 is 11 m, at the supports 7 and 10 the height is 4.50 m. The girders have a uniform width of 6 m; the arrangement for each road bed is approximately 11 m wide. A wide set of sensors have been installed, including both traditional and SOFO fiber optic sensors and, due to the large dimensions of the section, a data acquisition system able to collect widely distributed sensing units was also installed (Figure 7). Wireless serial communication is used to transfer the measured data from the almost inaccessible locations on the bridge to the location of the personal computer used to evaluate the measured data.

Data evaluation is performed by a combination of analytical modeling and fine-tuning of the system parameters. The system aims to the creation of the appropriate match between the non-linear simulation and the measured data. Since the measurement processes usually introduce a certain amount of variability and uncertainty into the results due to the limited number of measurement points and the partial knowledge on the actions, this randomness can affect the conclusions drawn from measurements. Randomness in measured variables can however be accounted for by their probability density functions. Once a model and its calibration has gained a certain level of completeness, analytical prediction provides a quantitative knowledge and hence it becomes a useful tool to support structural evaluation, decision making, and maintenance strategies. This ambitious project aims to a full integration of instrumentation into the decision-support system for structural maintenance.

2.2 Pile loading test

A new semi-conductor production facility in the Tainan Scientific Park, Taiwan, is to be founded on a soil consisting mainly of clay and sand with poor mechanical properties. To assess the foundation performance, it was decided to perform an axial compression, pullout and flexure test in full-scale on-site condition. Four meters SOFO sensors were used. The pile was divided into eight zones (called

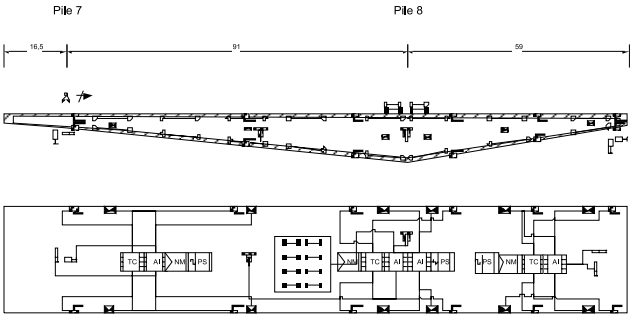

LEGEND

- SoFo Sensors
- Humidity/Temperature (Air)
- LVDTs at Bearings
- Thermocouples
- Inclinometers
- Strain Gauges on Reinforcement and Prestressing Cables
- Anemometer
- Wind Vane
- FP1001 Network Module
- Thermocouple Input Module (8)
- Analog Voltage Input Module (8)

Fig. 7: Layout of the Colle Isarco Bridge Instrumentation (courtesy of K. Bergmeister)

cells). In the case of axial compression and pullout tests, a simple topology was used: the eight sensors were installed in a single chain, placed along one the main rebar, one sensor in each cell, as shown in Figure 8. To detect and compensate for a possible load eccentricity, the top cell was equipped with one more sensor installed on the opposite rebar with respect to the pile axis (see Figure 5).

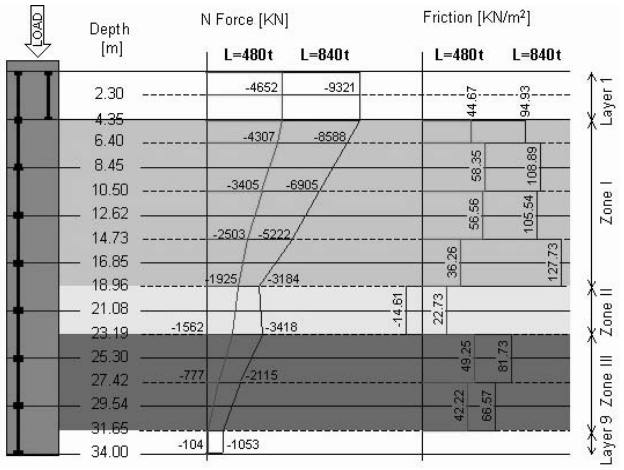

Fig. 8: Sensor topology and results obtained by monitoring during the axial compression test

As a result of monitoring rich information concerning the structural behavior of the piles is collected. Important parameters were determined such as distributions of strain, normal forces (see Figure 9), displacement in the pile, distribution of frictional forces between the pile and the soil, determination of Young modulus, ultimate load capacity and failure mode of the piles as well as qualitative determination of mechanical properties of the soil (three zones are distinguished in Figure 5).

In case of flexure test, a parallel topology was used: each cell contained two parallel sensors (as in cell 1 in Figure 8) installed on two opposite main rebars, constituting two chains of sensors. This topology allowed de-termination of average curvature in each cell, calculation of deformed shape and identification of failure point. Diagram of horizontal displacement for different steps of load as well as failure location on the pile are presented in Figure 6. In Figures 5 and 6 loads are presented in tons /8/.

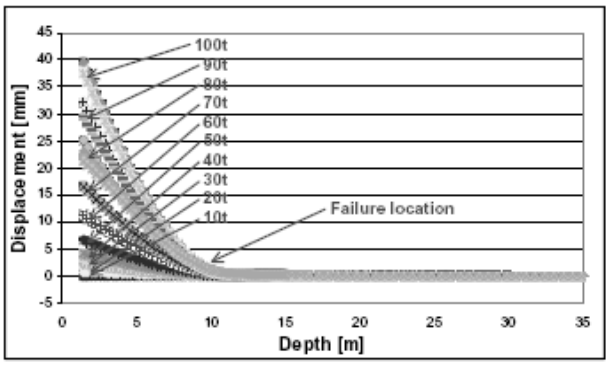

Fig. 9: Deformed shapes of the pile and identification of failure location

2.3 I35W Bridge, Minneapolis

This application example is a good example of a truly integrated structural health monitoring system, combining different sensing technologies to achieve the desired level of monitoring.

The collapse of the old I35W Bridge in Minneapolis in 2007 shook the confidence of the public in the safety of the infrastructure that we use every day. As a result, the construction of the replacement bridge (see Figure 10) must rebuild this confidence, by demonstrating that a high level of safety can not only be attained during construction, but also maintained throughout the projected 100-year lifespan of the bridge.

One of the central factors contributing to this is the design and installation of a comprehensive structural health monitoring system, which incorporates many different types of sensors measuring parameters related to the bridge performance and ageing behavior. This system continuously gathers data and allows, through appropriate analysis, to obtain actionable data on the bridge performance and health evolution /9/. The data provided is be used for op-

Fig. 10: New I35W Bridge in Minneapolis

erational functions, as well as for the management of ongoing bridge mainteonance, cmplementing and targeting the information gathered with routine inspections.

The monitoring system was designed and implemented through a close cooperation between the designer, the owner, the instrumentation supplier and University of Minesota.

The main objectives of the system are to support the construction process, record the structural behavior of the bridge, and contribute to the intelligent transportation system as well as to the bridge security.

The design of the system was an integral part of the overall bridge design process allowing the SHM system to both receive and provide useful information about the bridge performance, behavior and expected lifetime evolution.

Monitoring instruments on the new St Anthony Falls Bridge measure dynamic and static parameter points to enable close behavioral monitoring during the bridge's life span. Hence, this bridge can be considered to be one of the first 'smart' bridges of this scale to be built in the United States.

The system includes a range of sensors which are capable of measuring various parameters to enable the behavior of the bridge to be monitored. Strain gauges measure local static strain, local curvature and concrete creep and shrinkage; thermistors measure temperature, temperature gradient and thermal strain, while linear potentiometers measure joint movements. At the mid-spans, accelerometers are incorporated to measure traffic-induced vibrations and modal frequencies (Eigen frequencies). SensCore corrosion sensors are installed to measure the concrete resistivity and corrosion current.

Meanwhile there are long-gauge SOFO fiber optic sensors which measure a wide range of parameters, such as average strains, strain distribution along the main span, average curvature, deformed shape, dynamic strains, dynamic deformed shape, vertical mode shapes and dynam-

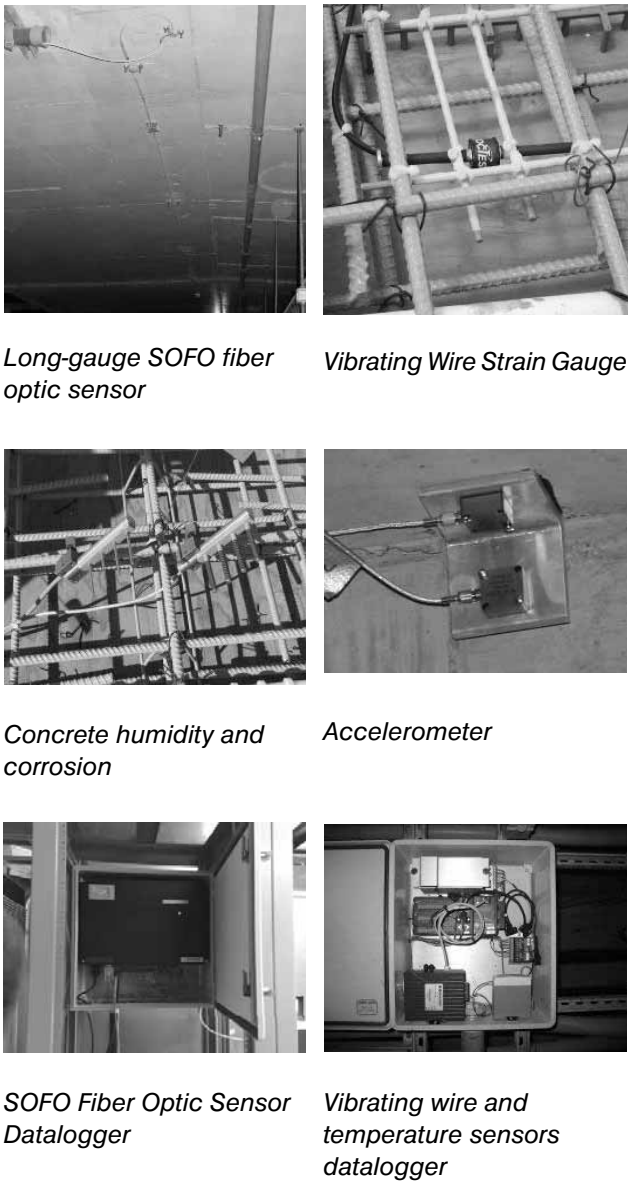

Long-gauge SOFO fiber optic sensor

Vibrating Wire Strain Gauge

Concrete humidity and corrosion

Accelerometer

SOFO Fiber Optic Sensor Datalogger

Vibrating wire and temperature sensors datalogger

Fig. 11: Sensing components

ic damping – they also detect crack formation. Some of the installed sensors are shown in Figure 11.

The sensors are located throughout the two bridges, the northbound and southbound lanes, and are in all spans. However, a denser instrumentation is installed in the southbound main span over the Mississippi river, as depicted in Figure 12. This span will therefore serve as sample to observe behaviors that are considered as similar in the other girders and spans.

This project is one of the first to combine very diverse technologies, including vibrating wire sensors, fiber optic sensors, corrosion sensors and concrete humidity sensors into a seamless system using a single database and user interface.

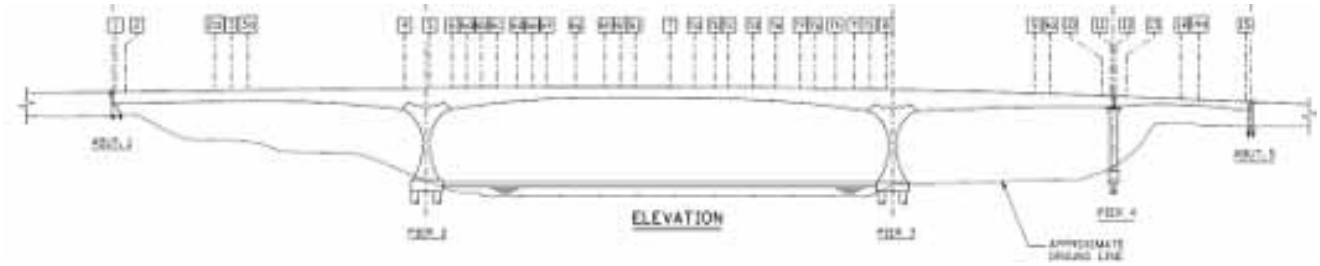

Fig. 12: Sensor locations

2.4 Luzzone Dam

Distributed temperature measurements are highly interesting for the monitoring of large structures. In the presented application, SMARTEC and the MET-EPFL group used the DiTeSt system to monitor the temperature development of the concrete used to build a dam /10/.

The Luzzone dam was recently raised by 17 meters to increase the capacity of the reservoir (Figure 13). The raising was realized by successively concreting 3m thick blocks. The tests concentrated on the largest block to be poured, the one resting against the rock foundation on one end of the dam. An armored telecom cable installed in serpentine during concrete pouring constituted the Brillouin sensor.

Fig. 13: Luzzone Dam raising works

The temperature measurements started immediately after pouring and extended over 6 months. The measurement system proved reliable even in the demanding environment present at the dam (dust, snow, and temperature excursions). The temperature distributions after 15 and 55 days from concrete pouring are shown in Figure 14. Comparative measurements obtained locally with conventional thermocouples showed agreement within the error of both systems.

This example shows how it is possible to obtain a large number of measurement points with relatively simple sensors. The distributed nature of Brillouin sensing make it particularly adapted to the monitoring of large structures were the use of more conventional sensors would require extensive cabling.

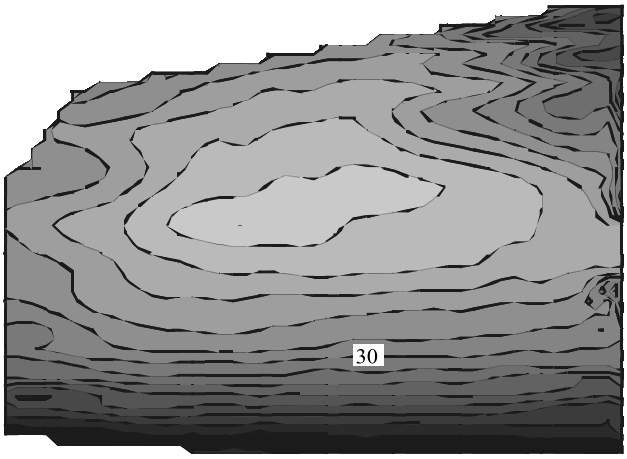

Fig. 14: Temperature measurements in the Luzzone Dam 15 days after concrete pouring

2.5 Bridge crack detection

Götaälvbron, the bridge over Göta River (Figure 15), was built in thirties and is now more than seventy years old. The steel girders were cracked and two issues are in cause of steel cracking: fatigue and mediocre quality of the steel. The bridge authorities repaired the bridge and decided to keep it in service for the next fifteen years, but in order to increase the safety and reduce uncertainties related to the bridge performance and integrity monitoring system has been mandatory.

Fig. 15: View to nearly one kilometer long Götaälvbron Bridge.

The main issue related to selection of the monitoring system has been the total length of the girders which is for all the nine girders more than 9 km. It was therefore decided to monitor the most loaded five girders (total length of 5 km approximately) and logically a fiber optic distributed sensing system have been selected. For the first time a truly distributed fiber optic sensing system, based on Brillouin scattering effect is employed on such large scale to monitor new crack occurrence and unusual strain development /11/.

In order for system to be able to detect the cracks in every point, it was decided to glue the SMARTape to the steel girder. The crack should not damage the sensor, but create its delaminating from the bridge (otherwise the sensor would be damaged and should be repaired). The gluing procedure was therefore established and rigorously tested in laboratory and on-site. Photograph of on-site gluing operation is presented in Figure 16. The full performance was also tested in laboratory and on-site, and photograph of tested SMARTapes installed on the bridge is presented in the same figure.

Fig. 16: On-site test of SMARTape gluing procedure (left) and installed SMARTapes.

The installation of SMARTape sensors was challenge itself. Good treatment of surfaces was necessary and number of transversal girders had to be crossed. Limited access and working space in form of lift basket, often combined with cold and windy environment and sometimes with the night work, made the installation particularly difficult. The measurements of SMARTape are compensated for temperature using the temperature sensing cable that has also the function of bringing back the optical signal to the DiTeSt reading unit.

2.6 Bitumen Joint Monitoring

Plavinu hes is a dam belongs to the complex of three most important hydropower stations on the Daugava River in Latvia (see figure 17). In terms of capacity this is the largest hydropower plant in Latvia and is considered to be the third level of the Daugavas hydroelectric cascade. It was constructed 107 km distant from the firth of Daugava and is unique in terms of its construction - for the first time in the history of hydro-construction practice; a hydropower plant was built on clay-sand and sand-clay foundations with a maximum pressure limit of 40 m. The HPP building is merged with a water spillway. The entire building complex is extremely compact. There are ten hydro-aggregates installed at the hydropower plant and its current capacity is 870,000 kW.

One of the dam inspection galleries coincides with a system of three bitumen joints that connects two separate blocks of the dam. Due to abrasion of water, the joints lose bitumen and the redistribution of loads in concrete arms appears. Since the structure is nearly 40 years old, the structural condition of the concrete can be compromised due to ageing. Thus, the redistribution of loads can provoke damage of concrete arm and as a consequence the inundation of the gallery. In order to increase the safety and enhance the management activities it was decided to monitor the average strain in the concrete arm next to the joints /12/. The DiTeSt system with SMARTape deformation (see Figure 18) sensor and Temperature Sensing Cable is used for this. The sensors were installed by company VND2 with SMARTEC support and configured remotely from the SMARTEC office. Threshold detection software with SPST (open-ground) module was installed in order to send pre-warnings and warnings from the DiTeSt instrument to the Control Office.

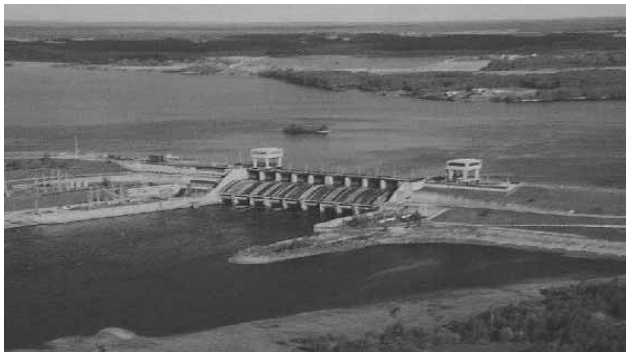

Fig. 17: Plavinu dam in Latvia

2.7 Gas Pipeline Monitoring

About 500 meters of a buried, 35 years old gas pipeline, located near Rimini, Italy, lie in an unstable area. Distributed strain monitoring could be useful in order to improve vibrating wire strain gauges monitoring system, actually used in the site. The landslide progress with time and could damage pipelines up to be put out of service. Three symmetrically disposed vibrating wires were installed in several sections at a distance typically of 50/100 m chosen as the most stressed ones according a preliminary engineering evaluation. These sensors were very helpful, but could not fully cover the length of the pipeline and only provide local measurements.

Different types of distributed sensors were used: SMARTape and Temperature Sensing Cable /13/. Three parallel lines constituted of five segments of SMARTape sensor were installed over whole concerned length of the pipeline (see figure 19). The lengths of segments were ranged from 71 m to 132 m, and the position of the sensors with respect to the pipeline axis were at 0°, 120° and –120° approximately. The strain resolution of the SMARTape is 20 micro-strains, with spatial resolution of 1.5 m (and an acquisition range of 0.25m) and provides the monitoring

Fig. 18: SMARTape installation in the inspection gallery

Fig. 19: SMARTape on the gas pipeline.

of average strains, average curvatures and deformed shape of the pipeline. The Temperature Sensing Cable was installed onto the upper line (0°) of the pipeline in order to compensate the strain measurements for temperature. The temperature resolution of the sensor is 1°C with the same resolution and acquisition of the SMARTape. All the sensors are connected to a Central Measurement Point by means of extension optical cables and connection boxes. They are read from this point using a single DiTeSt® reading unit. Since the landslide process is slow, the measurements sessions are performed manually once a month. In case of earthquake a session of measurements is performed immediately after the event. All the measurements obtained with the DiTeSt® system are correlated with the measurements obtained with vibrating wires. The sensors have been measured for a period of two years, providing interesting information on the deformation induced by burying and by the landslide progression. A gas leakage simulation was also performed with success using the temperature sensing cable.

3 Conclusions

Structural health monitoring is not a new technology or trend. Since ancient times, engineers, architects and artisans have been keen on observing the behavior of built structures to discover any sign of degradation and to extend their knowledge and improve the design of future structures. Ancient builders would observe and record crack patterns in stone and masonry bridges. Longer spans and more slender arches were constructed and sometimes failed during construction or after a short time /14/. Those failures and their analysis have led to new insight and improved design of future structures. This continued struggle for improving our structures is driven by engineering curiosity, but also by economic considerations.

As for any engineering problem, obtaining reliable data is always the first and fundamental step towards finding a solution. Monitoring structures is our way to get quantitative data about our bridges and help us in taking informed decisions about their health and destiny. This paper has presented the ad-vantages and challenges related to the implementation of an integrated structural health monitoring system, guiding the reader in the process of analyzing the risks, uncertainties and opportunities associated with the construction and operation of a specific bridge and the design of a matching monitoring system and data analysis strategy. Acknowledgments

Acknowledgments (if any) should appear as a separate non-numbered section before the list of references.

References

/1/ B. Glisic and D. Inaudi, "Fibre Optic Methods for Structural Health Monitoring", John Wiley & Sons, Ltd, 2007.

/2/ D. Inaudi, A. Elemari, S. Vurpillot, "Low-coherence interferometry for the monitoring of civil engineering structures", SPIE, Second European Conference on Smart Structures and Materials, Glasgow, UK, Vol. 2361, p 216-219, 1994.

/3/ D. Inaudi, "Application of civil structural monitoring in Europe using fiber optic sensors", Progress in Structural Engineering and Materials, Vol. 2, No 3, p 351-358, 2000.

/4/ É. Pinet, C. Hamel, B. Glišic, D. Inaudi, N. Miron, "Health monitoring with optical fiber sensors: from human body to civil structures", 14th SPIE Annual Symposium on Smart Structures and Materials & Nondestructive Evaluation and Health Monitoring, San Diego (CA), USA, 6532-19, 2007.

/5/ J. P. Dakin et al., "Distributed optical fiber Ra-man temperature sensor using a semiconductor light source and detector", Proc, IEE Colloq. on Distributed Optical Fiber sensors, 1986.

/6/ M. Niklčs et al., "Simple Distributed temperature sensor based on Brillouin gain spectrum analysis", Tenth International Conference on Optical Fiber Sensors OFS 10, Glasgow, UK, SPIE Vol. 2360, pp. 138-141, 1994.

/7/ A. Del Grosso, K. Bergmeister, D. Inaudi, U. Santa, "Monitoring of Bridges and Concrete Structures with Fibre Optic Sensors in Europe", IABSE Conference, Seoul, Korea, August 2001.

/8/ B. Glisic, D. Inaudi, C. Nan, "Piles monitoring during the axial compression, pullout and flexure test using fiber optic sensors", 81st Annual Meeting of the Transportation Research Board (TRB), on CD , 02-2701, 2002.

/9/ D. Inaudi, M. Bolster, R. Deblois, C. French, A. Phipps, J. Sebasky, K. Western, "Structural Health Monitoring System for the new I-35W St Anthony Falls Bridge", 4th International Conference on Structural Health Monitoring on Intelligent Infrastructure (SHMII-4) 2009, 22-24 July 2009, Zurich, Switzerland, 2009.

/10/ D. Inaudi, B. Glisic, "Distributed Fiber optic Strain and Temperature Sensing for Structural Health Monitoring", IABMAS'06 The Third Int'l Conference on Bridge Maintenance, Safety and Management, 16 - 19 July 2006, Porto, Portugal, 2006.

/11/ B. Glisic, D. Posenato, D. Inaudi, "Integrity monitoring of old steel bridge using fiber optic distributed sensors based on Brillouin scattering", 14th SPIE Annual Symposium on Smart Structures and Materials & Nondestructive Evaluation and Health Monitoring, San Diego (CA), USA, 6531-25, 2007.

/12/ D. Inaudi, B. Glisic, "Distributed Fiber Optic Sensors: Novel Tools for the Monitoring of Large Structures", Geotechnical News, Volume 25, Number 3, Pages 8-12, 2007.

/13/ D. Inaudi, B. Glisic, "Long-Range Pipeline Monitoring By Distributed Fiber Optic Sensing", 6th International Pipeline Conference September 25 - 29, 2006, Calgary, Alberta, Canada, 2006.

/14/ M. Levi, and M. Salvadori, "Why Buildings Fall Down", W.W. Norton & Company, New York, USA, 1992.

Daniele Inaudi
SMARTEC / Roctest

Prispelo (Arrived): 01.09.2010 *Sprejeto (Accepted): 15.09.2010*

TEMPERATURE FIBER-OPTIC POINT SENSORS: COMMERCIAL TECHNOLOGIES AND INDUSTRIAL APPLICATIONS

Éric Pinet, Sébastien Ellyson and Frédéric Borne

FISO Technologies

Key words: temperature fiber-optic point sensors, commercial technologies, industrial applications

Abstract: Temperature fiber-optic point-sensors have been commercialized for about two decades. Among the various available optical sensing technologies, only few ones have lead to commercial successes. For instance, temperature could be measured by fluorescence decay time of a phosphorus compound excited with UV light; the higher the temperature, the faster the decay. Semiconductor band-gap thermal properties could also be used for temperature sensing. As an example for GaAs, the wavelengths transmission cut-off is increasing al linearly with temperature (~0.3 nm/°C). By analyzing with a spectrometer the reflected spectrum of a white-light source, temperature could be deduced. Interferometry-based technology such as Fabry-Pérot is also a field-proven method for accurate measurement of temperature in various applications. In this case, the optical path of a Fabry-Pérot cavity is changing with temperature (~20 nm/°C). Finally with fiber Bragg grating technology, a Bragg grating is written inside the fiber and reflects a given wavelength which is slightly shifting with temperature (~10 pm/°C).

Several industrial applications involving temperature measurement contributed to the development of commercial optical fiber sensing technologies. Those include for instance the real-time temperature monitoring of hot spots in high-power transformers, of semiconductor plasma etchers or of microwave chemical reactors. Applications in the food industry or in the medical field are now also appearing.

Temperaturni koničasti optični senzorji: komercialne tehnologije in industrijska uporaba

Kjučne besede: temperaturni optični točkovni senzorji, komercialne tehnologije, industrijske aplikacije

Izvleček: Temperaturni točkovni senzorji na osnovi optičnih vlaken se tržijo že približno dve desetletji. Med različnimi dostopnimi optičnimi tehnologijami zaznave, jih je le nekaj doseglo komercialen uspeh. Na primer, temperaturo lahko merimo z meritvijo časovnega poteka fluorescence fosforne spojine, ki je vzbujena z UV svetlobo; višja kot je temperatura, hitrejši je upad fluorescence. Termične lastnosti prepovedanega pasu v polprevodniku prav tako lahko uporabljamo za zaznavanje temperature. Kot primer vzemimo GaAs, kjer mejna valovna dolžina linearno narašča s temperaturo (~0.3 nm/°C). Temperatura lahko ocenimo že s spektralno analizo sevanja izvora bele svetlobe. Tehnologija, ki temelji na interferometriji, kot npr. Fabry-Perot, je prav tako priznana kot metoda za natančno merjenje temperature v različnih aplikacijah. V tem primeru se optična pot Fabry-Perot votline spreminja s temperaturo (~20 nm/°C). Z Braggovo uklonsko mrežico, ki je vpisana v optično vlakno dosežemo, da se valovna dolžina odbite svetlobe spreminja s temperaturo (~10 pm/°C). Veliko industrijskih aplikacij za merjenje temperature je pripomoglo h komercialnemu razvoju tehnologij zaznavanja z optičnimi vlakni. To so npr. spremljanje temperature vročih točk v realnem času v transformatorjih velikih moči, v plazemskih jedkalnikih ali v mikrovalovnih kemijskih reaktorjih. Pojavljajo se tudi aplikacije v prehrambeni industriji in na področju medicine.

1 Introduction

Since now about two decades, optical fiber sensors /1-4/ (OFS) left academic research laboratories to enter the real industrial world. Several companies started to commercialize such sensors with however a slower than expected market penetration. Being more expensive than conventional technologies, OFS were confined to usually low-volume niche applications where they remained the only possible choice.

Among the various available technologies, pointsensing as opposed to quasi- or fully-distributed OFS was probably the most successful in terms of sold units. For such sensors, the sensing element is typically positioned at or near the end of an optical fiber used as a link between the sensing element and the light source/interrogator. Point-sensors are particularly well-adapted for applications where only a limited number of measuring points are needed, typically 1 to 10. Over 10-20 measuring points, multiplexing interrogation OFS technologies are often financially or technically more interesting since a same optical fiber (or channel) could be used to interrogate a lot of different sensing locations. Such multiplexing OFS interrogators are however usually much more expensive than single-point modules, they are thus often only considered in expensive projects such as for instance in civil engineering structures instrumentation where their cost investment represents only a small fraction of the overall project.

Since there are however a lot of industrial applications requiring only limited number of measuring locations, single-point OFS technologies were able to find interesting niche markets that could be developed thanks to the unique advantages provided by the use of optical fiber connecting the measuring location to the interrogating unit. Among the most important ones, total immunity to any electromagnetic interferences (EMI) such as radio frequency (RF) or mi-

crowaves (MW) is probably the first to come to mind as it clearly differentiates OFS to their electrical less expensive and well-established counterparts. The fact that OFS provides a truly intrinsically safe sensing measurement is certainly another key advantage in applications with explosions risks such as in the oil and gas or chemical industries. The chemical and thermal resistance of OFS is also noticeable for applications with environments too harsh for electronic sensors. Finally the miniature size (< 1 mm) of packaged industrial OFS temperature sensors is probably also one important technological advantage since miniature shielded electrical sensors are usually more expensive.

The purpose of this paper is to present some pointsensing OFS technologies currently well-accepted in the industry for measuring temperature. Selected industrial applications where such sensors provide a competitive advantage are also described.

2 Commercial technologies

Several optical point-sensing technologies are now commercially available, especially for temperature sensing which is probably the most widely spread OFS in the industry: applications range from industrial process control, energy, civil engineering to medical /5-7/. Although many concepts could be used to design an optical temperature sensor /8/, there are presently only four main OFS technologies that dominate temperature point-sensing:

- Fluorescence decay
- Semi-conductor band-gap variation
- Fabry-Pérot interferometry
- Fiber Bragg grating

2.1 Fluorescence decay temperature sensor

In fluorescence decay technology, a fluorescent compound (typically phosphorus-based although other options are possible /9/) is assembled and protected usually at the tip of an optical fiber (or could be part of the fiber itself /10/). The compound is excited with high energy short light pulses typically selected in the ultra-violet (UV) region (usually 400-420 nm). As shown at the top of Figure 1 describing fluorescence decay technology, such quantum energy moves electrons of the ground state to excited states where they move more or less rapidly depending on temperature to lower energy excitation states from which they can return to the ground state by emitting lower energy light quanta (usually in the 500-600 nm region). Such emitted light is partially captured by the multimode optical fiber, returned to the interrogator and detected with a cheap silicon broadband light detector such as photodiode or phototransistor. In order to be able collect as much reflected light as possible, very large core optical fibers are typically used. For applications where temperatures do not exceed 70°C, for instance in the medical field, Φ 0.25-1 mm plastic optical fibers (POF) could advantageously be used. For higher temperatures, silica-based multimode optical fibers /11/ or even sapphiretipped probe /12/ are preferred.

When measured over time, the light intensity could be separated in two distinct phases as shown at the bottom of Figure 1: after an intense reflected excitation pulse (at t_0), decreasing emitted light could be recorded between t_1 and t_2 to be able to calculate the fluorescent decay time (τ) without being fooled by reflected excitation pulse. Such first-order exponential decay time, typically in the 1-4 ms range, is directly linked to the temperature seen by the fluorescent compound: the higher the temperature, the faster the decay. Since such technology is based on time-dependent light intensity measurements, optical losses induced in the fiber, such as the ones due to bending which is more important for large core fibers, should be evaluated in order to have a more robust measurement. The intensity of the reflected excitation pulse could be used for that purpose, assuming that such reference intensity remains more or less constant between two pulses, which is often the case since acquisition rate is typically 1-4 Hz per channel. Due to the way the optical signal is obtained and processed, it is hard for this technology to achieve faster acquisition rates, which is a limitation for applications where a fast temperature feedback is required.

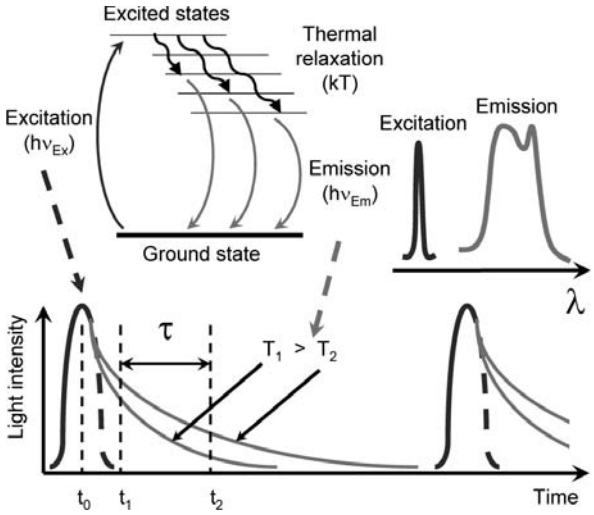

Fig. 1: Schematic description of the fluorescence decay technology. Electronic transitions (top left), typical excitation and emission spectra (top right), reflected light intensity with time (bottom).

The precision that could be obtained by fluorescence decay technology is highly dependent on the selected fluorescent compound (its electronic properties, thermal resistance and stability…) but it is also related to the sensor design /13/ and to the way the data is processed /14/. A typical ±2°C accuracy is usually available for temperatures ranging from about -30°C to +200°C which is suitable for several industrial applications. If the temperatures range is reduced and stays within about 20°C of a reference cali-

bration point, the accuracy could however be reduced to more or less one order of magnitude.

Such fluorescence decay technology, which has been on the market for now more than 15 years, has the main advantage of offering a low-cost interrogator. In its simplest version, optical interface could be limited to a UV light emitting photodiode (LED) and a silicon photo-detector placed at 90° in front of a 50/50 separating plate facing the optical connector of the fluorescent temperature OFS.

2.2 Semiconductor band-gap temperature sensor

In the semiconductor band-gap technology, a semiconductor small chip terminated by a mirror layer is glued at the tip of a multimode optical fiber. Several semiconductors could theoretically be used but practically, GaAs is the only one which has been successfully commercialized for more than 15 years.

A continuous broadband light source (such as halogen light bulb) is used to illuminate the semiconductor chip through the multimode fiber. Photons with sufficient energy could be absorbed by elastic collision with electrons of the valence band that are thus allowed to jump to the conduction band. Both bands are separated by an energy gap (*Eg* expressed in eV) which of course depends on the semiconductor structure, but also on hydrostatic pressure and on temperature as show by equations (1) and (2) respectively /15/:

$$E_g(P) = E_g(0) + b \cdot P - c \cdot P^2 \quad (1)$$

where *P* is pressure in GPa, and for GaAs at 300 K, *Eg*(0) = 1.43±0.01 eV, *b* = (10.8 ± 0.3)·10^{-2} eV/GPa and *c* = (14 ± 2)·10^{-4} eV/GPa^2.

$$E_g(T) = E_g(0) - \frac{\alpha \cdot T^2}{\beta + T} \quad (2)$$

where *T* is temperature in K (0 K < T < 10^3 K), and for GaAs at normal pressure, *Eg*(0) = 1.519 eV, α = 0.541·10^{-3} eV/K and β = 204 K.

In fact hydrostatic pressure does not affect much the energy gap as opposed to temperature, as a simple calculation could demonstrate. For instance assuming a pressure variation ΔP of 1 atm from normal pressure (which is an important pressure variation for most industrial applications), the energy gap will increase by only ΔEg = 1.1·10^{-5} eV. Now if we consider a temperature variation ΔT of only 20 K increasing from 300 K, the energy gap will show a much more important decrease (about 3 orders of magnitude higher, ΔEg = -9.1·10^{-3} eV).

When the semiconductor is illuminated with continuous broadband light, photons could interact with valence electrons depending on their energy given by equation:

$$E_\gamma(\lambda) = \frac{h \cdot c}{e \cdot \lambda} \approx \frac{1239.84}{\lambda} \quad (3)$$

where E_γ is photon energy in eV, λ is the photon wavelength in nm, *h* is the Planck constant, *c* is the light velocity in vacuum and *e* is the absolute value of the electron elementary charge.

High energy photons (lower wavelengths) will be absorbed approximately when $E_\gamma > E_g$. Photons with lower energy (higher wavelengths) will simply pass through the semiconductor and be returned to the optical fiber after a reflection on the mirror capping the chip. As a result, the light returned to the interrogator will have in wavelengths the form of a high-pass filter as shown in Figure 2. Since the energy band-gap (*Eg*) is mostly dependent on temperature as shown by equation (2), the position of the wavelengths cut-off is also temperature dependent. The light returned to the interrogator (which acts then as a low-resolution spectrometer) is wavelength spread geometrically over a charge coupled detector (CCD) and the wavelengths cut-off position is then evaluated by signal processing in order to determine the corresponding temperature seen by the sensor.

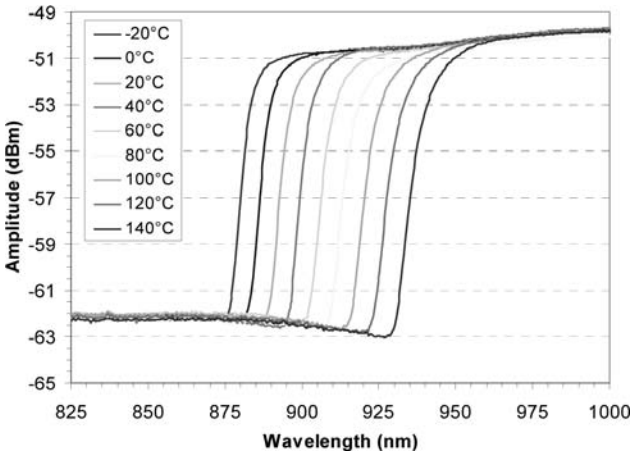

Fig. 2: Reflected spectrum of GaAs sensor measured with an OSA for temperatures from -20°C to +140°C in 20°C steps.

Figure 2 shows the experimental spectral distribution obtained with an optical spectrum analyzer (OSA) of the light reflected on a GaAs chip mounted at the tip an optical fiber for temperatures ranging from -20°C to +140°C with 20°C temperature steps. It could be seen on that figure that the reflected cut-off curves are almost equally spaced meaning that their position varies nearly linearly with temperature. Actually equation (2) could be better approximated by a polynomial fit rather than by a linear fit which would give a variation of about 0.3 nm/°C over the useful range of the sensor (typically from -50°C to +250°C).

If we calculate the energy gap at -20°C using equation (2) we obtain *Eg*(253.16 K) = 1.443 eV. From equation (3) it could be deduced that the corresponding wavelength cut-off should be about 859 nm. Experimentally it is actually about 875 nm (first left curve on Figure 2) showing that considerations additional to band-gap energy transfer are

involved. Among the ones that should be cited, the temperature dependence of semiconductor refractive index (*n*) should be taken into account. For GaAs, it is following equation /15/:

$$n(T) = 3.255 \cdot (1 + 4.5 \cdot 10^{-5} \cdot T) \quad (4)$$

where *T* is the temperature in K.

However even with temperature dependence correction of the GaAs refractive index, the experimental cut-off wavelength could not precisely be calculated. With the previous example at -20°C, the correction would increase the cut-off wavelength to 869 nm. Other phenomena such as other electronic transitions or local effects of ionic distribution could explain the remaining difference but it is beyond the scope of this paper.

One big advantage of the band-gap technology is the fact that the evaluation of temperature is actually wavelength dependent instead of intensity dependent. Intensity light fluctuations due to lamp aging or to fiber bending are therefore not affecting the accuracy of the measurement. Another interesting advantage is the temperature dependent wavelengths cut-off which is only related to the semiconductor properties and the sensor chip design. Once the interrogator has been calibrated to link CCD pixels position of wavelengths cut-off to actual temperature, the band-gap temperature sensors do not theoretically need any specific calibration factor. This reduces the manufacturing cost of such sensors since sensor temperature calibration is often time consuming. Typically the precision obtained for such sensor stays around ±1-2°C for most sensors available on the market. Better accuracy of less than one order of magnitude is however always possible when specific calibration is an option.

As far as accuracy is concerned, this technology is more or less similar to fluorescence decay previously described, and due to packaging design considerations, both technologies are often competing on similar applications. However when faster acquisition rate are required, the GaAs is superior since the signal could be continuously processed whereas for fluorescence decay it is trigged by excitation pulses frequency which could not be reduced since limited by emission relaxation processes. Typically for GaAs, acquisition rate from 4-75 Hz are presently commercially available. *FISO Technologies* will also release soon a 125 Hz GaAs interrogator in order to offer a more interesting product suitable for medical applications where faster acquisition rates are necessary.

2.3 Fabry-Pérot temperature sensor

The Fabry-Pérot (F-P) interferometry could be used to point-measure many different physical parameters including temperature but also pressure, strain, displacement or refractive index /16/. The principle behind this patented technology using white-light interferometry /17, 18/ is sketched in Figure 3. In few words, a continuous broadband light source is injected into an optical fiber and lead to its tip where the F-P sensor is assembled. Such sensing element is made of two parallel semi-reflecting mirrors separated by a gap. The light passing through the first mirror is reflected back and forth a very large number of times between the two parallel planes forming the F-P interferometer as shown in Figure 3 (right). The light emerging from the interferometer travels back to the interrogator through the optical fiber where, thanks to a 2x2 coupler, it is redirected to an optical analyzer and projected over a linear

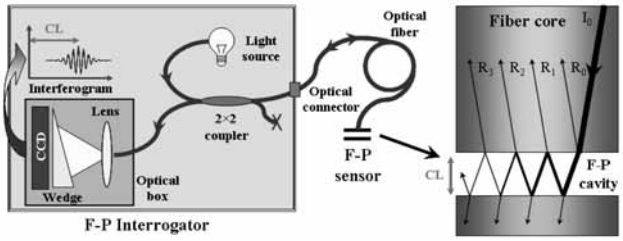

Fig. 3: Schematic description of the F-P absolute measurement signal conditioner from FISO Technologies *using patented white-light interferometry (left) and detail of F-P sensing interferometer showing ray traces obtained from a selected incident angle light beam propagating in the optical fiber core (right).*

CCD detector behind a Fizeau wedge. This last interferometric device reconstructs spatially the interference pattern. Due to the fact that white-light is used, all wavelengths are present and thus destructive interferences occur except for the zero order where all wavelengths are actually constructive. Thanks to the wedge that creates a linear variation of thicknesses, the cross-correlated interference pattern has a maximum intensity at the exact position where the optical path difference (OPD) equals the one created at the F-P sensor, and few lower intensity peaks symmetrically disposed around the central peak (as given by the interferometer cross-correlation function). Thus finding the sensor OPD related to the physical parameter to be measured simply consists of finding the position of the maximum peak in the CCD interference pattern (see interferogram of Figure 3).

This robust technology, commercialized by *FISO Technologies* since 1994, allows accurate and precise F-P cavity length measurement with sub-nanometer range precision over several decades of micrometer span, thus giving a very interesting dynamical range.

The greatest advantage of this interferometric equipment, beside the fact that it is suitable for sensing various physical parameters, is that the measurement is truly absolute which means that the sensor could be disconnected and reconnected and still give the same reading without any adjustment or referencing. Due to light source and detector limitations, such technology allows also sampling rates in the ~10 Hz to kHz ranges which are compatible with most demanding practical applications (the recently released FPI-HS from *FISO Technologies* allows a 15 kHz

sampling rate). Another patented /19/ relative measurement F-P interrogating technology offering an acquisition rate of 0.2 MHz (2 MHz if data post processing is possible) is also available commercially /18/. Such very high acquisition rate is rarely needed for temperature applications but is very useful for monitoring pressure in very fast occurring events such as explosions or blasts /20/.

Two types of F-P temperature point-sensors are available commercially: capillary type and refractive index type. Both types are actually affecting the OPD differently: in the first, the cavity length (CL) of the F-P sensor is temperature dependent, whereas for the second, this is mainly the refractive index of the F-P sensor that contributes mostly to the OPD change with temperature.

The design of the capillary type temperature sensor consists basically on two flat-ended glass fibers that are assembled in a quartz capillary tube to form a F-P cavity. The material of one fiber is selected to have a high coefficient of thermal expansion (CTE). As the temperature increases, this fiber expands and as a result, reduces the F-P cavity length separating the two fiber end-faces (with a thermal expansion of typically ~20 nm/°C). Thanks to factory calibration, this length variation is translated into temperature value.

In order also to avoid that external strain could be transmitted to the sensing capillary tube, this one is encapsulated into a bigger tube. Several packaging and thermal ranges are available for such sensors and could be selected depending on the specific needs of the application. Response time of the sensor will of course depend on the selected packaging but less than 0.5 s is a typical value for a packaged sensor and about 1 ms for a bare sensor. A typical accuracy for this sensor is ±0.3°C for a medical temperature range (20°C to 85°C) and ±1°C for an industrial temperature range (-40°C to 300°C).

Another type of F-P temperature sensor is also available. This time, instead of material thermal dilatation, temperature dependent refractive index is rather used to change the OPD of the F-P sensor. A tiny chip of a semiconductor material with high thermal refractive index dependence and two semireflective surfaces constituting a F-P cavity is assembled at the tip of the lead optical fiber. This solid compact design is actually the smallest optical fiber temperature sensor available on the market (150 µm square). Its sensitivity is about one order of magnitude lower than the capillary type temperature sensor but due to its extremely low thermal mass, its response time is better than 5 µs for a bare sensor which makes this sensor extremely interesting for fast temperature changes monitoring or for precise spatial point temperature mapping applications.

2.4 Fiber Bragg grating temperature sensor

The fiber Bragg grating (FBG) temperature sensor technology /21/ is quite different from the 3 previously cited ones. First instead of using multimode fiber (MMF), a low-cost single-mode fiber (SMF) is preferred (although MMF version of FBG is possible /22/). For SMF, the core is much smaller (8-10 µm) than for MMF (50-230 µm or up to ~1 mm for POF) to allow only one mode of light propagation. Such propagation mode is very interesting as SMF exhibits a narrower modal dispersion and has a higher bandwidth than MMF and also can retain the fidelity of each light pulse over a longer distance. Those are the reasons why SMF is now a standard in the telecommunication industry. Even though such fiber is usually cheaper in bulk, equipments for SMF are generally more expensive than for MMF. For instance, optical connectors need to have better mechanical tolerances to align correctly the smaller cores. Such connectors are also more sensitive to dust particles encountered in industrial environments and that could unfortunately cover the whole fiber core.

Another important difference with the 3 previously cited OFS technologies resides in the fact that the sensor is actually written inside the fiber itself and it is not mounted at the tip of the fiber. It consists of a periodic modification of the SMF core refractive index with sections having a slightly higher index than the rest of the core. Several methods could be used to write the FBG, but the most common one involves core refractive index modification of a special germanium-doped silica fiber through intense UV laser illumination patterned by interferences or by masking technologies. Many types of grating structure are available (uniform, chirped, tilted…) but the most common are FBG with uniform index period (Λ).

The fundamental principle behind FBG technology is Fresnel reflection as illustrated by Figure 4. The FBG is illuminated with a broadband infra-red (IR) light source (typically around 1510-1590 nm) and when light traveling in the core reaches the different refractive indices it may both reflect and refract at the interface. Part of the light is reflected

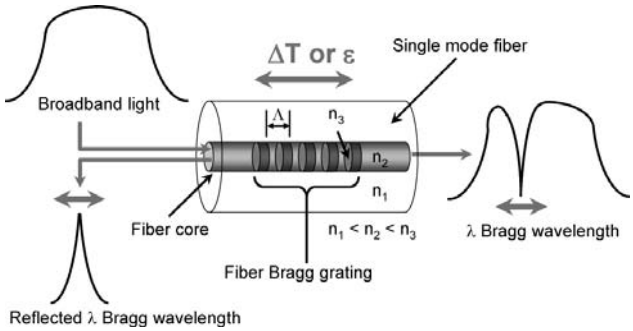

Fig. 4: General principle of the FBG technology. The FBG is written into the core of a SMF. It consists of periodic slight variations of the core refractive index which affects the spectral response of the light passing through it. The FBG period Λ is affected by stretching due to temperature variation or strain impacting the reflected λ_B (red horizontal arrows).

depending on its wavelength, called the Bragg wavelength (λ_B), which is defined by the equation:

$$\lambda_B = 2 \cdot n_e \cdot \Lambda \quad (5)$$

where n_e is the effective refractive index of the grating in the fiber core and Λ is the grating period. In SMF, n_e depends on the wavelength since only one propagation mode exists in such waveguide.

FBG could be used in many ways in optical telecommunication systems (such as notch filter, multiplexers and demultiplexers…) but also it is widely used for sensing applications involving temperature but also strain/deformation, pressure depending on how the sensor is encapsulated. If the grating period Λ is modified due to fiber thermal elongation or strain applied to the fiber, the Bragg wavelength λ_B will also be modified according to equation (6). Actually the relative shift of the Bragg wavelength ($\Delta\lambda_B$ / λ_B) due to an applied strain (ε) and a change in temperature (ΔT) is given by equation /23/:

$$\frac{\Delta\lambda_B}{\lambda_B} = C_S \cdot \varepsilon + C_T \cdot \Delta T \quad (6)$$

where λ_B is the Bragg wavelength, C_S is the coefficient of strain, C_T is the coefficient of temperature.

An accurate determination with an optical spectrum analyzer (OSA) of the reflected narrow band around λ_B allows the evaluation of the actual combination of temperature and strain. In order to limit the strain contribution, special packaging care should be taken to ensure that the FBG is free from any constraints on it whole length (typically 5-10 mm). This is usually achieved by placing the FBG fiber inside a capillary with an internal diameter sufficiently large to avoid any contact between its surface and the sensing part of the fiber. This yields an encapsulated sensor with an outside diameter typically greater than 1 mm.

The Bragg wavelength would shift usually ~10 pm/°C which is sufficient to achieve an accuracy usually around ±0.5-1°C for a temperature range covering -40°C to ~120°C. Precision will naturally depend on the FBG interrogator performances as well as on the scan frequency (which could vary from 1 Hz to 1 kHz).

Since several FBG with slightly different grating period Λ could be written on the same SMF, multiple measuring points could be multiplexed and interrogated by the same channel, provided that λ_B dynamic overlaps are avoided by design. This is a great advantage offered by this quasi-distributed sensing technology. However since FBG interrogators and often packaged sensors are much more expensive than other cited technologies their use are practically limited to applications where cost is not a critical issue.

3 Industrial applications

Fiber-optic temperature point-sensors have found several markets where they progressively became industry standards. Such niche markets were actually not correctly addressed by conventional electrical sensing technologies whereas OFS advantages made optical sensors the most reliable, simpler and sometimes even the cheaper solution. Some important examples are presented in this section.

3.1 Hot spot monitoring in transformers

One of the applications which made temperature OFS first commercial success is the hot spot monitoring in high-power transformers. Power transformers are always present as soon as electricity tension conversion is needed. Everybody is familiar with small power transformers used to charge their computer or cell phone, but much bigger ones have actually a very different design. They are present in areas where high-tension alternative current (110-1 200 kV) arriving from remote electricity power plants are converted into lower and less dangerous tension, typically 110 V or 220 V depending on the country.

The tension conversion is usually realized by induction between windings. The windings are made with copper wires separated with insulating layers. For the low-tension transformers of our day-to-day life the copper wires have simply a varnish as insulating layer, but for the high-tension transformers, higher dielectric properties are needed and dry cellulose paperboard is usually preferred. In order to maintain for decades the dielectric properties of the insulating paperboard, the assembled windings are dried and immersed in highdielectric mineral oil and the whole assembly is sealed in a hermetic container. Even if the windings are low resistive, they always produce heat which increases with current power. For our low-tension transformers we could feel that heat which is easily dissipated. For high-tension transformers which cost several million USD, this is another story since heat generated is much more important and the consequence of overheating could be as catastrophic as an impressive explosion since they have a good source of electrical energy and a huge reservoir of easy-to-burn oil and paperboard.

Actually the life of a transformer (expected to be over 20-30 years) depends on the life of the insulation system. This life is defined by the chemical degradation processes which depend primarily on temperature and time. Other factors such as the presence of oxygen or moisture could be considered as accelerating the aging process. It is therefore very important to have a way to monitor not only the overall average temperature of the system but also it is essential to evaluate the temperature in strategic locations known as "hot spots". In those spots where temperature is more elevated than in the rest of the winding often due to design considerations, the degradation processes are locally accelerated, leading to aging of the cellulose though polymer chain breakdown generating byproducts such as glucose monomers further transformed to furanic compounds /24/. Those degradation products are partially soluble in the oil reducing its dielectric properties not only locally but

also in the whole transformer through oil convection processes.

Due to the presence of very high levels of EMI, *in situ* hot spot temperature measurement is impossible for conventional electrical sensors which are therefore confined in areas where they could be shielded such as at the top of the high-power transformer. Such measurements are not very precise and give only an idea of the thermal operating status of the transformer but no accurate evaluation of its windings hot spots. Those conventional methods have errors from inferring hot spots by trying to simulate or calculate the temperature versus directly measuring it. Inaccurate estimations could have drastic impact on the real life expectancy of the transformer as it decreases exponentially with the temperature of the hottest spot in the winding as shown in Figure 5: a slight 5-10°C increase of the hot spot reduces dramatically the life of the transformer, thus the returns on investments made for this very expensive utility.

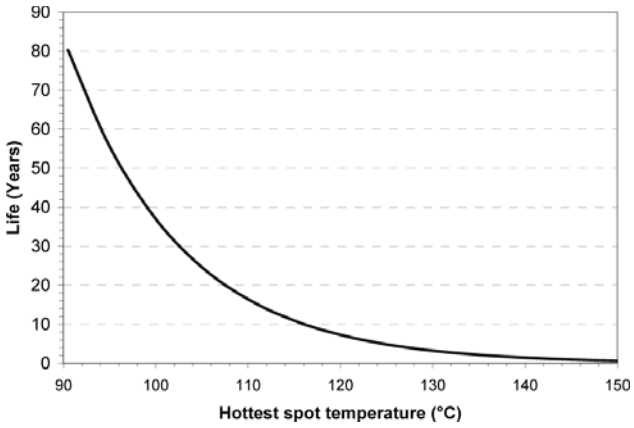

Fig. 5: Minimum life expectancy for liquidimmersed transformer rated in accordance with IEEE Std C57.12.00-1993 (65°C average rise, 80°C hottestspot rise). Graph adapted from IEEE C57.91-1995.

All penalties of conventional methods are overcome by *in situ* temperature measurements using fiber-optic point-sensors which could be installed directly into strategic points of the windings where hot spots are most suspected. Since such sensors are insensitive to the strong EMI and vibrating environments, they could perform where electrical counterparts are failing. The two OFS technologies which are now well accepted by the transformer industry are the fluorescence decay and the GaAs temperature sensors. Both types of sensors have been used with success in operating high-power transformers for now over 15 years. Their technical performances with a ±2°C accuracy with low-speed acquisition rate are satisfactory for this type of application.

Even though OFS are insensitive to strong EMI they could fail in this harsh environment if no attention is paid to the packaging of the sensor itself. For instance, the presence of air bubbles trapped into the sensor cable or tip assembly will be the source of partial discharges generated by the kV potential environment. Such discharges could lead with time to the sensor failure or worst, to a transformer failure since they may accelerate degradation of the dielectric medium. Thus specific care are taken to avoid such problems and all the cables used to protect the optical fibers are slotted or perforated (as shown on Figure 6) in order to allow ingression of insulating transformer oil into all possible voids of the sensor assembly.

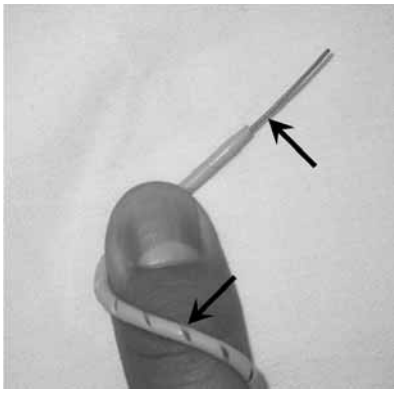

Fig. 6: GaAs TPT-32 or TPT-62 temperature sensor from FISO Technologies*. Slots (arrows) in the Teflon® cables are used to allow transformer immersing oil to fill all the voids of the sensor assembly.*

A typical installation scheme of a power transformer is presented in Figure 7 with GaAs bandgap temperature sensing technology from *FISO Technologies*. The sensors are placed in different locations directly into the windings of the transformer during their manufacturing. Optical connectors are then plugged into a hermetic optical pass-through when the windings are inserted into the transformer casing. After a drying process involving heat and harsh solvents to remove as much as possible moisture and oxygen, the transformer casing is sealed permanently. The temperature sensors are then connected to the signal conditioner using patch cords in order to record actual temperature data.

Their use was originally very important for design and manufacturing steps of the transformers as they could give pertinent information that helped to reduce the temperature of hot spots and to improve utility general quality. They are also now often used as quality acceptance when the transformer is delivered to the final customer. As the transformer is in operation, the temperature OFS could be used as safety monitoring devices, as the OFS interrogator is often connected to relays and warning procedures could be activated when safety temperature limits are reached. With a better understanding of the actual temperature status of the transformer, the operator could even decide to use shortly the utility in overload mode in order to respond to a power peak demand, still preventing overheating and winding failure.

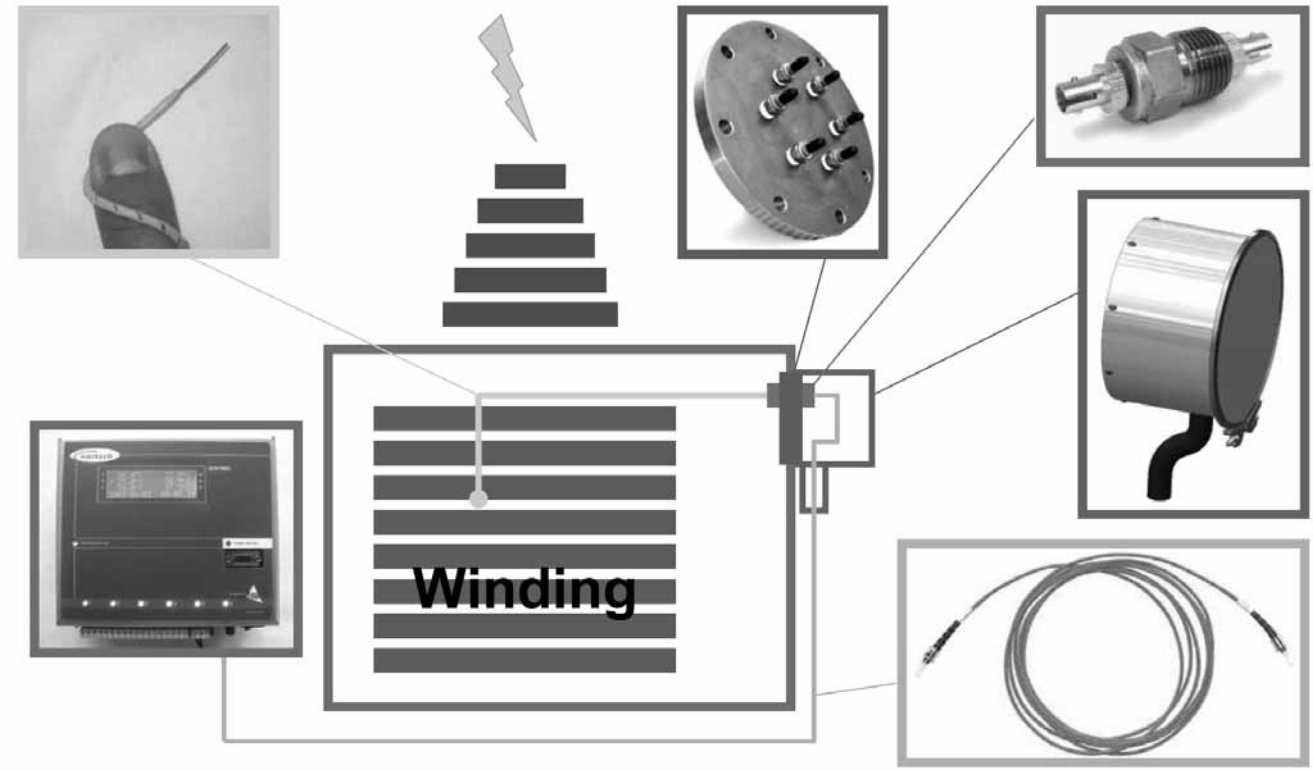

Fig. 7: Typical installation scheme of OFS for hot spots monitoring in high-power transformers. Illustrated is the GaAs technology from FISO Technologies*: Sensor (top left),* Easyplate® *(top center)* Easythrough® *(top right),* Easycover® *(middle right), patch-cord (bottom right) and 6 channels* Sentinel® *interrogator (bottom left).*

In the early times when OFS was introduced to this industrial application, their use was limited only to very high power (>100 MVA) and very expensive transformers. But with the OFS prices decrease of the last few years, this technology is now much more accessible to the whole industry and it started to be used for smaller transformers (20-100 MVA). More transformers are now instrumented with an increased number of sensors since redundancy enhances also their safety level. In the up-coming 2010 edition of the international standard IEC 60076-2 on power transformers, it will be recommended to instrument ≥ 50 MVA single-phase and ≥ 20 MVA 3-phase oilfilled transformers with at least 4 and 6-8 temperature OFS respectively, depending on their cooling system.

3.2 Semiconductor plasma etcher

In the semiconductor industry, plasma etcher is a key tool to pattern multi-layers trace paths for integrated circuits on silicon wafers using photolithography technologies. A plasma-assisted dry etch is often performed on masked wafers so that fine structured etching could be achieved at temperatures lower than possible without the help of the plasma. In normal procedure, the air is vacuumed and replaced by a process gas and a high-speed stream of glow discharge (plasma) is initiated using a highfrequency electric field (typically 13.56 MHz). The plasma could be used to grow silicon dioxide films on silicon wafers (oxygen plasma) or to remove silicon dioxide by using a fluorine or chlorine bearing gas. The process allows a reproducible, uniform etching of all materials used in silicon and III-V semiconductor technology. The performance of this tool is however highly dependent on pressure and temperature control. Temperature steps are included in the etching process and in order to increase throughput and uniformity there was a need for a temperature sensor that could perform in a plasma environment. Such harsh environment application with a limited number of measurement points on wafer holder was ideal for market penetration of temperature OFS.

3.3 Microwave chemistry and food applications

Microwave (MW) environment is also an area where temperature OFS have a clear advantage over electrical sensors as they are not affected by the EMI. In this area two major applications have been opportunities for the development of temperature OFS niche markets: microwave chemistry and food applications.

Microwave chemistry is the science of applying MW to chemical reactions /25-27/. As all electromagnetic radiations, MW radiation consists of two components: magnetic and electric field components. The MW electric field oscillates very quickly (at 2.45 GHz the field oscillates 4.9 $x10^9$ times per second) and this strong agitation is responsible for dielectric heating mechanism, either through molecular motion of ionic species (conduction mechanism) or rotation of dipolar species (dipolar polarization mecha-

nism). This cyclic reorientation of molecules can result in an intense internal heating with heating rates of > 10°C/s when MW radiation of 1 kW capacity source is used.

Such advantage combined with the fact that heating of chemicals is performed through their volume instead of through their surface provides interesting benefits over conventional ovens. Since all chemical reactions are dependent on temperature activation, reaction rates are accelerated and reaction conditions are usually milder. As a result, chemical yields are often higher as fewer by-products have time to be generated. Also, since heat is generated only inside the MW radiation-absorbing elements of the chemical reactor, lower energy is used. Finally different reaction selectivities could be achieved as MW radiation energy transfer depends on polarization properties and physical state of the chemicals involved in the reaction. Selective heating can also be achieved which is of particular interest for heterogeneous systems (comprising different substances or different phases) where MW energy is converted to heat by different amounts in different parts of the system. For binary systems such as polar and non-polar solvents, different temperatures could be achieved. For instance phase transfer reaction could be done with a temperature different for each phase, such as ~100°C for water while maintaining only ~50°C for chloroform.

Microwave chemistry began to gain popularity in the labs more than 20 years ago but really expanded in the industry with the introduction of temperature OFS in commercial MW reactor ovens. *In situ* temperature measurement during the MW heating allows a better control of MW activated chemical reactions since a feedback loop involving real-time temperature could be implemented in the process. F-P temperature sensors are commercially successful for such applications, since sensor precision and response time are important specifications to consider together with the reasonable cost of the system. In order to be fully MW compatible, the optical sensor assembly has to be metal free, and if the sensor has to be connected inside the MW oven, this should include the optical connector where usually metal parts are present, for instance in the spring holding the ferula. An example of a F-P temperature sensor designed by *FISO Technologies* for MW chemistry is presented in Figure 8. The whole sensor is protected by encapsulation inside chemically inert Teflon® tubing.

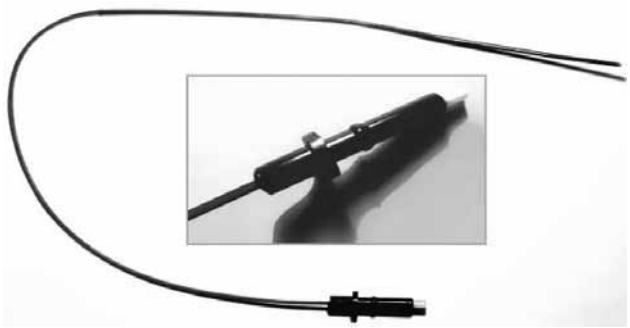

Fig. 8: Example of a F-P temperature sensor designed by FISO Technologies *for MW chemistry. Insert is a detail of the metal-free connector.*

Another application involving temperature measurement in MW environment concerns food industry. Small MW ovens have now invaded our modern kitchens and are part of our busy day-to-day life where less time is available for cooking. As a result, this task is partially transferred to the food industry which now prepares various ready-to-serve meals which jump directly from the freezer to the MW oven to end few minutes later on the kitchen table.

Since MW heating depends on the chemical nature of the food and since the MW power is rarely uniform in the MW oven, it is very important to have a tool for real-time evaluation of the food temperature uniformity in order to know precisely how the heat is transferred from water-rich sections to others where MW energy is less absorbed. If the food disposition is not optimized, it is not rare to have hot-burning sections while others are still frozen, even if the food is rotated during the MW heating.

FISO Technologies is the only company which commercializes since several years OFS instrumented kitchen MW ovens which help food industry engineers to improve performances either of the MW heating program or of the food packaging itself, for instance by introducing honey-comb MW reflectors in strategic places of the packaging. In the microwave station (MWS) shown in Figure 9, four to eight F-P temperature sensors (FOT-L) could be connected to the interrogator mounted on the top of the oven. The MWS interrogator is rotating with the MW plate in order to avoid sensors cables entanglement.

Fig. 9: Commercial kitchen MW oven instrumented by FISO Technologies *for multiple point-sensing with F-P temperature sensors.*

3.4 Medical applications

More recently, optical temperature point-sensors have found many applications in the medical field. Again such

sensors offer a solution in applications where electrical sensors do not perform correctly, mostly due to the presence of strong EMI. For instance the very strong permanent magnetic field (typically 1.5-3 T) that is present in magnetic resonance imaging (MRI) is a true obstacle for metallic sensors which can not be used in such environment. Although MRI equipments are very expensive (~1-1.5 million USD for 1.5 T scanner) they are progressively invading the modern hospitals since they provide a unique non-invasive medical imaging tool used in radiology to visualize precisely in 2D or 3D detailed internal tissues as well as limited functions of the body.

Unlike the competitive and complementary traditional computational tomography (CT) imaging which uses ionizing radiations (X-rays) to acquire its images, MRI uses non-ionizing RF signals (strong magnetic fields) that are believed to be harmless to the patients (provided that they do not have MRI non compatible implants). As a result, the patients can undergo exams several times successively in the short term which is advantageous for close follow-up of some diagnosis or therapies. Also because MRI uses spin modifications induced in hydrogen nuclei, it is best suited for imaging soft tissues with many hydrogen nuclei and little density contrast, making it especially useful in neurological (brain), musculoskeletal, cardiovascular, and oncological (cancer) imaging.

Due to the construction of some MRI scanners which have small diameter bore (especially the old models since modern scanners have larger bores, up to 70 cm) and since imaging procedure could last up to 40 min during which patient should lie without moving in a very stressful noisy clicking and beeping environment (up to 120 dB equivalent to a jet engine at take-off /28/), for those reasons, some MRI patients suffer from claustrophobia and discomfort and in many cases they have to be sedated. This is particularly the case if MRI is used during surgery (such as for instance for brain surgery) or when small children have to undergo this imaging procedure.

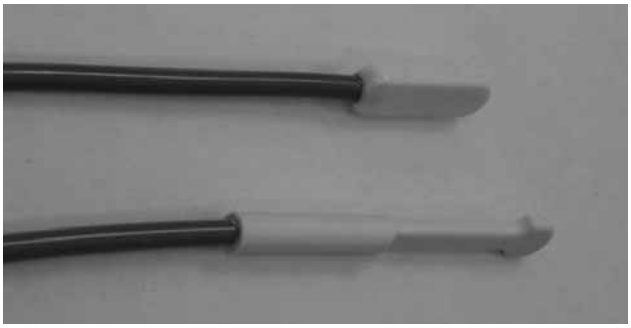

Fig. 10: Example of medical OFS assembly developed by FISO Technologies *for skin surface temperature sensing of patient during MRI procedure. The diameter of the blue cables is 3 mm.*

It is important during patient sedation to monitor their vital signs such as temperature, in order to be able to react and interrupt the procedure if some abnormal situation is encountered. Some examples of skin surface temperature F-P sensors used during MRI procedure are presented in Figure 10.

Other applications of optical point-sensors in MRI field concern for instance MRI safety evaluation of implants, medical devices or materials. Under very strong magnetic fields, even non-ferromagnetic materials could experience some effects depending on the design. In some cases local elevation of temperature could be recorded and provide useful information to engineers. Minimally invasive temperature OFS insensitive to magnetic fields are successfully used to find hot spots generated in MRI environment. They could also be used for improving the design of custom coils that are used for imaging specific parts of the human body.

Optical temperature point-sensors could be used as well in medical therapies such as hyperthermia therapy which is used to help treating some cancers. Hyperthermia therapy is a medical treatment consisting of exposing body tissues to high temperature to damage and kill cancer cells or to make them more sensitive to the effects of radiations and certain anti-cancer drugs. The problem of this therapy is to localize and control temperature elevation and heat transfer to limit deleterious effects to tumor cells without damaging too much healthy cells and without elevating too much the whole body temperature (normally around 37.6°C, 42°C being maximum temperature compatible with life). Fortunately tumor cells are disorganized and have a compact vascular structure which makes them have more difficulties dissipating heat. In moderate hyperthermia, a local temperature of 40-43°C is usually generated to kill the cells. Very high temperatures (above 50°C) are used for ablation of some tumors which are so to speak literally burned (thermal ablation).

Miniaturization of heat treatment is actually quite important: the smaller the area that is heated and the shorter the treatment time with associated the lower the side effects. Depending on the location of the tumor, heat could be applied to the surface of the body, inside normal body cavities or through tissues using needles or probes. Several sources are used to generate heat tissues locally and among them MW and RF sources offer interesting advantages. However they make real-time temperature feedback control difficult due to the presence of EMI… unless OFS are utilized. The use of temperature OFS is furthermore recommended when the hyperthermia therapy is done under MRI which could be used as a way for correctly positioning the heating elements on the right spot of tumor cells.

Since heat is transferred and dissipated in neighbor tissues, having information on thermal distribution within the surrounding tissues is also very useful. This is the reason why equally spaced temperature optical point-sensors integrated into a small instrumented catheter as shown in Figure 11 provide an interesting tool helping the therapy.

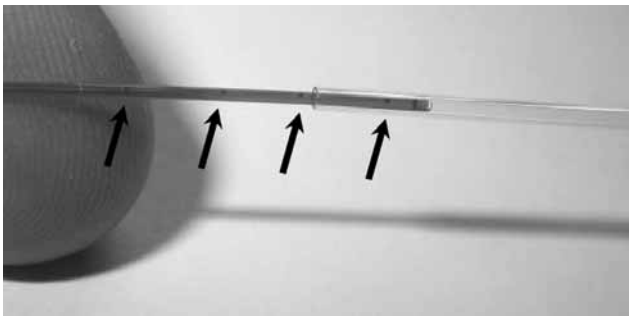

Fig. 11: Example of an 840 µm OD instrumented catheter designed by FISO Technologies *for multiple point temperature sensing compatible with RF/MW hyperthermia therapy or thermal ablation. Arrows show the positions of four GaAs sensors.*

4 Conclusion

Emergence of commercial fiber-optic temperature sensors in the industrial world was originally possible due to the unique sensing advantages provided by such technologies. They could perform better in many environments where other sensors fail: mainly environments with any type of strong EMI, with fire or explosion risks or simply with harsh temperature or chemical conditions. Among all the possible technologies developed by academic research, only very few ended to actual commercial success. Unfortunately OFS are still more expensive than conventional technologies and can therefore compete only in few niche-markets where they have technological advantages. As a result, the four robust temperature point-sensing OFS technologies which are presently successfully commercialized are fluorescence decay, GaAs band-gap variation, F-P interferometry and FBG. Each of them has its own advantages and limitations which make them suitable for various industrial applications as presented in this paper.

Over years passed sensing temperature in the "real world", OFS proved that they have unique and reliable performances which make them players impossible to circumvent when safety or robustness are concerned. With the progresses made by the OFS companies for pushing those technologies to their limits while decreasing as much as possible the selling price, one can guess that new niche-markets will emerge or expand at it is presently the case for hot spot monitoring in power transformers as explained in this paper. The fact also that such technology is now better known and well accepted in the scientific and engineer communities will contribute for sure to better market opportunities as they will be more and more tested in new applications…

References

/1/ D. A. Krohn, *Fiber Optic Sensors: Fundamentals and Applications*, Instrument Society of America (Pub.), Research Triangle Park, NC, USA, 2nd ed., ISBN 0-55617-010-6, 1992

/2/ J. M. López-Higuera, *Handbook of Optical Fibre Sensing Technology*, John Wiley & Sons (Pub.), Chichester, West Sussex, England, ISBN 0-471-82053-9, 2002

/3/ W. J. Bock, I. Gannot and S. Tanev, *Optical Waveguide Sensing and Imaging*, Springer (Pub.), Dordrecht, The Netherlands, ISBN 978-1-4020-6951-2, 2006

/4/ S. Yin, P. B. Ruffin and F. T. S. Yu, *Fiber Optic Sensors*, CRC Press (Pub.), Taylor & Francis Group, Boca Raton, FL, USA, 2nd ed., ISBN 978-1-4200-5365-4, 2008

/5/ D. Schaafsma, G. Palmer and J. H. Bechtel "Fiber optic temperature sensors for medical applications" *Optical Fibers and Sensors for Medical Applications III*, *Proc. SPIE*, Vol. 4957, pp. 162-169, 2003

/6/ É. Pinet, C. Hamel, B. Glišić, D. Inaudi, and N. Miron, "Health monitoring with optical fiber sensors: from human body to civil structures", *Proc. SPIE*, Vol. 6532, pp. 653219-1 to 653219-12, 2007

/7/ É. Pinet, "Medical applications / Saving lives", *Nature Photon. Tech. Focus* (special edition on fiber-optic sensors), Vol. 2, pp. 150-152, 2008

/8/ D. A. Krohn, "Temperature sensors" in *Fiber Optic Sensors: Fundamentals and Applications*, Instrument Society of America (Pub.), Research Triangle Park, NC, USA, 2nd ed., ISBN 0-55617- 010-6, Chap. 7, pp. 117-136, 1992

/9/ H. Aizawa, N. Ohishi, S. Ogawa, T. Katsumata, S. Komuro, T. Morikawa and E. Toba, "Fabrication of ruby sensor probe for the fiberoptic thermometer using fluorescence decay", *Rev. Sci. Instrum.*, Vol. 73, pp. 3656-3658, 2002

/10/ G. Paez and M. Strojnik, "Erbium-doped optical fiber fluorescence temperature sensor with enhanced sensitivity, a signal-to-noise ratio, and a power ratio in the 520-530- and 550-560-nm bands", *Appl. Opt.*, Vol. 42 (16), pp. 3251-3258, 2003

/11/ J.L. Wu, "A high-temperature sensor based fluorescence lifetime", *Proc. SPIE*, Vol. 6280, pp. 0347-0352, 2006

/12/ T. Katsumata, "Characteristics of Ti-doped sapphire for fluorescence thermo-sensor", *Int. Conf. Control Automat & Syst.*, Vol. 1-6, pp. 1025-1028, 2007

/13/ A. Babnik, A. Kobe, D. Kuzman, I. Bajsič and Možina, "Improved probe geometry for fluorescence-based fibre-optic temperature sensor", *Sensors and Actuators A*, Vol. 57, pp. 203-207, 1996

/14/ H. Chungai and W. Yutian, "Digital signal processing for fluorescence-based fiber-optic temperature sensor", *Proc. SPIE*, Vol. 4920, pp. 98-100, 2002

/15/ M. R. Brozel and G. E. Stillman (Eds.), "Properties of Gallium Arsenide", 3rd Ed. *Institution of Electrical Engineers*, London, 1996

/16/ É. Pinet "Fabry-Pérot fiber-optic sensors for physical parameters measurement in challenging conditions", *Journal of sensors*, Vol. 2009, Article ID 720980, 9 p., 2009, available at http://www.hindawi.com/journals/js/2009/720980 .html

17/ C. Belleville and G. Duplain, "Fabry-Perot optical sensing device for measuring a physical parameter", *US Patents* #5,202,939 1993 & #5,392,117, 1995

/18/ www.fiso.com

/19/ R. Van Neste, C. Belleville, D. Pronovost and A. Proulx, "System and method for measuring an optical path difference in a sensing interferometer", *US patent*, #2004/0075841 A1, 2004

/20/ M. Chavko, W.A. Koller, W.K Prusaczyk and R.M. McCarron, "Measurement of blast wave by miniature fiber optic pressure transducer in the rat brain", *J. Neurosci. Meth.*, Vol. 159 (2), pp. 227-281, 2007

/21/ L. Zhang, W. Zhang and I. Bennion, "In-fiber grating optic sensors" in *Fiber Optic Sensors*, CRC Press (Pub.), Taylor & Francis Group, Boca Raton, FL, USA, 2nd edition, ISBN 978-1-4200-5365-4, Chap. 4, pp. 109-162, 2008

/22/ S. Yin, C. Zhan and P.B. Ruffin, "Femtosecond laser-inscribed harsh environment fiber Bragg grating sensors" in *Fiber Optic Sensors*, CRC Press (Pub.), Taylor & Francis Group, Boca Raton, FL, USA, 2nd edition, ISBN 978-1-4200-5365-4, Chap. 5, pp. 163-200, 2008

/23/ A. Othonos and K. Kalli, "Fiber Bragg gratings: Fundamentals and applications in telecommunications and sensing", Artech House, ISBN 0890063443, 1999

/24/ D.H. Shroff and A.W. Stannet, "A review of paper aging in transformers", *IEEE Proc.*, Vol. 132 (6), part C, Nov 1985

/25/ A. Loupy Ed., "Microwave in organic synthesis", Wiley-VCH, Weinheim, 2006

/26/ D. Bogdal, "Microwave-assisted organic synthesis, One hundred reaction procedures", *Tetrahedron Organic Chemistry*, Vol. 25, Elsevier Ltd (Pub.), Oxford, UK, 2005

/27/ A. de la Hoz, A. Diaz-Ortiz and A. Moreno, "Microwaves in organic synthesis. Thermal and non-thermal microwave effects", *Chem. Soc. Rev.*, Vol. 34 (2), pp. 164-178, 2005

/28/ D.L. Price, J.P. de Wilde, A.M. Papadaki, J.S. Curan and R.I. Kitney, "Investigation of acoustic noise on 15 MRI scanners from 0.2 T to 3 T", *J. Magn. Res. Imag.*, Vol. 13 (2), pp. 288-293, 2001

Éric Pinet, Sébastien Ellyson and Frédéric Borne
FISO Technologies

Prispelo (Arrived): 01.09.2010 *Sprejeto (Accepted): 15.09.2010*

SPECIALTY OPTICAL FIBRES FOR A SENSING APPLICATION

Yuri Chamorovskiy

Institute of Radioengineering and Electronics Russian Academy of Science, Moscow, Russian Federation

Key words: optical fibres sensors, OFS, advantages of OFS, application area of OFS, sensing application

Abstract: Development of the optical fibre sensor (OFS) becomes an important real practical task due to a number advantages of a such sensors. The main are : the immunity to external influences, flexibility and long distance operation, high stability and sensitivity to various measurands, high resistance to a harsh environmental , possibility of nonelectrical operation and other. The application area for OFS is very wide and roughly could be divided in the following general categories: sensing of temperature; mechanical stress and displacement; acoustics waves; chemical and biosensing, electromagnetic fields. Some OFS could control only point data, other could measures many points over a fibre length simultaneously – these are called distributed type OFS. The development of OFS requires many types of optical fibres with very wide range of parameters and design are needed. In the present paper some more common speciality types optical fibre are described and several examples are given, based on researches made by author group.

Uporaba posebnih optičnih vlaken za zaznavanje

Kjučne besede: optična vlakna, optični senzorji, prednosti optičnih senzorjev, uporabna področja optičnih senzorjev, zaznavne aplikacije

Izvleček: razvoj senzorjev na osnovi optičnih vlaken (OFS) postaja pomembna naloga zaradi številnih njihovih prednosti, ki jih nudijo. Glavne prednosti so: imunost na zunanje vplive, prilagodljivost, delo na daljave, visoka stabilnost in občutljivost na različne merjene veličine, visoka odpornost na kruto okolje, možnost delovanja brez elektrike in druge. Aplikacijsko območje OFS je zelo široko in ga lahko grobo razdelimo v naslednje splošne kategorije: zaznavanje temperature, merjenje mehanskih obremenitev in premikov, zvočni valovi, kemično in biološko zaznavanje, elektromagnetna polja. Nekateri optični senzorji lahko kontrolirajo samo točkovne podatke, drugi lahko hkrati merijo več točk po celi dolžini vlakna-tem pravimo porazdeljeni OFS. Razvoj OFS zahteva veliko različnih vrst optičnih vlaken s širokim razponom parametrov in oblik. V članku je opisanih nekaj vrst posebnih optičnih vlaken in podanih je nekaj primerov, ki temeljijo na raziskavah, ki jih je opravila avtorjeva skupina.

1 Introduction

The speciality types optical fibre (SOF) were developed practically just after the development of telecommunication types optical fibre- i.e. at the end of 70th years. There are several types of SOF, but 2 main groups are an active, or lasing types optical fibres and fibres for sensing application. The last one is the topic of present paper, reviewing the main applications areas and designs of SOF for fibre optical sensors (OFS).

Development of the OFS becomes an important real practical task due to a number advantages of a such sensors. The main are : the immunity to external influences, flexibility and long distance operation, high stability and sensitivity to various measurants, high resistance to a harsh environmental , possibility of nonelectrical operation and other. OFS at present penetrates to many real application areas, but only few of them are really big commercial values. Probably the most bright example is the OFS for angular rotation control, often called as a gyro sensor /1/. Thus , real value of the total market for OFS is not easy to specify and one of a recent market estimation gives a value of about 1 bln $ (see Fig.1 /2/) . It is significantly less than telecom one, but grows quickly and has a big potential.

The application area for OFS is very wide and roughly could be divided in the following general categories: sensing of temperature; mechanical stress and displacement; acoustics waves; chemical and biosensing, electromagnetic fields. Some OFS could control only point data, other could measures many points over a fibre length simultaneously – these are called distributed type OFS. Principles of operation of OFS are also very different and most common are : interferometer schemes, Raman and Brillouin scattering , in- fibre Bragg gratings, small scale infibre resonators, amplitude modulation of light in a fibre under external influence and other.

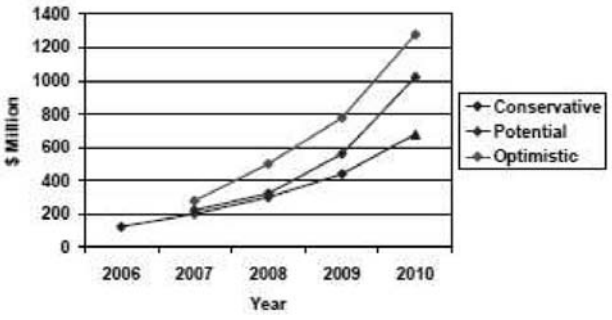

Fig.1: OFS market estimation (from /2/). Lower curve- conservative, upper- optimistic

It is clear that OFF should have a very wide range of the design and optical characteristics to fit the particular OFS application goal and engineering parameters. This is in a contrast with requirements for optical fibres for telecom applications where tight specification and unification as well as very low price are related with mass production conditions. Some main requirements for optical fibres are given in a Tab.1, of course this is a general consideration and can't be applied for absolutely all applications.

Table 1: Comparison of main parameters of the telecom fibres and SOF for sensors.

Parameter	Telecom fibre	SOF
Optical loss	< 0.5 dB/km	1-100 dB/km
Outer diameter	125 µm	40-2000 µm
Core diameter	10,50,62.5 µm	1-2000 µm
Mode dispersion	As low as possible	Could be very high for
		polarization types
Numerical aperture	0.1- 0.15	0.07- 0.6
Geometry	Circular (perfect)	Could be shaped in different forms
	0.2-	
Coating	Standard polymers	Standard, silicone, PI, metal
Sample length	10^4-10^5 m	1-10^4 m
Typical price	< 0.5 Eu/m	0.5-500 Eu/m
Operating temperature	-40 ÷ 80 C	-270 ÷ 700C

Below in section 2 we give a short description of most common types of SOF, based on their application for different physical values and measurement conditions. An example the optical fibre current transformer having a very high accuracy of about 0.1% , stability and wide dynamic range is considered. Such OFS is developed in our research group and uses a several types of SOF, including an advanced microstructured type fibre. It should be noted, that the question of SOF manufacturing process is not discussed in this paper, and one interesting in this could be referred to /3/.

2 Main types of SOF

2.1 SOF for chemical and bio-medical sensing

The basic principle of such OFS is the measurement of changing of some optical parameters (color, losses, polarization) of sensing element under presence of specific materials. Normally the SOF in such schemes must supply and collect light to/from sensing elements –such FOS are called as extrinsic sensors. Main demand to a fibre in this case is a core size and NA to collect enough light and medical compatibility of a fiber coating for medical applications. The typical examples of such FOS is given e.g. in /4/. The sensing elements could be placed at fiber endface or at outer surface, in later case it is necessary to modify fiber geometry to force the optical field to come out of boundary. This can be achieved e.g. by tapering of optical fibre or by making it D-shaped. Recently another approach was suggested for a such SOF, based on a new type of fiber – so called holey, or photonic crystal fibre /5/. Operation principle in this case is the high fraction of evanescent field (field out of fiber core) due very small core size – about wavelength. Thus the field propagating in a cladding, which is really an air holes, could be affected by the material penetrating to these holes. Simplest case of course is a gas, filling a holes. Typical structures of such SOF are presentaed at Fig.2: left is a common suspended core structure, with the core being placed between 3 holes (dark areas) and core size is less than 1 µm; right one shows the co-called " open" structure, where one holes is open to surrounding atmosphere. It gives a possibility to make gas penetration much faster and decrease time response of OFS. Another similar approach is to use the air hole core photonic crystal fibre /6/ and now a number of researches is made to optimize a design of OFS.

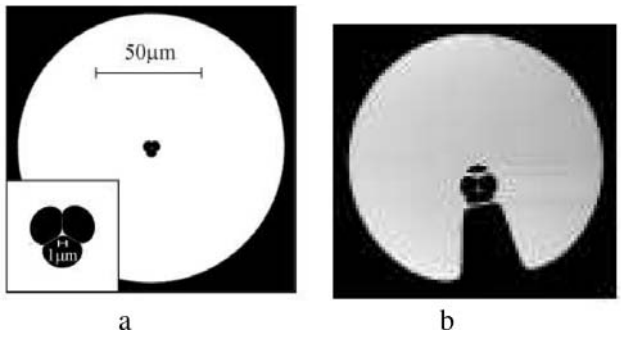

Fig. 2: Structures of holley type SOF for gas sensing a- suspended core structure, b-"open" hole structure.

2.2 Temperature sensors and high temperature applications

OFS for temperature measurements is probably the most wide type of sensors, at least in a number of units and operation principles. They use e.g. change of light transmission amplitude, color, polarization, as well as Fabry-Perot resonator and Bragg grating frequency shift or change of luminescence decay time constant with a temperature change. The review of such sensors is not a goal of paper and we should only point out that for all above design a telecom type fibres could be used with only a moderate modification for optimization sensors parameters. But situation changes dramatically if OFS should be used or measure the high temperature, say above 150 °C. This is because standard polymer coatings resist only a temperature about 100 °C and not higher. So even silica itself could work up to 1000 °C, damage of coating gives in result very quick mechanical damage of a fibre. For a temperature about 300 °C there is an alternative version with PI (polyimide) coating /7/, but for many application higher temperature is needed. We performed a research for applying of metal coating and investigation of high temperature behavior of SOF with metal coating. Two types of coatings were tested – Al and Cu based alloys. The gold coating also looks very promising with technical point of view, but a current gold price makes such experiments problemat-

ic. Shortly main results are the following. There are 2 reasons for loss increment in metal coated SOF- absorption and scattering due to microbending. Absorption increase depends on a preform and fibre design and environmental condition and is significantly higher for Al coated fibre /8/ (see Fig.3) Typical diagram for microbending induced losses for Cu coated fibre is presented at Fig.4

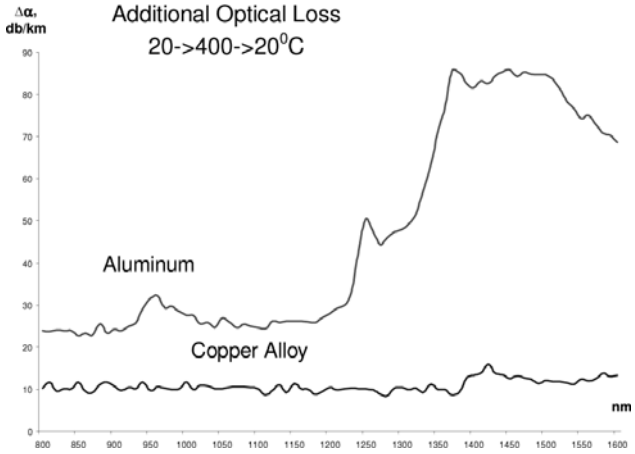

Fig. 3: Additional losses induced in Cu-alloy (lower curve) and Al coated fibre after heat cycling To 400 °C and back

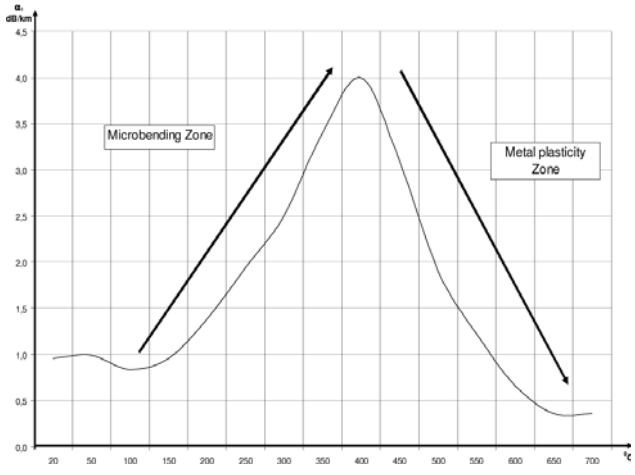

Fig. 4: Microbending induced losses at 1300 nm in optical fibre with Cu alloy coating .

It should be mentioned one application of a metal coated fibre- OFS for high temperature based on a fibre Bragg grating (FBG). As it is known the normal FBG written in GeO_2 fibre destroyed at high temperature /9/, but it was found that doping with N could resolve this problem and FBG in such fibre operates at rather high temperature, over 500 °C /10/. We combine N doped fibre with a Cu coting and obtain in this way a sensitive element for high temperature OFS /11/- example is given at Fig.5 and comparison of GeO_2 and N doped FBG behavior under high temperature annealing at Fig. 6

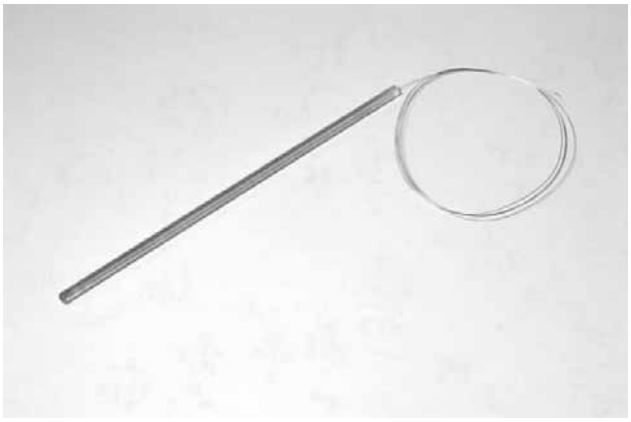

Fig. 5: High temperature Bragg type sensing element with N-doped and Cu coated fibre

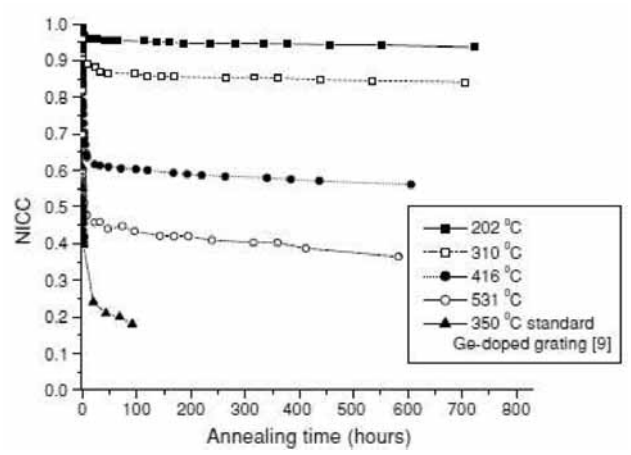

Fig. 6: Isothermal annealing of FBG written in an N-doped fibre compared with that of a Ge-doped.

Here NICC parameter (normalized integrated couple constant) defined as NICC $=\tanh^{-1}(\sqrt{R})/\tanh^{-1}(\sqrt{R_0})$ where , R_0 and R are the initial and current reflection coefficients of the grating at the resonance wavelength, respectively.

2.3 SOF for stress and displacement monitoring systems

The fibers used for this application are very similar to the fibers for temperature sensing because physical phenomena are practically the same for these sensors. For example, shift of central wavelength of FBG, resonator frequency or fiber interferometer phase shift depend both on temperature and stress in a fiber and separation of different influences is a common problem for OFS design. Of course some OFS measure the single measurand – e.g. Raman scattering or luminescence based sensors affected by temperature only, but from fiber point of view differences of the two OFS are very small. May be the remarkable one is related with the object of monitoring of the stress and deformation. As a rule it is a long haul and big in size objects –e.g. bridge, oil hole, gas or oil pipe, etc. and hence normally one have to control the distributed or multipoint pa-

rameters. For many of engineering objects the hard environmental conditions are also proper. Thus, SOF for monitoring system normally must be strong enough at length up to several km, resists relatively high temperature, in some cases (e.g. in oil mines) be hermetical to avoid H penetration. Some of these parameters could be achieved by using SOF with combined coating : carbon layers plus PI layers / 7/, but in general the problem needs more effort to develop SOF adequate to practical problems and advanced types of modern opto-electronic measuring devices, such as Raman, Brillouin or polarization reflectometers /12/.

2.4 Polarization types SOF. Optical fibre current transformer

The interest to polarization type SOF was generated in a first turn by the development of angular velocity OFS, often called as gyro sensor /1/. For such an OFS the fibre preserving linear polarization state (HB fibre) was necessary and several types were successfully designed – PANDA type, bow-tie, elliptical stress jacket, elliptical core. Basic design and principle of operation of these SOF are described in a classic paper /12/, and in many more modern papers, e.g. / 3/. Shortly, two main mechanisms could lead to strong linear birefringence and hence to polarization holding property. First is the creation of anythotropic mechanical stress due to adding an elements or making an uncercular internal regions in the fibre with big thermoelastic coefficient, second is making uncercular core shape and obtaining of waveguiding birefringence. The properties of HB fibres are now investigated in details, including relation between fibre design and birefringence value and its temperature dependence. An example of most common type HB fibre- PANDA fibre is presented at Fig7 a. Bright area in a center corresponds to a core, and two black circulars to stress applying rods.

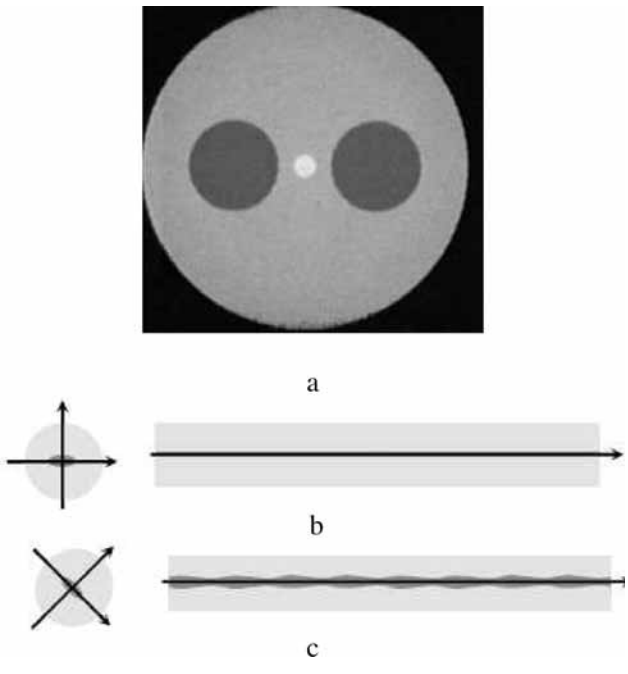

Fig. 7: Cross section of a typical HB SOF PANDA type (a) and comparison of HB (b) and SPUN (c) fibres structures.

The fibre, preserving elliptical (“circular like”) polarization states is not so common and isn’t investigated in all details. On our opinion this fibre has at least the same importance as HB fibre as they could be used for creation of optical current sensors or optical current transformer (OCT) based on a Faraday effect. Such OCT could have an extremely high characteristic and are very perspective for application in electro energetic and some other industrial areas /13/. The SOF using for Faraday OCT is made by fast rotation of a fibre during its drawing and as a result the birefringence axes rotated along a fibre length in a spiral manner. As a starting preform we use a HB type preform in this case and the fibre obtained in this way is called SPUN type fibre. Schematically, the difference between HB and SPUN fibres is clear from Fig.7 b and c.

The principle scheme of OCT is given at Fig.8. It is interesting to point out that such OFS uses 6 different SOFs in a real design. They are:

- Active Er-doped optical fibre wide spectrum light source at 1550 nm
- Polarizing fibre
- Delivery fibre PANDA type (up to 1 km)
- Fibre phase modulator
- Fibre quarter wavelength thermo stable plate
- Sensitive SPUN type fibre

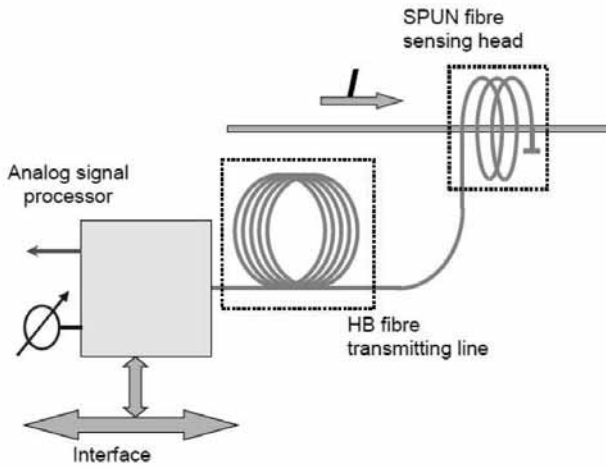

Fig. 8: Principle scheme for OCT,using SPUN fibre. I- electrical current coming through sensing fibre coil.

Characteristics of developed OCT based on a “ classical” SPUN type fibre are very high: accuracy of measurement is better than 0.2 % over a 1000 ^{o}C range, dynamic range is better than 10^5, maximal current – up to 10^5 A, high linearity and total immunity to electromagnetic interference.

We show recently /13,14/ that replacing of a "classical" SPUN fibre by an advanced holey type SPUN fibre open it out that parameters could be further improved. First, it is possible to make a coil with up to 10^5 fibre turns without degradation of optical parameters (loss and magneto-optical sensitivity) and also thermal stability becomes higher due to fact of very high insensitivity of holey SPUN fibre to temperature. The cross section of advanced SPUN fibre is given at Fig.9 a . Also shown are sensitive coils with 10^2 and 10^5 turns number (Fig.9 b,c)

We think that now it is obvious that holey fibre could be used in a many modern practical OFS. Another fact confirming it is for example a value of linear birefringence- in our fibre we achieve a value of about $2x10^{-2}$, what is about 20 times higher than for best PANDA type fibre /14/.

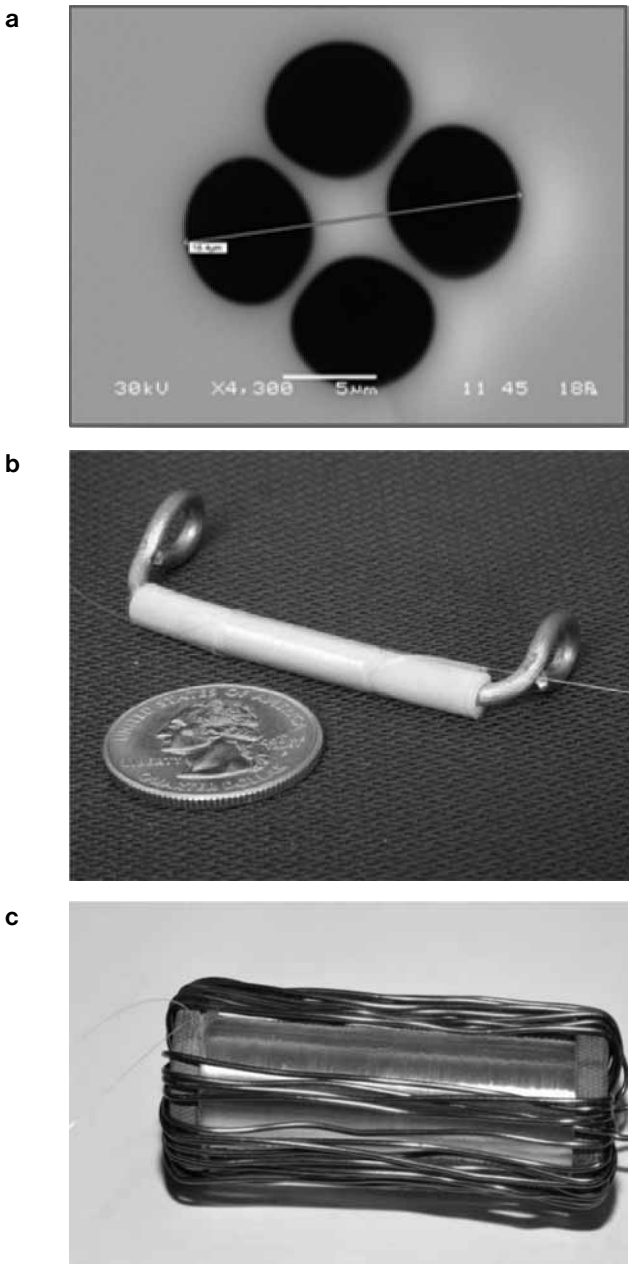

Fig. 9: a-Cross section of central region of holey SPUN fibre, 4 dark regions- air holes, inside-core region; b- SPUN holey fibre sensitive coil with 100 turns; c-the same but with 10000 turns.

3 Conclusions

The brief review of main types of SOF for sensing applications is presented. Developed SOF could tolerate to a very wide spectrum of OFS differing by physical operation principles, measured parameters and design. Probably the most important type of SOF which needs a further serious development is the SOF for very high temperature and harsh environmental conditions. OFS with such fibre could be used in multiple monitoring systems – smart oil holes, engine, engineering structures and have a big commercial potential. Application of a new advanced holey or photonic crystal fibres gives a possibility for remarkable improvement of OFS parameters.

Acknowledgments

Author thank to a members of speciality fibre division of IRE RAS for help at preparing this article.

References

/1/ B. Culshaw, "Optical fibre sensor technologies: Opportunities and perhaps pitfalls", J. Lightwave Technol., 22, No 1, pp. 39-50, 2004

/2/ P. E. Sanders, D. A. Krohn, "Market Opportunities for Photonic and Optical Fiber Sensors", OFC/NFOEC 2007, Workshop: Future of Fiber Optic Sensors, 2007

/3/ A.Mendez, T.F.Morse "Speciality Optical Fibers Handbook", Elsevier AP, 2007.

/4/ F. Baldini, "Advanced biomedical optical fibre sensors", 20th International Conference on Optical Fibre Sensors, Proc. of SPIE Vol. 7503, 75030Q, 2009

/5/ E. P. Schartner, R. T. White, S. C. Warren-Smith, T. M. Monro, "Practical sensitive fluorescence sensing with microstructured fibres", 20th International Conference on Optical Fibre Sensors, Proc. of SPIE Vol. 7503, 75035X, 2009

/6/ T. Ritari, J. Tuominen, H.Ludvigsen, J. Petersen, T. Sřrensen, T. Hansen, H.Simonsen, "Gas sensing using airguiding photonic bandgap fibers," Opt. Express, 12, pp. 4080-4087, 2004.

/7/ C.Wang, A.Soufiane, I. Majid, K. Wei, "High reliability hermetic optical fiber for oil and gas application", Proceedings of the SPIE, Volume 5855, pp. 563-566, 2005.

/8/ V. V. Voloshin, I. L. Vorob'ev, G. A. Ivanov, V. A. Isaev, A. O. Kolosovskii,S. M. Popov*, and Yu. K. Chamorovskii," Effect of Metal Coating on the Optical Losses in Heated Optical Fibers", Technical Physics Letters, Vol. 35, No. 4, pp. 365–367, 2009

/9/ D. Razafimahatratra, P. Niay, M. Douay, B. Poumellec , I.Riant " Comparison of isochronal and isothermal decays of Bragg gratings written through continuous-wave exposure of an unloaded germanosilicate fiber" Appl. Opt.39 pp.1924–33, 2000

/10/ O.V. Butov, E.M. Dianov, K. M. Golant, " Nitrogen- doped silica-core fibres for Bragg grating sensors operating at elevated temperatures", Meas. Sci. Technol. 17 pp.975–979, 2006

/11/ O.V. Butov, K.M. Golant, Yu.K. Chamorovsky, V.A. Isaev, I.L. Vorobjev, V.V. Voloshin, A.O. Kolosovsky, Ya. V. Gusev, I.V. Sokolov "In fiber Bragg graiting for sensor application at high temperatures" // Proc.. OFC-2004, Los Angelos, Febr. 22-27, đ.Fc5, 2004.

/12/ M.N.Alahbabi, Y.T.Cho, T.P.Newson, "Simultaneous temperature and strain measurement with combined spontaneous Raman and Brillouin scattering", Optics Letters , V.30(11) pp.1276-1278, 2005

/13/ Yu K Chamorovsky, N I Starostin, S K Morshnev, V P Gubin, M V Ryabko, A I Sazonov, I L Vorob'ev, "Spun microstructured optical fibres for Faraday effect current sensors", QUANTUM ELECTRON , 39 (11), pp.1074–1077, 2009

/14/ / Yu.K. Chamorovskiy, N.I. Starostin, M.V. Ryabko, A.I. Sazonov, S.K. Morshnev, V.P. Gubin, I.L. Vorob'ev, S.A. Nikitov, "Miniature microstructured fiber coil with high magneto-optical sensitivity", Optics Communications, V. 282, 23, pp. 4618-4621, 2009

Yuri Chamorovskiy

Institute of Radioengineering and Electronics Russian Academy of Science, Mokhovaya str.11 bld.7, Moscow, 125009, Russian Federation
yurichamor@gmail.com

Prispelo (Arrived): 01.09.2010 *Sprejeto (Accepted): 15.09.2010*

LUMINESCENT CHEMOSENSORS – ADVANCED TOOLS IN ANALYTICAL CHEMISTRY

Sergey M. Borisov and Ingo Klimant

Institute of Analytical Chemistry and Food Chemistry, Graz University of Technology, Graz, Austria

Key words: luminiscent chemosensors, advanced tool, analytical chemistry

Abstract: Optical chemosensors represent smart analytical tools which become very popular in the last decades. They are advantageous due to the number of features such as non-invasiveness, absence of electromagnetic interferences, possibility of miniaturization, suitability for imaging etc. Optical chemosnesors are very versatile in their formats which include planar optodes, fiber-optic (micro)sensors, sensor paints, nanoparticles etc. This paper briefly reviews the main sensing principles and materials used in optical chemosensors and provides an overview of the novel luminescent chemosensors recently developed in the Institute of Analytical Chemistry and Food Chemistry in Graz University of Technology.

Luminiscenčni kemosenzorji – napredno orodje v analitični kemiji

Kjučne besede: luminiscentni kemosenzorji, napredno orodje, analitična kemija

Izvleček: Optični kemosenzorji predstavljajo pametno analitično orodje, ki je postalo priljubljeno v zadnjih desetletjih. Njihove prednosti so neinvazivnost, odpornost na elektromagnetne motnje, možnost miniaturizacije, ustreznost za slikanje itn. Optični kemosenzorji so zelo vsestranskih oblik kot so planarne optode, mikro senzorji na osnovi optičnih vlaken, senzorske barve, nanodelci.itn. V članku so na kratko opisani principi zaznavanja in uporabljeni materiali pri optičnih kemosenzorjih. Članek poda pregled novih luminiscentnih kemosenzorjev, ki so bili pred kratkim razviti na Inštitutu za analitično kemijo in prehransko kemijo na Tehnološki univerzi v Gradcu.

1 Introduction

Optical chemosensors became increasingly popular in the last decades /1-3/. They can be defined as devices capable of continuous monitoring of chemical or biological parameter by optically transforming the information into an analytically useful signal. Several features of optical chemosensors make them promising alternatives to other analytical techniques. Particularly, they are free of electromagnetic interferences, are non-invasive or minimally invasive, enable simultaneous measurements of several parameters, imaging over a surface or in volume, and, finally, they are very versatile and can be realized in a variety of formats. The most common sensor formats include planar foils, paints, fiber-optic sensors and microsensors and analyte-sensitive nano- and microparticles. The latter represent self-contained analytical tools which can be used on their own (e.g. as an aqueous dispersion) or combined in a composite material, for example to enable multi-analyte sensing. Optical chemosensors rely on the use of indicators which respond to a particular analyte in altering their optical properties (absorption, emission intensity, decay time, anisotropy etc). The chemosensors based on luminescent indicators are particularly promising due their high sensitivity and versatility /1/. The requirements to the indicators include high selectivity to the analyte of interest, selectivity in the desired range, high luminescence brightness, preferably long Stokes´ shifts and high photostability. However, the state-of-the-art indicators not always fulfill these requirements. Moreover, for many important applications indicators and sensors with tailor-made properties are required.

In this contribution we report the recent progress on optical chemosensors and novel sensing materials developed in our institute.

2 Results and discussion

2.1 Optical oxygen sensors

Oxygen belongs to one of the key analytes and its determination is of utmost importance in various fields of science and technology including biology, medicine, environmental monitoring, marine science etc., to mention only a few. Optical oxygen sensors rely on dynamic quenching of the luminescence of an indicator /4/. Upon the collision of an excited indicator molecule and molecular oxygen (in ground triplet state) the indicator is deactivated and the oxygen is promoted to the excited singlet state (Fig. 1). Since the singlet oxygen rapidly returns to the ground state, no consumption of the analyte occurs as e.g. in Clark electrode. In optical oxygen sensors the luminescence intensity and the decay time are directly related to oxygen concentration (Stern-Volmer equation).

Oxygen indicators are mostly represented by metal complexes which possess relatively long-lived luminescence (µs-ms). These mainly include ruthenium(II)-tris-polypyridyls and platinum(II) and palladium(II) porphyrins, but some

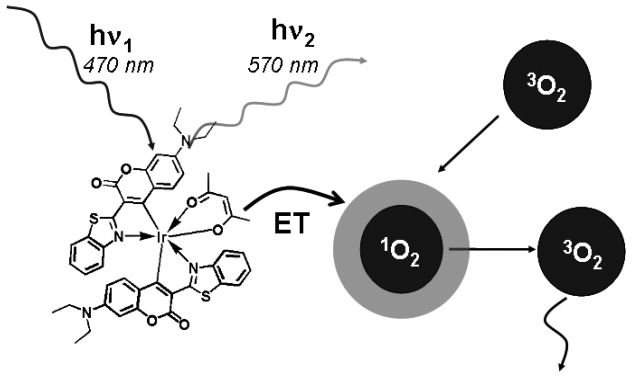

Fig. 1: Oxygen sensing scheme with an iridium(III) coumarin complex Ir(C_s)$_2$(acac) as an indicator

complexes of osmium(II), rhenium(I) or copper(I) were also reported. Unfortunately, the state-of-the-art complexes do not fully fulfill the requirements of luminescence brightness (defined as a product of molar absorption coefficient and luminescence quantum yield), photostability or spectral compatibility to the light sources (e.g. LEDs or laser diodes). Therefore, several novel indicators and oxygen sensing materials were developed in our laboratory to overcome these drawbacks.

2.1.1 Ultrabright oxygen optodes

These are based on the cyclometallated iridium(III) complexes with coumarin ligands (Fig. 1). Compared to conventional cyclometallated complexes the new indicators are distinguished by very high molar absorption coefficients in the blue part of the spectrum (ε ~ 90,000 $M^{-1}cm^{-1}$ at 450-480 nm) and also possess high luminescence quantum yields approaching 60% /5/. This results in very high luminescence brightness which exceeds the brightness of the conventional indicators (ruthenium(II) polypyridyls and platinum(II) porphyrins) by ~10-fold (Table 1). Therefore, preparation of very thin fast responding optodes (response times < 1 s) became possible. The decay time of the complexes is ~ 10µs so that when embedded in polystyrene and similar materials the optodes show optimal sensitivity to oxygen at physiologically relevant concentrations.

Table 1: Photophysical properties of the iridium coumarin complex and two most common oxygen indicators

Indicator	λ_{abs}, nm	ε, $M^{-1}cm^{-1}$	QY	BS
Ir(C_s)$_2$(acac)	472	92800	0.54	50000
Ru-dpp	463	28600	0.37	10600
PtTFPP	504	23200	0.2	4600

2.1.2 NIR-emitting oxygen indicators

The red-light excitable near-infrared emitting indicators and sensors are generally attractive for the following reasons: (i) they are less prone to interferences e.g. from backgroung fluorescence and light scattering; (ii) they can be compatible with cheap red-laser diodes and 632.8 nm line of the He-Ne laser (confocal imaging applications); (iii) they can be used for subcutaneous determination of oxygen – "smart tattoos" /6/. Since the optical glucose biosensors rely on oxygen transducers the NIR indicators can be used to subcutaneously monitor the glucose levels in blood (artificial pancreas) which may provide a convenient solution to diabetic patients. The state-of-the art NIR indicators included metal complexes of benzo- and naphoporphyrins /7-9/, Fig. 2. We developed platinum(II) and palladium(II) complexes with fluorinated benzoporphyrins which have improved photophysical properties (higher emission quantum yields and better photostability) /10,11/. Notably, these indicators can be excited both in the red (600-630 nm) and in the blue part of the spectrum (430-460 nm). The long Stokes´ shift helps to eliminate the autofluorescence almost completely. Thus, measurements even in photosynthetically active biological media (which show intense chlorophyll fluorescence) become possible which makes the new materials especially attractive for a number of applications.

Additionally, molecular hybrids of benzoporphyrins and phthalocyanines were developed /12/. The novel azotetrabenzoporphyrin complexes occupy intermediate position between the two classes and combine the advantages of both which include high luminescence brightness, good solubility and extreme photostability. Particularly, photostability was found to increase by ~ 10 fold compared to the respective benzoporphyrins. Additionally, the platinum(II) and palladium(II) complexes possess bathochromically shifted absorption in the red part of the spectrum and become fully compatible with the red laser diodes (635 and 645 nm, respectively).

A palette of oxygen indicators with tailor-made spectral properties was also developed /13/. These represent the hybrids between benzo- and naphthoporphyrins. Both the absorption and the emission maxima are systematically tuned and shift bathochromically ~ 20 nm per each naphtho-group introduced in the porphyrin macrocycle. Thus, the excitation of the sensing materials can be performed at a preferred wavelength varying from 600 to 700 nm. The new indicators enable multiplexing – i.e. they can be separately excited to obtain several independent informations (e.g. oxygen and glucose concentration). Additionally, the benzo-naphthoporphyrin hybrids possess tunable decay times (which become shorter with naphthosubstitution) which makes possible to adjust the sensitivity to oxygen.

2.1.3 Trace oxygen sensors

Sensing of low oxygen concentrations is also of much interest in many areas of science and technology. For example, continuous monitoring of dissolved oxygen (DO) is essential in breweries since high oxygen concentrations negatively influence the taste of beer (typical concentrations of DO in beer are in the range of 10-50 ppb). In water boilers the concentration of DO is kept at ~ 7 ppb to prevent corrosion. Monitoring of ultra-low concentrations of DO is of

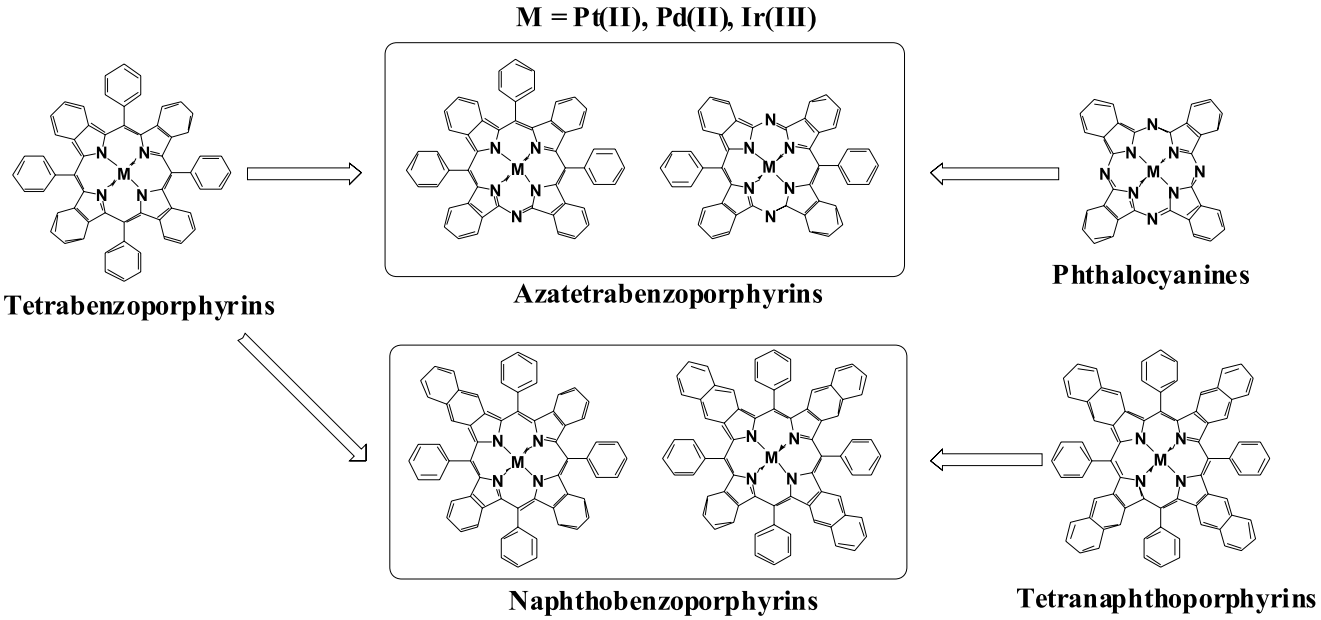

Fig. 2: Chemical structures of the state-of-the-art and novel NIR emitting oxygen indicators

particular interest in aquatic biology and oceanography. For example, some marine ecosystems such as oxygen minimum zones and other oxygen-deficient environments contain less than 70 ppb of DO and sometimes as low as 0.06 ppb. Notably, conventional luminescent oxygen sensors do not provide such high sensitivities and are more suitable for monitoring of oxygen at physiologically relevant conditions. The sensors for trace oxygen determination usually rely on highly gas permeable polymers but often suffer from solubility (such as e.g. in case of Teflon AF) and stability (e.g. in case of poly(1-trimethylsilyl-1-propine) issues. Therefore, development of new materials for trace oxygen sensors is still of high importance.

We present a new approach based on covalent coupling of the highly photostable commercially available oxygen indicators to micrometer-sized silica-gel beads /14/. The palladium(II) and platinum(II) complexes with *meso*-pentafluorophenyl porphyrin can be easily covalently immobilized onto amino-modified silica-gel particles. These particles are dispersed in silicone. Notably, covalent coupling prevents aggregation and migration of the dye into silicone and also enables high dye loading. As demonstrated, the novel materials are suitable for monitoring of oxygen traces in ppb range and below.

2.2 Optical temperature probes

It is well known that the performance of all optical chemosensors (e.g. for oxygen, carbon dioxide, ammonia, pH) is compromised by temperature. In fact, temperature has pronounced effect on the diffusion of species inside the polymeric matrix, on their solubility, equilibrium constants etc. Moreover, the luminescence properties of the indicators are also affected by temperature. Thermal quenching (decrease of the luminescence quantum yields and the decay times) can be often very pronounced, e.g. in case of ruthenium(II) polypyridyl complexes. Fig. 3 provides an example of temperature effects in case of an oxygen sensor (extreme case).

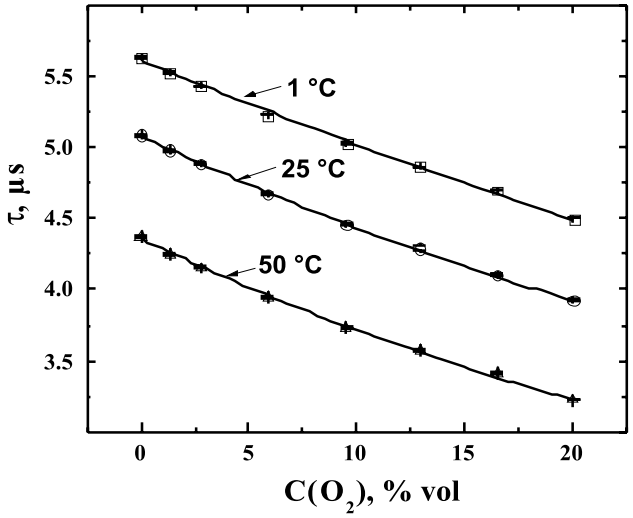

Fig. 3: Oxygen calibration plots for a ruthenium(II) complex Ru-dpp embedded in polystyrene.

Evidently, reliable measurements are only possible if temperature is kept constant or is known. This lead to development of so called "dual sensors" which are capable of simultaneous monitoring of temperature and a chemical parameter /15,16/. The probes employed in such composite materials respond to temperature in altering their luminescent properties (intensity and/or decay time) and therefore are advantageous to other methods of temperature measurements. For example, simultaneous imaging of both parameters on surfaces becomes possible. These luminescent temperature probes are mostly represented by ruthenium(II) polypyridyl complexes and europium(III)-tris-b-diketonates. Thermographic inorganic phosphors are

also used but they commonly respond at rather high temperatures. The sensitivity of these phosphors at ambient temperatures is rather low (~0.2% decay time change per K). Often the brightness of such phosphors is not sufficient for practical applications. We realized a new thermographic phosphor, chromium(III)-doped yttrium aluminium borate (YAB) which overcomes these drawbacks /17/, Fig. 4. The phosphor is excitable in the blue and in the red parts of the spectrum and emits in the NIR. The luminescence decay time decreases with increasing temperature and the sensitivity approaches 1%/K. Moreover, the luminescence intensity remains virtually constant in this temperature range so that the S/N ratio is not influenced. Compared to the luminescent probes based on metal complexes, Cr(III)-doped YAB also benefits from high chemical and photochemical stability. The phosphor can be easily obtained in large quantities via solution combustion technique.

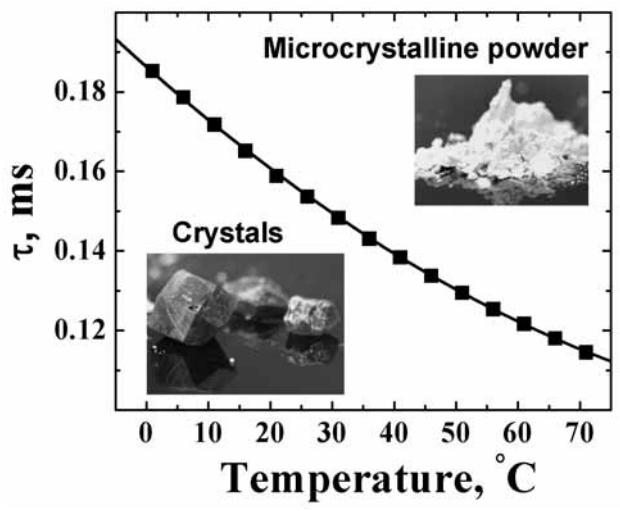

Fig. 4: Calibration plot for the new Cr(III)-doped YAB temperature phosphor. The inserts show the photographic images of the two phosphor forms.

Recently we demonstrated the application of the novel phosphor for temperature compensation of the pH chemosensors /18/. The composite material relied on the fluorescent red light-excitable pH indicator dissolved in a polyurethane hydrogel where the phosphor particles were also dispersed. The phosphor not only served as a temperature probe but also as a reference for the pH indicator with help of Dual Lifetime Referencing technique.

2.3 Luminescent nanochemosensors for various analytes

Nanosensors belong to smart analytical tools which became popular in the last decade /19,20/. They are rather small (Φ < 1 μm and more often <100 nm) and therefore respond to the analytes of interest virtually in real time. Many of them can be used for intracellular monitoring of important parameters. The nanosensors are simply dispersed in the analyzed media in which they behave similarly to dissolved indicators with notable exception that the indicator inside is protected from undesired interferences (e.g. from other analytes) and is much less prone to nonspecific binding. Many typical nanosensors are designed by immobilizing an indicator into polymeric nanoparticles, inorganic sol-gel particles or hybrid Ormosil materials. Notably, the indicator behaves similarly to the balk optodes since the material also serves a solvent and a support for the indicator, and as a permeation-selective membrane. Many other types of nanosensors exist (based on quantum dots, metal particles etc. /20/) but they are more or less limited to specific analytes.

Recently we developed a versatile material for designing optical nanosensors /21/. A block polymer of styrene and vinylpyrrolidone is used as a matrix. The polymer is commercially available in form of the nanobeads (Φ ~220 nm) which in aqueous dispersion possess core-shell structure, Fig. 5.

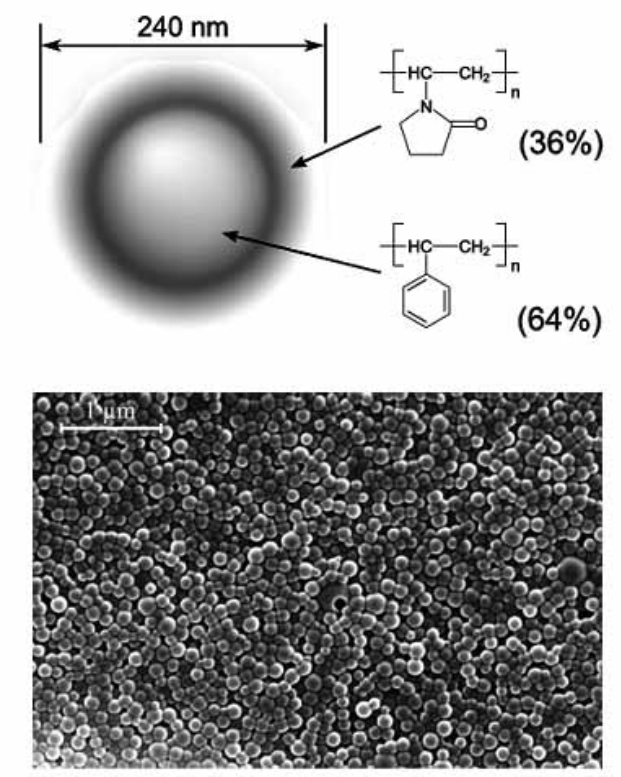

Fig. 5: Schematic representation of the structure of poly(styrene-block-vinylpyrrolidone) nanoparticles (upper part) and scanning electron microscopy image of the nanoparticles.

As we have demonstrated this determines the unique stability of the particles which do not aggregate even at very high concentrations in presence of inorganic salts and other substances, and can be freeze-dried and redispersed afterwards. The lipophilic indicators are easily immobilized by swelling (the beads are swollen in the mixture of an organic solvent and water, an indicator is added and the or-

ganic solvent is slowly removed under reduced pressure) into the core or into the shell of the nanobeads. Particularly, immobilization into the core is performed from tetrahydrofurane:water mixtures, and the shell of the beads can be stained from ethanol:water. A palette of oxygen nanosensors was prepared by staining into the core, which possessed desirable spectral properties and sensitivity /22/. Temperature probes were also manufacturing by immobilizing a europium(III) complex into the core /21/. On the other hand, the nanosensors for pH and ions were prepared by immobilizing lipophilic indicators into the shell of the beads /21/. Particularly, the nanosesnors covering the dynamic ranges of interest (pH 5-9) were prepared and are likely to be suitable for applications in biotechnology, biology, medicine and marine science /23/.

On the basis of the oxygen nanosensors we designed the first water dispersible and washable Pressure Sensitive Paint (PSP) /24/. The state-of-the-art PSPs are widely used in aeronautics, aircraft and automobile industries for determining pressure distribution on the models. A relatively new technique relies on use of oxygen sensors to measure total pressure via oxygen partial pressure. In this case the whole model is usually imaged with a CCD camera. Unfortunately the materials used require expensive and environmentally harmful solvents for polymers and indicators. Our novel material represents an aqueous dispersion of dye-doped poly(styrene-block-vinylpyrrolidone) beads which is sprayable on various surfaces including e.g. aluminium. Notably, upon drying the dense mechanically stable layer is formed and enables imaging of oxygen partial pressure and temperature (in case of the temperature probes dispersed along with the oxygen-sensitive nanospheres). The layer can be removed simply by washing with water.

We also developed a simple method for preparation of optical nanosensors via precipitation /25/. Briefly, a polymer and an indicator are dissolved in organic solvent (miscible with water) and water is added to the solution. The size of the particles is determined by the nature of the polymer but can be also tuned by the concentration of the components, the solvents used, speed of water addition etc. This highly versatile technique works with many indicators and polymers. For example, nanosensors for oxygen, pH, temperature were manufactured from neutral, cationic and anionic polymers. The positively charged Rl-100 beads, particularly, are rather small ($\Phi \sim 40$ nm) and are found to penetrate through the cell membranes to enable intracellular monitoring of various parameters.

2.4 Novel optical pH sensors

Most state-of-the-art optical pH sensors rely on use of fluorescent indicators such as fluoresceins, 8-hydroxypyrene-1,3,6-trisulfonate and naphthalimide derivatives. All these indicators have some disadvantages. Fluoresceins, particularly, are prone to self-quenching and possess low photostability. The brightness of the naphthalimides is not sufficient for many applications due to low molar absorption coefficients. Therefore, development of new materials with improved photophysical properties is still of much importance. Photoinduced electron transfer (PET) is widely used for designing pH and ion sensors (mainly on the basis of naphthalimides). We recently developed the new optical pH sensors based on perylene dyes and relying on PET. Perylenes are known as chemically and photochemically robust chromophores that possess high molar absorption coefficients and fluorescence quantum yields approaching 100%. The perylene structure can also be modified to enable dyes with different spectral properties. Moreover, NIR analogous (terrylenes) are available and, in principle, can be used to design pH sensors. We have shown that preparation of the pH sensors on the perylene basis is feasible /26/. The pK_a values can be tuned over a broad range to enable different applications. This is achieved by varying the nature of amine substituent (primary, secondary or tertiary) responsible for PET. Covalent immobilization of the indicators also is possible and will be realized in future work.

2.5 Trace ammonia sensors

Ammonia is known to be very harmful for aquatic organisms even in very small quantities. Ammonia concentration is also an important parameter in biotechnology. Therefore, its precise monitoring is particularly important in many biological applications and in fish farming. Our group developed novel optical sensors for detection of trace ammonia. They rely on lipophilic xantene dyes (eosin and 2,7-dichlorofluorescein) embedded into a gas permeable polymeric matrix /27,28/. The trace quantities in the ppb range can be reliably monitored. Referenced sensors based on nanoparticle materials also were prepared /29/.

2.6 Sensing materials with magnetic properties

Optical sensing materials with magnetic properties become increasingly popular in the last few years. Compared to the conventional materials they provide possibility of manipulation. For example, the sensors based on micro- or nanoparticles can be collected in the region of interest, manipulated there and easily removed from the analyzed media with magnetic forces. The signal intensity of the sensor spot formed from magnetic particles is comparable to conventional planar spots. We developed a variety of magnetic sensing materials ranging from nanoparticles ($\Phi \sim 100$ nm)/30/ to microparticles ($2<\Phi<100$ µm) /31/ and to magnetic macrospheres (Φ of few mm) /32/, Fig. 6. Basically, these materials bear similar sensing chemistry as the conventional ones but also incorporate magnetite to render them magnetic. The primary applications of magnetic nanoparticles are those in microscopy and microfluidics, however, photodynamic therapy, drug delivery etc. are also considered. The magnetic microparticles are collected much fasted and manipulated more easily due to their larger dimensions. Finally, magnetic macrospheres

(produced by coating of iron balls with sensing composition) are collected virtually instantaneous and can be easily moved in reactors /32/. They can also be used in 24-channel plate readers to substitute the sensor spots. Special magnetic adaptors for collecting the magnetic sensors directly in front of an optical fiber also were developed /33/. So far, magnetic materials fro sensing pH and oxygen were realized but sensing of other analytes is certainly feasible.

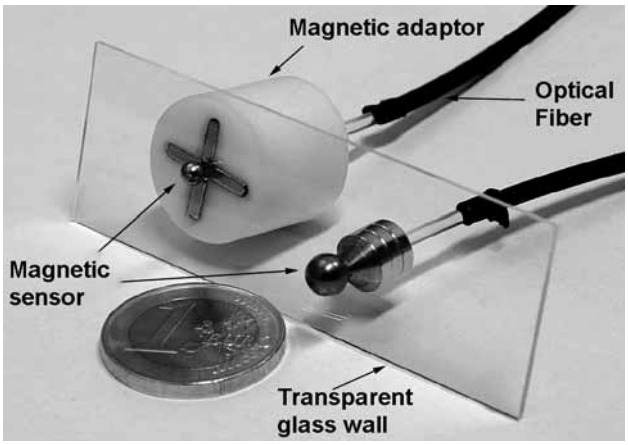

Fig. 6: Photographic image of the optical magnetic spherical sensors

3 Conclusions

Novel luminescent indicators and optical sensing materials were developed which substantially improve the performance of optical chemosensors and open new frontiers for their application is science and technology. Particularly, ultrabright oxygen sensors, novel NIR oxygen and pH sensors, nanoparticle-based sensors, sensors with magnetic properties as well as optical temperature-sensitive materials were described. They are expected to find numerous applications in biology, biotechnology, marine science, medicine etc.

Acknowledgments

The financial support from the Austrian Science Fund FWF (projects P 21192-N17 and M 1107-N22) is gratefully acknowledged.

References

/1/ O.S. Wolfbeis, Materials for Fluorescence-Based Optical Chemical Sensors, J. Mater. Chem., vol. 15, pp. 2657-2669, 2005.

/2/ O.S. Wolfbeis, Fiber-Optic Chemical Sensors and Biosensors, Anal. Chem., vol. 78, pp. 3859-3874, 2006.

/3/ O.S. Wolfbeis, Fiber-Optic Chemical Sensors and Biosensors, Anal. Chem., vol. 80, pp. 4269-4283, 2008.

/4/ Y. Amao, Probes and Polymers for Optical Sensing of Oxygen, Microchim. Acta, vol. 143, pp. 1-12 (2003).

/5/ S.M. Borisov, I. Klimant, Ultrabright Oxygen Optodes Based on Cyclometalated Iridium(III) Coumarin Complexes, Anal. Chem., vol. 79, pp. 7501-7509, 2007.

/6/ E.W. Stein, P.S. Grant, H. Zhu, M.J. McShane, Microscale Enzymatic Optical Biosensors Using Mass Transport Limiting Nanofilms. 1. Fabrication and Characterization Using Glucose as a Model Analyte, Anal. Chem., vol. 79, pp. 1339-1348, 2007.

/7/ A.V. Cheprakov, M.A. Filatov, The dihydroisoindole approach to linearly annelated d-extended porphyrins, J. Porphyrins Phthalocyanines, vol. 13, pp. 291-303, 2009.

/8/ O.S. Finikova, A.V. Cheprakov, I.P. Beletskaya, P.J. Carroll, S.A. Vinogradov, Novel Versatile Synthesis of Substituted Tetrabenzoporphyrins, J. Org. Chem., vol. 69, pp. 522-535, 2004.

/9/ J.R. Sommer, R.T. Farley, K.R. Graham, Y. Yang, J.R. Reynolds, J. Xue, et al., Efficient Near-Infrared Polymer and Organic Light-Emitting Diodes Based on Electrophosphorescence from (Tetraphenyltetranaphtho/2,3/porphyrin)platinum(II), ACS Appl. Mater. Interfaces, vol. 1, pp. 274-278, 2009.

/10/ S.M. Borisov, G. Nuss, W. Haas, R. Saf, M. Schmuck, I. Klimant, New NIR-emitting Complexes of Platinum(II) and Palladium(II) with Fluorinated Benzoporphyrins, J. Photochem. Photobiol. A, vol. 201, pp. 128-135, 2009.

/11/ S.M. Borisov, G. Nuss, I. Klimant, Red Light-Excitable Oxygen Sensing Materials Based on Platinum(II) and Palladium(II) Benzoporphyrins, Anal. Chem., vol. 80, pp. 9435-9442, 2008.

/12/ S.M. Borisov, G. Zenkl, I. Klimant, Phosphorescent Platinum(II) and Palladium(II) Complexes with Azatetrabenzoporphyrins—New Red Laser Diode-Compatible Indicators for Optical Oxygen Sensing, ACS Appl. Mater. Interfaces, vol. 2, pp. 366-374, 2010.

/13/ F. Niedermair, S.M. Borisov, G. Zenkl, O. Hofmann, H. Weber, R. Saf, I. Klimant, Tunable Phosphorescent NIR Oxygen Indicators Based on Mixed Benzo- and Naphthoporphyrin Complexes. Inorg. Chem., submitted.

/14/ S.M. Borisov, P. Lehner, I. Klimant, Trace Oxygen Sensors Based on Platinum(II) and Palladium(II) Complexes of 5,10,15,20-meso-tetrakis-(2,3,4,5,6-pentafluorphenyl)-porphyrin Covalently Immobilized on Silica Gel Particles, in preparation.

/15/ S. Nagl, O.S. Wolfbeis, Optical multiple chemical sensing: status and current challenges, Analyst, vol. 132, pp. 507-511, 2007.

/16/ M.I.J. Stich, L.H. Fischer, O.S. Wolfbeis, Multiple fluorescent chemical sensing and imaging, Chem. Soc. Rev., vol. 39, pp. 3102-3114, 2010.

/17/ S.M. Borisov, K. Gatterer, B. Bitschnau, I. Klimant, Preparation and Characterization of Chromium(III)-Activated Yttrium Aluminum Borate: A New Thermographic Phosphor for Optical Sensing and Imaging at Ambient Temperatures, J. Phys. Chem. C., vol. 114, pp. 9118-9124, 2010.

/18/ S.M. Borisov, K. Gatterer, I. Klimant, Red light-excitable dual lifetime referenced optical pH sensors with intrinsic temperature compensation, Analyst, vol. 135, pp. 1711-1717, 2010.

/19/ J.W. Aylott, Optical nanosensors-an enabling technology for intracellular measurements, Analyst, vol. 128, pp. 309-312, 2003.

/20/ S.M. Borisov, I. Klimant, Optical nanosensors-smart tools in bioanalytics, Analyst, vol. 133, pp. 1302-1307, 2008.

/21/ S.M. Borisov, T. Mayr, I. Klimant, Poly(styrene-block-vinylpyrrolidone) Beads as a Versatile Material for Simple Fabrication of Optical Nanosensors, Anal. Chem., vol. 80, pp. 573-582, 2008.

/22/ S.M. Borisov, I. Klimant, Luminescent nanobeads for optical sensing and imaging of dissolved oxygen, Microchim. Acta, vol. 164, pp. 7-15, 2008.

/23/ S.M. Borisov, D.L. Herrod, I. Klimant, Fluorescent poly(styrene-block-vinylpyrrolidone) nanobeads for optical sensing of pH, Sens. Actuators B, vol. 139, pp. 52-58, 2009.

/24/ L. Fischer, S. Borisov, M. Schaeferling, I. Klimant, O. Wolfbeis, Dual sensing of pO2 and temperature using a water-based and sprayable fluorescent paint, Analyst, vol. 135, pp. 1224-1229, 2010.

/25/ S.M. Borisov, T. Mayr, G. Mistlberger, K. Waich, K. Koren, P. Chojnacki, I. Klimant Precipitation as a simple and versatile meth-

od for preparation of optical nanochemosensors, Talanta, vol. 79, pp.1322-1330, 2009.

/26/ D. Aigner, S.M. Borisov, I. Klimant, New optical pH sensors based on perylene dyes, in preparation.

/27/ K. Waich, T. Mayr, I. Klimant, Microsensors for detection of ammonia at ppb-concentration levels, Meas. Sci. Technol., vol. 18, pp. 3195-3201, 2007.

/28/ K. Waich, T. Mayr, I. Klimant, Fluorescence sensors for trace monitoring of dissolved ammonia, Talanta, vol. 77, pp. 66-72, 2008.

/29/ K. Waich, S. Borisov, T. Mayr, I. Klimant, Dual lifetime referenced trace ammonia sensors, Sens. Actuators B, vol. 139, pp. 132-138, 2009.

/30/ G. Mistlberger, K. Koren, E. Scheucher, D. Aigner, S.M. Borisov, A. Zankel, I. Klimant. Multifunctional Magnetic Optical Sensor Particles with Tunable Sizes for Monitoring Metabolic Parameters and as a Basis for Nanotherapeutics, Adv. Funct. Mater., vol. 20, pp. 1842-1851, 2010.

/31/ G. Mistlberger, S.M. Borisov, I. Klimant, Enhancing performance in optical sensing with magnetic nanoparticles, Sens. Actuators B, vol. 139, pp. 174-180, 2009.

/32/ G. Mistlberger, K. Koren, S.M. Borisov, I. Klimant, Magnetically Remote-Controlled Optical Sensor Spheres for Monitoring Oxygen or pH, Anal. Chem., vol. 82, pp. 2124-2128, 2010.

/33/ G. Mistlberger, P. Chojnacki, I. Klimant, Magnetic sensor particles: an optimized magnetic separator with an optical window, J. Phys. D: Appl. Phys., vol. 41, pp. 085003 (1-8), 2008.

Sergey M. Borisov and Ingo Klimant

Institute of Analytical Chemistry and Food Chemistry,
Graz University of Technology, Stremayrgasse 9,
A-8010 Graz, Austria.
E-mail: sergey.borisov@tugraz.at

Prispelo (Arrived): 01.09.2010 *Sprejeto (Accepted): 15.09.2010*

VAPOR PHASE DEPOSITION PROCESSES FOR FABRICATION OF SENSOR AND SPECIALTY OPTICAL FIBER PREFORMS

Borut Lenardič

Optacore d.o.o. Ljubljana, Slovenia

Key words: vapor phase, fabrication of optical fibre preform, special optical fibres

Abstract: An overview of vapor phase doping methods in fabrication of optical fiber preform using different technologies is presented. Advantages of vapor phase processes are discussed and evaluated based on several samples developed for applications in sensorics, MOEMS and photonic component design. Vapor phase methods have shown good potential and are suitable tools for further development of standard and novel glass structures.

Uporaba tehnologije nanosa v parni fazi za izdelavo senzorjev in posebnih optičnih vlaken

Kjučne besede: parna faza, izdelava preforme optiÄnih senzorjev, posebna optična vlakna

Izvleček: Predstavljena je tehnologija dopiranja in nanosa v parni fazi za izdelavo optičnih vlaken. Predstavimo prednosti nanosa v parni fazi na osnovi mnogih vzorcev, razvitih za aplikacije v senzoriki, MOEMS in načrtovanja fotoničnih komponent. Metode nanosa v parni fazi so se pokazale kot obetavno orodje za razvoj standardnih in novih struktur.

1 Introduction

Optical fibers for sensor and specialty application require silica glass layers to be doped with a number of dopants not used in fabrication of telecommunication fibers/1/. Many such dopants like heavy metal- and rare earth ions, do not offer precursor materials in gaseous form or have very low vapor pressures. One way to deal with this limitation is to use a process, based on soaking of porous silica layers by solution, containing dopant ions (so-called "solution doping" method)/2/. Solution doping technology has some limitations and recently vapor phase doping methods are gaining wider acceptance. These methods rely on presence of dopant precursor vapor in the reaction zone where silica is formed. The advantage of vapor-phase doping methods over soaking is in reduced complexity, improved purity, wide choice of precursors and possibility to produce larger preforms with improved yield.

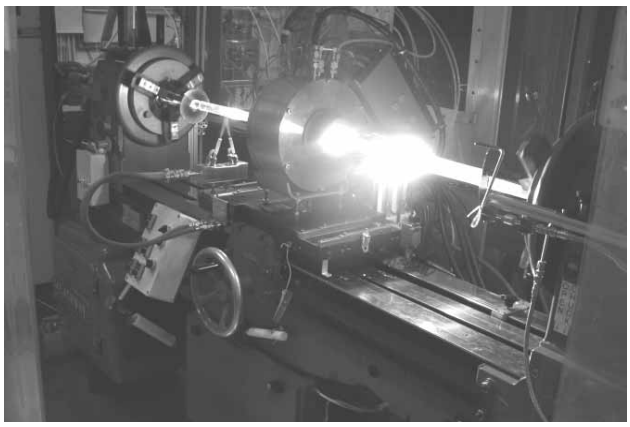

Fig. 1: View of MCVD preform fabrication system.

Vapor phase methods have been known since late 80's but did not gain wider acceptance due to the lack of feasible fabrication equipment. Recently, semi-industrial devices were introduced and several new methods can be used on standard optical fiber preform fabrication equipment.

The first such method is so-called "chelate doping" /3/, based on high temperature evaporation of solids (powders or sands). The second method is so-called "flash vaporization" method, based on impulse evaporation of solutions containing proper precursors.

An option to vapor phase doping method is "aerosol" method, offering advantages of both liquid and vapor phase methods.

Vapor phase methods have shown good potential and are suitable tools for further development of standard and novel glass structures.

2 Chelate doping method

2.1 Raw materials

Precursors in chelate rare earth-doping system are organometalic compounds of the 2,2,6,6-tetramethyl-3,5-heptanedionate (tmhd) or acetyl acetonate (acac) type. They are widely available from commercial sources, with typical purity between 99.9 and 99.999% in regard to metal impurities.

2.2 Device concept

In a chelate doping system precursors have to be heated over 150°C to provide high enough vapor pressure for use in MCVD process. Powders typically melt at temperatures

over 170°C and they decompose at temperatures over 280°C while boiling.

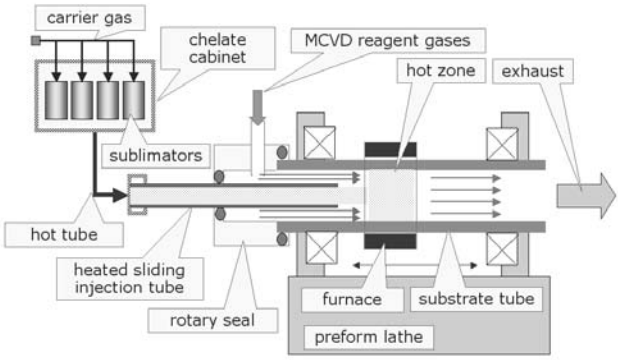

Fig. 2: Schematical view of chelate doping device on MCVD preform fabrication system

Chelates (and AlCl3) are evaporated from special heated vessels called sublimators. A standard sublimator design is shown schematically on Fig. 3A. It is usually filled by powder in bulk, possibly mixed with some inert material as filler. This simple design has been tested by fabrication of several preforms (Yb content results are indicated as area A in Fig. 4) It was found that such devices have poor performance due to small active surface interacting with carrier gas flow and due to agglomeration with prolonged use, preventing repeated use of the same materials.

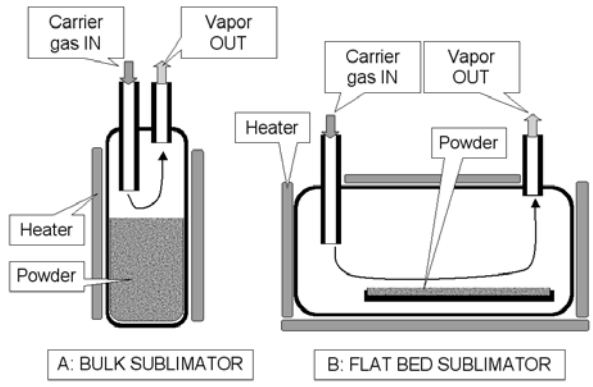

Fig. 3A: Typical design of a bulk sublimator; 3B: design of improved flat bed sublimator.

It was found that for deposition of highly-doped thick core layers, required for LMA fibers, sublimator has to be heated above precursor melting temperature. Therefore, a new type of sublimator (flat bed, Fig. 3B) had to be developed and tested on a series of preforms (Yb content results are indicated as area B in Fig. 4).

Relationship between evaporation rate (normalized to standard SiCl4 vapor flow and carrier flow) and Yb2O3 concentration in fabricated glass (each dot for one measured preform) is shown in Fig. 4. opposite.

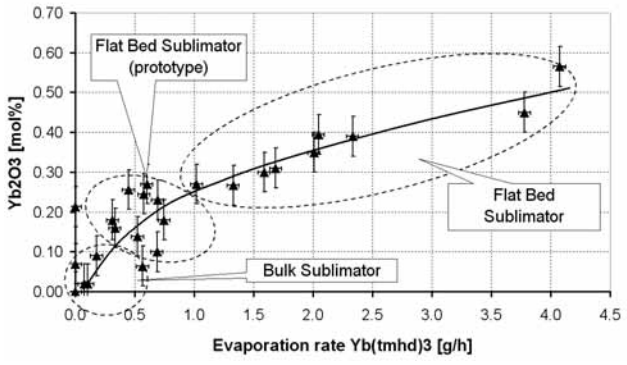

Fig. 4: Evaporation rates and deposition efficiency for different sublimator designs are shown.

2.3 Experimental

An MCVD preform fabrication system equipped with induction furnace was used. Chelate delivery system, connected to preform lathe as add-on device was a prototype of a commercial device. Precursor vapors, volatized at temperatures between 100°C to 220°C, were transported and injected into reaction hot zone by a system of heated conduits, valves, specially constructed high-temperature rotary seal and sliding precursor vapor injection tube.

Each precursor was sent to the hot zone in its own conduit to prevent chemical reaction between them. Each individual conduit (PTFE tube) can be exchanged quickly and conveniently, as it has been noticed that using same conduit for different precursor resulted in cross-contamination.

Preform fabrication was carried out in standard MCVD fashion. Cladding deposition was followed by active core deposition using chelate doping system.. Volatized precursors were transported and injected into reaction hot zone by a system of heated conduits, high-temperature rotary seal and sliding injection tube. An inert gas was used as carrier to prevent chemical reaction between constituents. They were allowed to mix with oxygen and SiCl4 vapors (and other gases and vapors GeCl4, POCl3, BCl3 and fluorine containing gas) delivered from standard MCVD gas cabinet only in the hot zone.

Prototype chelate doping system permitted deposition of multiple layers (up to 20 or more, depending on charge) but typically 5 – 9 layers were used to form core. SiCl4 carrier flow (O2) in core was typically set for 100 to 250 sccm with bubbler temperature 35°C and carriage traverse speed was 100 mm/min. Deposition was typically made over 600 mm and preforms with useful length between 250 and 350 mm and OD of 12 – 15 mm were produced.

After deposition of core layers, substrate tube was collapsed into solid rod preform in the conventional MCVD way, with the exception that furnace was used as heat source, which permitted significant acceleration of collapse process (more than twice faster) with generally improved geometrical characteristics.

3 Flash vaporization doping method

3.1 Flash Vaporization Concept

A new type of high performance vaporizers were developed for ALD, CVD, MOCVD (Metal Organic CVD), PECVD(Plasma Enhanced CVD), PEALD (Plasma Enhanced ALD) and all other gas phase processes containing vapors of solid or liquid compounds. New type of vaporizers can vaporize pure liquid compounds and solid ones dissolved in a carrier liquid (organic solvent). Their operation is based on a very fine atomization of a pulsed liquid flow, mixed with carrier gas prior to injection into vaporizer chamber.

Generated vapors can be used, for instance, for the synthesis by ALD and CVD of thin films, nanoparticles and nano-objects of numerous functional materials such as: dielectrics (low-k and high-k), barrier layers (Ta, Ti and Nb nitrides), ferroelectrics, piezoelectrics, metals (Cu, Ru, Rh, Pd, Ag, Ir, Pt…), III-V, II-V, chalcogenides (GST, CIS, CIGS,…), transparent conductive oxides, photovoltaic ones, low friction coatings, hard coatings and superconductors. In this described case we employed vaporizers as vapor delivery for optical fiber preform fabrication.

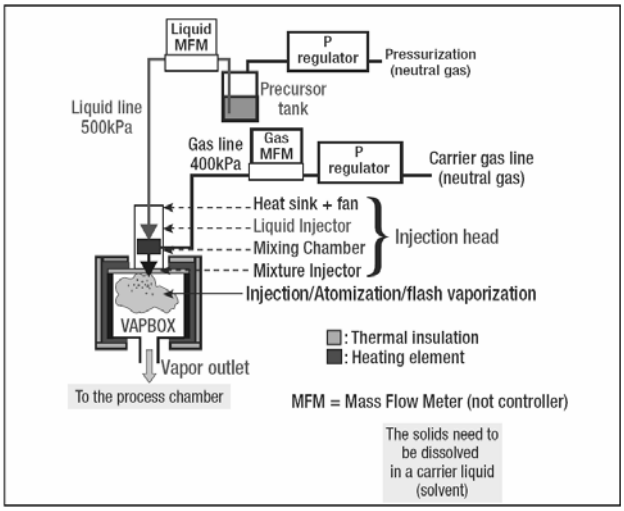

Fig. 5: Flash vaporization principle as employed in VapBox devices, single injector is shown.

VapBox vaporizers employ a proprietary way to deliver and atomize the liquid inside the vaporizer. They feature what is termed an injection head (see Figure 5 opposite). The injection head consists of multiple components: one liquid injector, one mixing chamber and one mixture injector. These three components are surrounded by a heat sink with a cooling fan. This arrangement keeps liquid or solution at room temperature, as long as it is not injected in the vaporizer. Premature precursor decomposition is thus avoided. Both the liquid and mixture injectors are normally closed fast solenoid valves working in a pulsed regime. The liquid to be vaporized is stored at room temperature in a pressurized tank at a higher pressure than the mixing chamber that is maintained under constant inert carrier gas pressure. The liquid injector pulses the cool fluid into the mixing chamber. The mixing chamber blends this fluid with the inert carrier gas. Finally, the mixture injector injects this mixture into the vaporizer in a pulsed regime. Pulsed flow combined with the blasting effect of the carrier gas pressure allows atomization of the blended fluid into an aerosol with extremely small droplets, typically 10 µm in diameter, with narrow distribution.

The surface of evaporation is thus very large. Furthermore, the droplets are very uniformly distributed over the carrier gas volume. Since the carrier gas serves as a heat transfer medium between the hot vaporizer walls and the droplets, heat transfer is very efficient. This provides efficient and truly non-contact flash vaporization to happen. The pulsed two-phase flow regime at the outlet of the mixture injector is highly turbulent and therefore the mean residence time of the droplets inside the vaporizer is largely increased, as compared to a stationary flow situation, avoiding the presence of non-vaporized droplets at the outlet of the vaporizer. A large amount of the droplets vaporize before touching the hot vaporizer walls of the vaporization chamber, limiting the clogging risks and allowing for generation of particle-free vapors. It is thus possible to efficiently vaporize thermally unstable compounds without clogging. These vaporizers can operate from vacuum to atmospheric pressure.

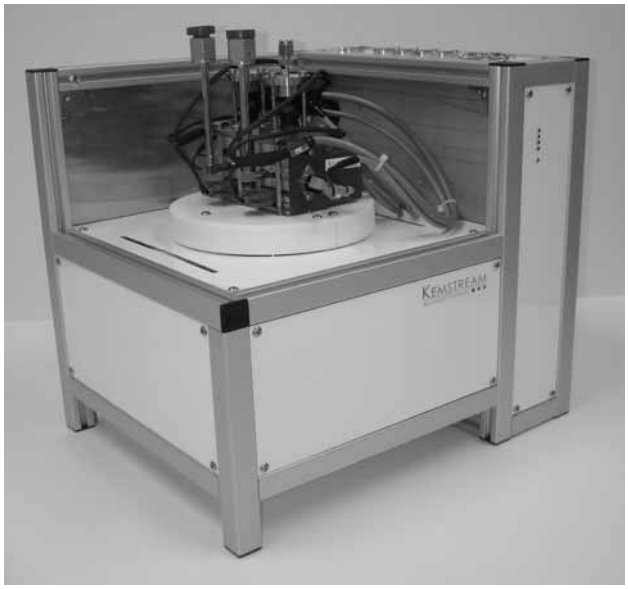

Fig. 6: Commercial version of Vapbox flash vaporization device with two injectors.

Vapbox vaporizer was adopted as vapor source for novel MCVD-like process for deposition of silica layers highly doped by lanthanides or metal ions. Figure 6 shows Vapbox device with two injection heads.

3.2 Raw Materials

Flash vaporization process relies on use of organometallic compounds as precursors for deposition process. It is not possible to combine standard halides like $SiCl_4$ in combination with organometallic materials or organic solvent vapors. Therefore chloride was replaced by TEOS (tetraethyl orthosilicate, Si(OC2H5)4), a material widely used in electronic industry. TEOS easily converts to silica by hydrolysis (sol-gel process) or at higher than 600 °C in presence of oxygen to SiO2 and diethyether. TEOS is readily available in ultra high purity and does not require complex handling.

There are other options, among which octamethylcyclotetrasiloxane (OMCTS or D4) or tetramethylcyclotetrasiloxane (TMCTS, precursor for gate dielectrics in thin-film transistors) have reportedly been used in specialty optical fiber preform fabrication by Morse /5/. They both have much higher content of silicon than TEOS and their reaction with oxygen is strongly exothermic.

β-diketonates have been chosen as organometallic precursors for lanthanide and transition metal ions. The reason for this was good availability from several commercial sources, relatively high purity, simple handling (with exception mentioned below) and good solubility in organic solvents. Most often used materials are chelates (tmhd) or acetyl acetonates (acac) as in case described above in chapter 2.

Organic solvents for preparation of solutions were, i.e. diglyme, 1,3-dimethoxyethane, tetrahydrofuran (THF) or chloroform, p.a. pure. Solution preparation and filling of precursor containers was made under dry and neutral (nitrogen) atmosphere, when necessary.

3.3 Experimental

Standard MCVD preform system has been used for fabrication of preforms. Flash vaporization doping system, connected to preform lathe as add-on device was a prototype of a commercial device. Schematic view of the complete set-up is shown on Figure. 7.

Precursor liquid or solution was injected into Vapbox vaporizer, volatized at temperatures between 180°C and 220°C, transported and injected into reaction hot zone by a system of heated conduits, valves, specially constructed high-temperature rotary seal and sliding precursor vapor injection tube

An inert gas was used as a carrier to prevent chemical reaction between constituents. Precursors were allowed to mix with oxygen and other gases (i.e. fluorine containing gas) delivered from standard MCVD gas cabinet only in the hot zone. Vapor entering substrate tube is shown on Figure 4b.

Standard cladding layers were first deposited on synthetic fused silica tube as barrier against hydroxyl impurity diffusion. Cladding was followed by active core deposition using flash vaporization doping system. Core was deposited in multiple thin layers.

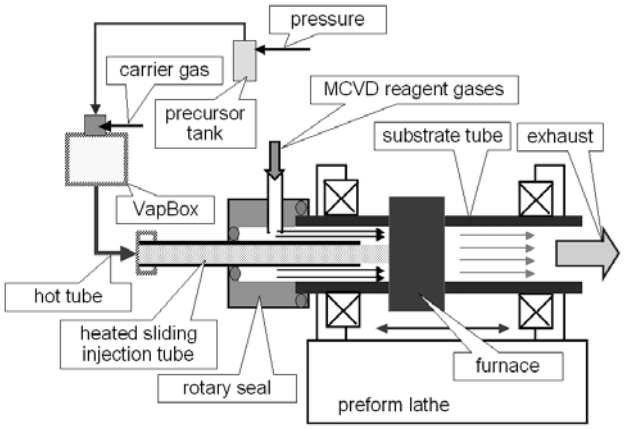

Fig. 7: Flash vaporization principle as employed in VapBox devices, single injector is shown.

Direct comparison with standard MCVD deposition is not possible, as TEOS was used in flash vaporization process as silicon precursor with evaporation rates between 0.25 and 2 g/min.

Core layers were deposited as thin porous doped silica layers (carriage forward motion) with low hot zone temperature of approx. 1450°C. At higher deposition rates, layers were filled with carbon soot (see Figure 8.) mainly from organic solvents and also partially from organometallic materials. At very high deposition rates, silica soot was filled with carbon to such an extent that the adherence to substrate tube wall was minimized and deposited layers detached themselves from the tube inner wall randomly.

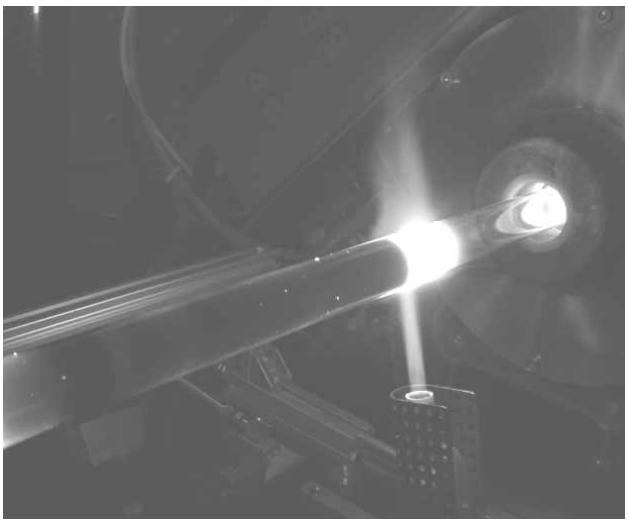

Fig. 8: Deposition of soot-filled layers during high deposition rate process.

Carbon was removed from soot-filled layers in oxygen-rich atmosphere at moderate to high temperatures, leaving

transparent and solid layer of doped silica. Chlorine was sometimes added to gas flow at this stage to remove hydroxyl and other impurities from deposited layers, and to reduce background loss /1/.

After deposition of several core layers, vapor injection tube was retracted and substrate tube was collapsed into solid rod preform. In these experiments furnace was used as heat source, permitting significant acceleration of collapse process (more than twice faster than with H2/O2 burner) with generally improved optical and geometrical characteristics.

4 Aerosol doping method

By modifying construction of flash vaporization doping device, a new type of devices is created. Instead of sending precursor and solvent vapor into process, a finely distributed aerosol is made from precursor-containing solution and guided into reaction by a system of heated conduits. Schematical view of such a doping system is shown on Fig. 9.

Aerosol enters reaction zone as very fine mist and evaporation process is initiated as soon as the substrate tube or burner flame (in outside deposition process) is hot enough. Therefore, vapors are produced on the spot where precursors are reacted with oxygen and other reagents.

Advantage of aerosol process over flash vaporization is in the capacity to use highly aggressive solutions or solutions based on alcohols or even water. Such process open the possibilities to use inorganic precursor materials which are most often available in higher purity.

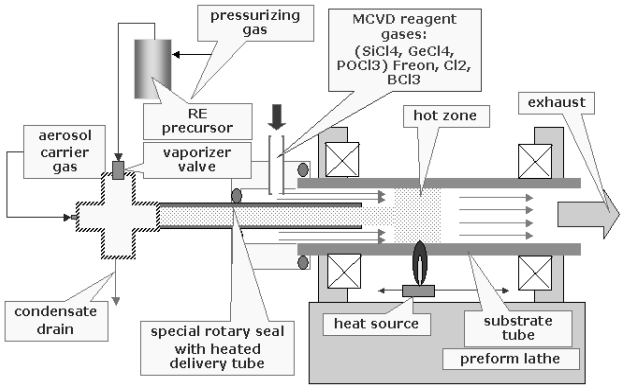

Fig. 9: Schematical view of aerosol doping device, based on flash vaporization process.

And, another important characteristics – due to use of injectors with higher injector orifice cross section, atomization causes no clogging or process problems even with precipitation of solids from solution. In all other aspects, the process is run as by the flash vaporization method.

5 Results and discussion

Most often specialty preforms are produced on request by customers developing new applications or devices. Deposited glass composition and characteristics have to provide behavior required by the sensor device or system. Such characteristics may range from optical to geometrical or even purely mechanical. A wide range of specialty preforms and glass compositions has been made in the recent years, based on above described doping methods and fabrication technologies.

5.1 Rare Earth-doped Performs and Fibers

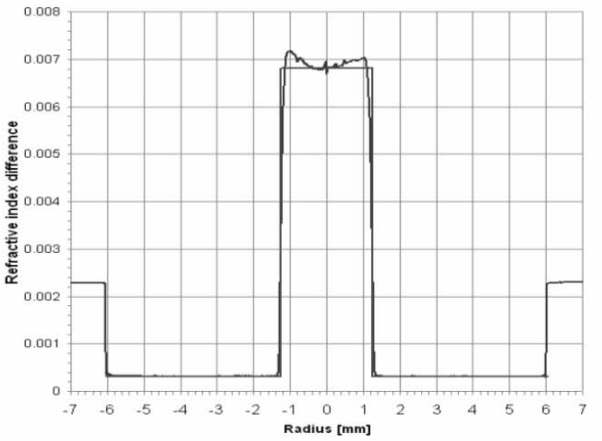

Fig. 10: Typical refractive index profile of a core preform made by flash vaporization doping process.

A number of experiments were carried out during evaluation of flash vaporization process and device. Preforms for laser fiber, co-doped by Yb^{3+} and Al^{3+}, (or phosphorous) were of most interest as they are currently very intensely investigated. A few experiments were made with other rare earth dopants (Er^{3+}, Tb^{3+}) to compare results of flash vaporization process with that of direct chelate evaporation / sublimation. For Yb^{3+}, the doping level achieved ranged from a few thousands to 70,000 ppmw with Al^{3+} or P^{5+} levels in appropriate ratio to rare earth, to prevent clustering.

Fibers were drawn from such preforms and it was demonstrated that chelate or flash vaporization doping can technology provides high quality glass, suitable for amplifier or laser operation.

Further testing is under way to confirm photodarkening characteristics of such glasses, while excellent slope efficiency performance has already been demonstrated. Background losses are well-controlled, both for chelate and flash vaporization made fibers.

Figure 10 demonstrates excellent refractive profile control for flash vaporization method. Figure 11 shows a typical octagonally-shaped preform for laser fiber (preform P0400 from Optacore).

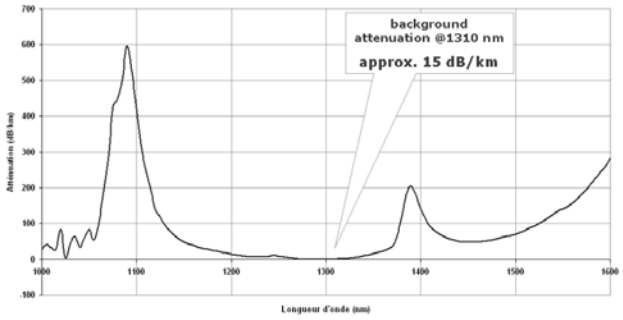

Fig. 11: Spectral atteenuation diagram for P0400 Yb^{3+}/Al^{3+}-codoped dual clad fiber

Fibers drawn from this preform were analyzed and spectral attenuation coefficient is shows on Fig. 12.

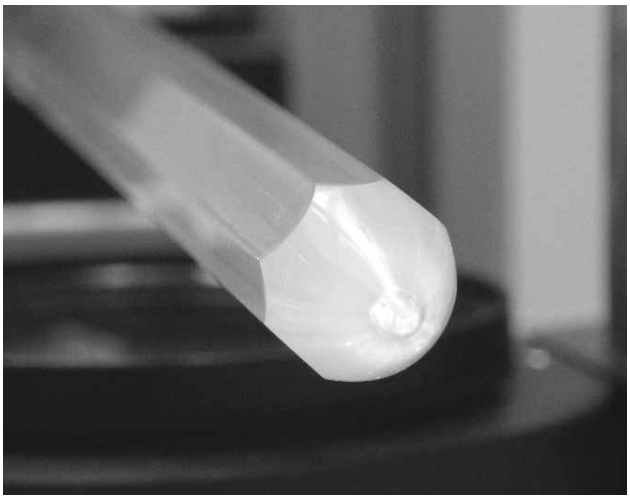

Fig. 12: Yb^{3+}/Al^{3+}-codoped dual clad preform produced in Optacore, ready for fiber drawing

5.2 Bismuth-doped Performs

Large interest in bismuth-doped fibers is related to search for laser white light sources. Bi-doped preforms were made by chelate and flash vaporization methods.

Bi-doping by chelate process is difficult, due to Bi-ion affinity to chlorine, which is always present when chloride is used as Si-precursor. Finding a Bi precursor for flash vaporization process is quite a complex task.

Bismuth chelate Bi(tmhd)3 is a very moisture sensitive compound which has to be handled under strict inert atmosphere and with anhydrous and deoxygenated solvents. Triphenyl bismuth Bi(C6H5)3O was identified as suitable Bi-dopant.

So far analysis of preform samples (slices) by X-ray microanalysis (EDS) has shown that bismuth content is below or at the detection level of the mentioned method (0.02 %at). Some of the preforms have shown bismuth luminescence (measured courtesy of FORC Moscow) but insufficient to proceed with preform or fiber analysis. Based on presented results and publications, new Bi dopants and modifications to precursor preparation process are currently investigated.

5.3 Metal ion-doped Performs and Fibers

Metal ions are used to produce glasses with very specific optical or mechanical characteristics. Vapor phase doping methods were tested with a number of dopants. Elements that are used as part of laser fiber fabrication process were not re-tested.

The following types of glasses have been deposited, and some were drawn to optical fibers:

- pure TiO2 on silica deposition
- highly vanadium-doped silica layers
- ZnO and CuO layer deposition on the inner wall of a quartz glass tube
- Fe-, Co- and Cr – doped preforms

Preforms have shown that significant doping levels, can be achieved while glass quality (in respect to bubbles and inclusion) and opto-mechanical characteristics remain suitable for use of drawn fibers in sensorics and photonic device development and fabrication.

6 Conclusions

Presented results and discussion demonstrate that vapor phase doping methods provide suitable and extremely flexible means for fabrication of different types of optical fiber preforms.

Experimental results have shown that highly rare-earth-doped fibers can be produced with sufficiently high deposition rate and repeatability to permit fabrication of high LMA laser fibers using chelate doping method.

Novel flash vaporization doping method has also demonstrated that fully vitrified transparent preforms without inclusions or bubbles can be fabricated using organometallic precursors for silicon, lanthanides, metal and transition element ions.

Fibers have been produced with suitable refractive index profiles and composition for intended purposes in laser and amplifier applications, for sensor applications and for fabrication of photonic devices. Champion data from such preforms and fibers show their characteristics are at least comparable to those of fibers produced by solution doping.

Wide range of precursors permits fabrication of diverse glass compositions thus making vapor phase methods and aerosol a versatile and reliable research tool, suitable for development and fabrication of novel glass structures and compositions.

Acknowledgments

Author would like to acknowledge support from Center of Excellence "En->Fist" and Slovenia Research Agency for part of the work presented here.

References

/1/ A. Mendez, T.F. Morse, ed., Specialty Optical Fibers Handbook, Academic, Burlington, 2007, Chap 7., 0-12-369406-X

/2/ Townsend, J.E. et al, "Fabrication of low loss optical fibres containing rare earth ions", Electr. Lett. 21, 737-738 (1987)

/3/ R.P. Tumminelli et al., Fabrication of High-Concentration Rare-Earth Doped Fibers Using Chelates, J. Light. Technol., Vol. 8 (1990)

/4/ B. Lenardič et al., Poster P09, ECOC Berlin, 2007

/5/ Materials from www. kemstream. com

/6/ B. Lenardič et al., Paper 1734, APOC Hanzhou, 2008

/7/ B. Lenardič et al., Paper OthK6, OFC San Diego, 2009

Borut Lenardič
Optacore d.o.o. Trpinčeva ul. 39, 1000 Ljubljana, Slovenia, borut.lenardic@optacore.si

Prispelo (Arrived): 01.09.2010 *Sprejeto (Accepted): 15.09.2010*

46. Mednarodna konferenca o mikroelektroniki, elektronskih sestavnih delih in materialih – MIDEM 2010
46nd International Conference on Microelectronics, Devices and Materials – MIDEM 2010

29. september – 01. oktober 2010 Zdravilišče Radenci, Radenci

Zaključno poročilo

Šestinštirideseta mednarodna konferenca o mikroelektroniki, elektronskih sestavnih delih in materialih – MIDEM 2010 (46th International Conference on Microelectronics, Devices and Materials) nadaljuje uspešno tradicijo mednarodnih konferenc MIDEM, ki jih vsako leto prireja Strokovno društvo za mikroelektroniko, elektronske sestavne dele in materiale - MIDEM. Področje elektronskih komponent je zelo pomembno in dinamično področje tehničnih znanosti in tehnologij. Problematika se zelo hitro spreminja, potrebno je slediti vsem spremembam, ki se pojavljajo v svetu in doma. Domačim in tujim strokovnjakom nudi možnost izmenjave izkušenj, primerjavo dosežkov in preverjanje raziskovalnih smeri. Na konferenci so se predstavili najnovejši dosežki na naslednjih področjih:

- senzorjev,
- tehnike načrtovanja monolitnih in hibridnih integriranih vezij,
- tehnologije izdelave monolitnih in hibridnih integriranih vezij,
- modeliranje tehnoloških procesov in delovanja sestavnih delov,
- tehnike testiranja vezij in podsistemov,
- fizika polprevodnikov,
- novi materiali za elektroniko in njihova uporaba,
- materialoznanstvo in tehnologije izdelave materialov za elektroniko,
- optoelektronika,
- polprevodniški, tankoplastni in debeloplastni senzorji,
- zanesljivost in analiza načinov odpovedi elektronskih komponent in vezij,
- analizne tehnike v elektroniki in materialoznanstvu.

Na konferenci je bilo letos predstavljeno 45 rednih in 10 vabljenih predavanj v šestih sekcijah z naslednjimi vsebinami:

- Materiali, tehnologije in elektronski sestavni deli,
- elektronika
- optoelektronika,
- tanki in debeli filmi,
- integrirana vezja,
- senzorji in aktuatorji.

Kot vsako leto je osrednji dogodek konference predstavljala enodnevna delavnica, tokrat na temo optičnih senzorjev z naslovom »Optical Sensors«. Na spremljajoči delavnici so bile predstavljene novosti s področja optičnih senzorjev ter njihove praktične uporabe. Vabljeni predavatelji so ugledni strokovnjaki iz akademskega in industrijskega okolja. Poleg akademskih dosežkov so bili predstavljeni tudi najnovejši dosežki na področju industrijskega razvoja naprednih senzorskih tehnologij s poudarkom na razvoju praktičnih aplikacij. Delavnica je dala vpogled v nove možnosti in trende, ki jih ponujajo sodobne optične senzorske tehnologije.

Na konferenci so bili predstavljeni najnovejši dosežki raziskovalcev iz domačih in tujih raziskovalnih skupin in podjetij. Pomembno vlogo so odigrala vabljena predavanja, ki so povzemala zadnje dosežke iz evropskega in svetovnega vrha izbranih tematik.

V delavnici je bilo predstavljeno osem vabljenih predavanj:

1. **J.P.Dakin**
   Optical Fibre Sensors, Past, Present and Future – A Personal View
2. **D.Inaudi**
   Overview of Fiber Optic Sensing Technologies for Structural Health Monitoring
3. **É.Pinet, S.Ellyson and F.Borne**
   Temperature Fiber-optic Point Sensors: Commercial Technologies and Industrial Applications
4. **K.Weir**
   Optical Measurements in Sensor Systems
5. **Y.Chamorovskiy**
   Specialty Optical Fibres for a Sensing Application
6. **S.M. Borisov and I.Klimant**
   Luminescent Chemosensors – Advanced Tools in Analytical Chemistry
7. **A.Leitner, N.Galler, J.Krenn**
   Sensing With Surface Plasmons
8. **B.Lenardič**
   Vapor Phase Deposition Processes For Fabrication of Sensor and Specialty Optical Fiber Preforms

Delavnica je privabila več kot 75 poslušalcev.

Pred konferenco je bil izdelan zbornik s 45 referati (10 tujih avtorjev), skupaj v obsegu 322 strani. Skupno število udeležencev konference je bilo 75, od tega 61 domačih in 14 tujih udeležencev, kar kaže na visok trend naraščanja obiska konferenc MIDEM.

Glede na navedene podatke in kvaliteto vabljenih in rednih prispevkov smo organizatorji, upamo pa tudi da udeleženci konference, z letošnjo konferenco zelo zadovoljni. To nam je v motivacijo in izziv pri pripravi aktualnih znanstvenih in razvojnih tem ter organizacije konference MIDEM 2011.

UDK621.3:(53+54+621+66), ISSN0352-9045 Informacije MIDEM 40(2010)1, Ljubljana

VSEBINA CONTENT

UDK621.3:(53+54+621+66), ISSN0352-9045 Informacije MIDEM 40(2010)2, Ljubljana

VSEBINA CONTENT

UDK621.3:(53+54+621+66), ISSN0352-9045 Informacije MIDEM 40(2010)3, Ljubljana

VSEBINA CONTENT

UDK621.3:(53+54+621+66), ISSN0352-9045 Informacije MIDEM 40(2010)4, Ljubljana

MIDEM
DRUŠTVO-SOCIETY
IMAPS Slovenia Chapter

M I D E M

Strokovno društvo za mikroelektroniko,
elektronske sestavne dele in materiale
MIDEM pri MIKROIKS
Stegne 11, 1521 Ljubljana
SLOVENIJA

TEL.: +386 (0)1 5133 768
FAX: +386 (0)1 5133 771
Email / WWW
iztok.sorli@guest.arnes.si
http://paris.fe.uni-lj.si/midem/

MIDEM SOCIETY REGISTRATION FORM

1. First Name ..... Last Name .....

   Adress .....

   City .....

   Country ..... Postal Code .....

2. Date of Birth .....

3. Education (please, circle whichever appropriate)

   PhD MSc BSc High School Student

3. Profession (please, circle whichever appropriate)

   Electronics Physics Chemistry Metallurgy Material Sc.

4. Company .....

   Adress .....

   City .....

   Country ..... Postal Code .....

   Tel.: ..... FAX: .....

   Email .....

5. Your Primary Job Function

   Fabrication Engineering Facilities QA/QC
   Management Purchasing Consulting Other

6. Please, send mail to a) Company adress b) Home Adress

7. I wil regularly pay MIDEM membership fee, 25,00 EUR/year

MIDEM member recive Journal "Informacije MIDEM" for free !!!

Signature ..... Date .....

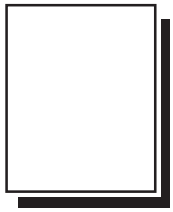

MIDEM at MIKROIKS
Stegne 11

1521 Ljubljana
Slovenija

Informacije MIDEM
Strokovna revija za mikroelektroniko, elektronske sestavine dele in materiale

NAVODILA AVTORJEM

Informacije MIDEM je znanstveno-strokovno-društvena publikacija Strokovnega društva za mikroelektroniko, elektronske sestavne dele in materiale - MIDEM. Revija objavlja prispevke s področja mikroelektronike, elektronskih sestavnih delov in materialov. Ob oddaji člankov morajo avtorji predlagati uredništvu razvrstitev dela v skladu s tipologijo za vodenje bibliografij v okviru sistema COBISS.
Znanstveni in strokovni prispevki bodo recenzirani.

Znanstveno-strokovni prispevki morajo biti pripravljeni na naslednji način:

1. Naslov dela, imena in priimki avtorjev brez titul, imena institucij in firm
2. Ključne besede in povzetek (največ 250 besed).
3. Naslov dela v angleščini.
4. Ključne besede v angleščini (Key words) in podaljšani povzetek (Extended Abstract) v angleščini, če je članek napisan v slovenščini
5. Uvod, glavni del, zaključek, zahvale, dodatki in literatura v skladu z IMRAD shemo (Introduction, Methods, Results And Discsussion).
6. Polna imena in priimki avtorjev s titulami, naslovi institucij in firm, v katerih so zaposleni ter tel./Fax/Email podatki.
7. Prispevki naj bodo oblikovani enostransko na A4 straneh v enem stolpcu z dvojnim razmikom, velikost črk namanj 12pt. Priporočena dolžina članka je 12-15 strani brez slik.

Ostali prispevki, kot so poljudni cčlanki, aplikacijski članki, novice iz stroke, vesti iz delovnih organizacij, inštitutov in fakultet, obvestila o akcijah društva MIDEM in njegovih članov ter drugi prispevki so dobrodošli.

Ostala splošna navodila

1. V članku je potrebno uporabljati SI sistem enot oz. v oklepaju navesti alternativne enote.
2. Risbe je potrebno izdelati ali iztiskati na belem papirju. Širina risb naj bo do 7.5 oz.15 cm. Vsaka risba, tabela ali fotografija naj ima številko in podnapis, ki označuje njeno vsebino. Risb, tabel in fotografij ni potrebno lepiti med tekst, ampak jih je potrebno ločeno priložiti članku. V tekstu je treba označiti mesto, kjer jih je potrebno vstaviti.
3. Delo je lahko napisano in bo objavljeno v slovenščini ali v angleščini.
4. Uredniški odbor ne bo sprejel strokovnih prispevkov, ki ne bodo poslani v dveh izvodih skupaj z elektronsko verzijo prispevka na disketi ali zgoščenki v formatih ASCII ali Word for Windows. Grafične datoteke naj bodo priložene ločeno in so lahko v formatu TIFF, EPS, JPEG, VMF ali GIF.
5. Avtorji so v celoti odgovorni za vsebino objavljenega sestavka.

Rokopisov ne vračamo. Rokopise pošljite na spodnji naslov.

Uredništvo Informacije MIDEM
MIDEM pri MIKROIKS
Stegne 11, 1521 Ljubljana, Slovenia
Email: Iztok.Sorli@guest.arnes.si
tel. (01) 5133 768, fax. (01) 5133 771

Informacije MIDEM
Journal of Microelectronics, Electronic Components and Materials

INSTRUCTIONS FOR AUTHORS

Informacije MIDEM is a scientific-professional-social publication of Professional Society for Microelectronics, Electronic Components and Materials – MIDEM. In the Journal, scientific and professional contributions are published covering the field of microelectronics, electronic components and materials.
Authors should suggest to the Editorial board the classification of their contribution such as : original scientific paper, review scientific paper, professional paper…
Scientific and professional papers are subject to review.

Each scientific contribution should include the following:

1. Title of the paper, authors' names, name of the institution/company.
2. Key Words (5-10 words) and Abstract (200-250 words), stating how the work advances state of the art in the field.
3. Introduction, main text, conclusion, acknowledgements, appendix and references following the IMRAD scheme (Introduction, Methods, Results And Discsussion).
4. Full authors' names, titles and complete company/institution address, including Tel./Fax/Email.
5. Manuscripts should be typed double-spaced on one side of A4 page format in font size 12pt. Recommended length of manuscript (figures not included) is 12-15 pages
6. Slovene authors writing in English language must submit title, key words and abstract also in Slovene language.
7. Authors writing in Slovene language must submit title, key words and extended abstract (500-700 words) also in English language.

Other types of contributions such as popular papers, application papers, scientific news, news from companies, institutes and universities, reports on actions of MIDEM Society and its members as well as other relevant contributions, of appropriate length , are also welcome.

General informations

1. Authors should use SI units and provide alternative units in parentheses wherever necessary.
2. Illustrations should be in black on white paper. Their width should be up to 7.5 or 15 cm. Each illustration, table or photograph should be numbered and with legend added. Illustrations, tables and photographs must not be included in the text but added separately. However, their position in the text should be clearly marked.
3. Contributions may be written and will be published in Slovene or English language.
4. Authors must send two hard copies of the complete contributon, together with all files on diskette or CD, in ASCII or Word for Windows format. Graphic files must be added separately and may be in TIFF, EPS, JPEG, VMF or GIF format.
5. Authors are fully responsible for the content of the paper.

Contributions are to be sent to the address below.

Uredništvo Informacije MIDEM
MIDEM pri MIKROIKS
Stegne 11, 1521 Ljubljana, Slovenia
Email: Iztok.Sorli@guest.arnes.si
tel.+386 1 5133 768, fax.+386 1 5133 771